

الجمهورية الجزائرية الديمقراطية الشعبية
République Algérienne Démocratique et Populaire
وزارة التعليم العالي و البحث العلمي
Ministère de l'enseignement supérieur et de la recherche scientifique

Université Mohamed Khider – Biskra
Faculté des Sciences et de la technologie
Département : Génie Mécanique
Réf.....:



جامعة محمد خيضر بسكرة
كلية العلوم و التكنولوجيا
قسم : الهندسة الميكانيكية
المرجع :

Thèse présentée en vue de l'obtention
du diplôme de

Doctorat en Sciences

Spécialité : Génie Mécanique

Option : Énergétique

Modélisation et simulation du refroidissement des éléments à base de composants électroniques par des nanofluides

Par :

CHADI Kamel

Devant le jury composé de :

<i>Mr. Noureddine MOUMMI</i>	<i>Professeur</i>	<i>Président</i>	<i>Université de Biskra</i>
<i>Mr. Noureddine BELGHAR</i>	<i>Professeur</i>	<i>Encadreur</i>	<i>Université de Biskra</i>
<i>Mr. Semch-Eddine DERFOUF</i>	<i>Professeur</i>	<i>Co- Encadreur</i>	<i>Université Batna 2</i>
<i>Mr. Foued CHABANE</i>	<i>M.Conférences A</i>	<i>Examineur</i>	<i>Université de Biskra</i>
<i>Mme. BATTIRA Mouna, Née MAACHE</i>	<i>M.Conférences A</i>	<i>Examineur</i>	<i>Université de Khenchela</i>
<i>Mr. Mourad CHIKHI</i>	<i>M.Conférences A</i>	<i>Examineur</i>	<i>U.D.E.S CDER Bou-Ismaïl</i>

ABSTRACT

In this thesis, we have studied and modeled by a numerical simulation in laminar and stationary, the cooling by convective flows of electronic components using nanofluids, with the aim of improving heat exchanges and to increase the cooling efficiency. For this reason, we have carried out several studies in the form of applications. The first application numerically examined heat transfer in three different geometries of mini-channels using Cu – water nanofluid with a volume concentration of 0.05.

As for the second, fourth and third applications devoted to the study of the effect of the type of nanofluids and their volume concentrations, as well as the effect of the sections and shapes of the mini channels on the heat exchange and on the cooling of the electronic component. In these studies we used three different types of nanofluids at different concentrations. These studies showed that the minichannels of the third and ninth case improve the heat transfer compared to other cases as well as the value of the maximum junction temperature of the electronic component and that the use of diamond-water nano-fluid gives significantly higher heat transfer coefficients than Ag-water and Cu-water nanofluids. And increase in the concentration of nanoparticles in the base fluid (water) improves the heat transfer coefficient.

The fifth application aims to determine the effect of the position of the obstacle inside a horizontal mini channel on the cooling of the electronic component using nano-fluids with a volume fraction of 0.05. In this study, we found that the position of the obstacle in the twelfth case offers much better thermal performance than the other cases.

In the sixth application, we investigated the effect of adding the pie shaped fins and parallelogram fins in the microchannels on thermal performance using a Diamond-water nanofluid with a volume fraction of 0.05. In this study, the heat flux generated by electronic components is equal $q = 100 \text{ W} / \text{cm}^2$. The Reynolds (Re) number was taken between 200 and 600. The results showed that the micro-channels in the seventeenth case which contained the parallelogram-shaped fins gave an improvement in heat transfer.

Key words: natural convection, nano-fluids, obstacle, electronic component, numerical simulation, CFD fluent, microchannels, mini channels, heat transfer, solid fraction, Pie shape ribs, parallelogram ribs.

RÉSUMÉ

Dans cette thèse, nous avons étudié et modélisé par une simulation numérique en régime laminaire et stationnaire, le refroidissement par les écoulements convectifs des composants électroniques en utilisant des nanofluides, dans le but d'amélioration des échanges thermiques et pour augmenter l'efficacité du refroidissement. Pour cette raison, nous avons réalisé plusieurs études sous forme des applications. La première application a examiné numériquement le transfert thermique dans trois géométries différentes des mini-canaux en utilisant nanofluide Cu-eau avec une concentration volumique de 0.05.

Quant aux deuxième, quatrième et troisième applications consacrées à l'étude de l'effet du type de nanofluides et de leurs concentrations volumiques, ainsi que de l'effet des sections et formes des mini canaux sur l'échange thermique et sur le refroidissement du composant électronique dans ces études, nous avons utilisé trois types différents de nanofluides à différentes concentrations et ces études ont montré que les minicanaux du troisième et neuvième cas améliorent le transfert de chaleur par rapport aux autres cas ainsi que la valeur de la température maximale de jonction du composant électronique et que l'utilisation de nano-fluide diamant-eau donne des coefficients de transfert de chaleur significativement plus élevés que les nanofluides Ag-eau et Cu-eau. Et L'augmentation de la concentration de nanoparticules dans le fluide de base (eau) permet d'améliorer le coefficient de transfert de chaleur.

La cinquième application vise à déterminer l'effet de la position de l'obstacle à l'intérieur d'un mini canal horizontal sur le refroidissement du composant électronique en utilisant de nano-fluides avec une fraction volumique de 0,05. Dans cette étude, nous avons constaté que la position de l'obstacle dans le douzième cas offre de bien meilleures performances thermiques que les autres cas.

Dans la sixième application, nous avons étudié l'effet de l'ajout des ailettes en forme de trois quarts du cercle et des ailettes en parallélogramme dans les micro-canaux sur les performances thermiques en utilisant un nanofluide Diamant - eau avec une fraction volumique de 0,05. Dans cette étude, le flux thermique généré par les composants électroniques est égal à $q = 100 \text{ W /cm}^2$. Le nombre de Reynolds (Re) a été pris entre 200 et 600. Les résultats ont montré que les micro-canax dans le dix-septième cas qui contiennent les ailettes en forme de parallélogramme ont donné une amélioration de transfert thermique.

Mots clés: convection naturelle, nanofluides, obstacle, composant électronique, simulation numérique, fluent CFD, microcanaux, minicanaux, transfert de chaleur, fraction volumique, ailettes en forme de trois quarts du cercle, ailettes en parallélogramme.

ملخص

في هاته الأطروحة ، قمنا بدراسة النمذجة والمحاكاة العددية لتدفق صفائحي ومستقر ، التبريد عن طريق الحمل الحراري لمكونات إلكترونية باستخدام الموائع النانوية ، بهدف تحسين التبادل الحراري وزيادة كفاءة التبريد. لهذا السبب ، قمنا بإجراء العديد من الدراسات في شكل تطبيقات. التطبيق الأول يتضمن فحص نقل الحرارة في ثلاث أشكال هندسية مختلفة للقنوات المصغرة باستخدام سائل نانوي ماء - النحاس بتركيز حجمي قدره 0.05.

بالنسبة للتطبيقات الثانية والثالثة والرابعة المخصصة لدراسة تأثير أنواع الموائع النانوية وكسورها الحجمية ، وكذلك تأثير مقاطع وأشكال القنوات الصغيرة على التبادل الحراري وعلى تبريد المكون الإلكتروني في هذه الدراسات استخدمنا ثلاثة أنواع مختلفة من السوائل النانوية بكسور مختلفة وأظهرت هذه الدراسات أن القنوات الصغيرة للحالة الثالثة والتاسعة تعمل على تحسين نقل الحرارة مقارنة بالحالات الأخرى بالإضافة إلى تحسين قيمة درجة حرارة القصوى للمكون الإلكتروني وأن استخدام سائل نانو الماء-الماس يعطي معاملات نقل حرارة أعلى بكثير من Ag-water و Cu-water كما أن زيادة تركيز الجسيمات النانوية في السائل الأساسي (الماء) يحسن معامل انتقال الحرارة

يهدف التطبيق الخامس إلى تحديد تأثير موضع العائق داخل قناة أفقية صغيرة على تبريد المكون الإلكتروني باستخدام سوائل نانوية بحجم كسر حجمه 0.05. في هذه الدراسة وجدنا أن موضع الحاجز في الحالة الثانية عشر يقدم أداء حراري أفضل بكثير من الحالات الأخرى

في التطبيق السادس ، درسنا تأثير إضافة زعانف على شكل ثلاثة أرباع دائرة وزعانف متوازية الأضلاع في قنوات متناهية الصغر على الأداء الحراري باستخدام المائع النانوي الماء-الماس مع جزء حجمي 0.05. في هذه الدراسة ، يكون التدفق الحراري الناتج عن المكونات الإلكترونية مساوياً لـ $q = 100 \text{ W/cm}^2$ تم أخذ عدد رينولدز (Re) بين 200 و 600. وأظهرت النتائج أن القنوات الصغيرة في الحالة السابعة عشر التي تحتوي على زعانف على شكل متوازي الأضلاع أعطت جودة في نقل الحرارة.

الكلمات الرئيسية: الحمل الحراري الطبيعي ، الموائع النانوية ، العائق ، المكون الإلكتروني ، المحاكاة العددية ، CFD ، القنوات الصغيرة ، نقل الحرارة ، الكسر الصلب ، أضلاع الشكل شبه الدائري ، متوازية الأضلاع.

Remerciements

Je souhaite rendre grâce à Dieu, le clément et miséricordieux de m'avoir donné la force, le courage et la patience de mener à bien ce modeste travail.

*Je tiens à remercier sincèrement mon encadreur Mr **N. BELGHAR**, Professeur à l'Université Mohamed Khider – Biskra, de m'avoir suivi et dirigé tout au long de la réalisation de cette thèse. Et aussi je tiens à remercier mon co-encadreur Mr **S. DERFOUF** Professeur à l'Université de Batna 2.*

*Je remercie Mr **N. MOUMMI**, Professeur à l'Université Mohamed Khider – Biskra, d'avoir accepté de présider le jury.*

*Je remercie Mr **F. CHABANE**, M.C.A à l'Université Mohamed Khider de Biskra, Mme : **BATTIRA M**, Née **MAACHE**, M.C.A à l'Université Abbès Laghrour - Khenchela et Mr **M. CHIKHI**, M.C.A à Unité de développement des équipements solaires (U.D.E.S) CDER - Bou-Ismaïl, d'avoir accepté de faire parti du jury ainsi que pour leur participation à l'évaluation du présent travail.*

Mes remerciements vont également à tous ceux et celles qui de près ou de loin m'ont apporté aide et encouragement.

kamel

Dédicaces

Je dédie ce modeste travail

A mes très chers parents

A mes très chers frères et sœurs

A tous mes professeurs

Et à tous mes amis

kamel

Summary

ABSTRACT	1
RESUME	2
ملخص	3
Remerciements	4
Dédicace	5
Nomenclature	11
List of Figures	13
List of Table	17
General introduction	18
Chapter I: Bibliographic review	21
Chapter II: Generality on thermal Properties of nanofluids	47
II.1.Introduction	47
II. 2. Types of nanofluids	47
II. 2.1. Single material nanofluids	48
II. 2.2. hybrid nanofluids	49
II.3. Nanofluid preparation	50
II.3.1. One-step method	51
II.3.2 Two-step method	51
II. 4. Thermophysical properties of nanofluids	52
II. 4. 1. The volume fraction (φ)	52
II. 4. 2. The density	53
II. 4. 3. Specific heat	54
II. 4. 4. The thermal expansion coefficient	54
II. 4. 5. The thermal conductivity of nanofluids	54
II. 4. 5. 1. Maxwell model	55
II. 4. 5. 2. Hamilton-Crosser Model	55
II. 4. 5. 3. Yu et Choi Model	56
II. 4. 5. 4. Bruggeman Model	56
II. 4. 6. Dynamic viscosity	57
II. 4. 6. 1. Einstein Model	57
II. 4. 6. 2. Batchelor Model	58
II. 4. 6. 3. Brinkman Model	58
II. 4. 6. 4. Pack et Cho Model	58

II. 4. 6. 5. Maiga et al. Model	58
II. 4. 7. The parameters affecting thermal conductivity	59
II. 4. 7. 1. Effect of temperature and nanoparticle size on thermal conductivity	59
II. 4. 7. 2. Effect of nanoparticle volume fraction on thermal conductivity	60
II. 4. 7. 3. Effect of the base liquid on thermal conductivity	61
II. 4. 7. 4. Effect of particle shape on thermal conductivity	62
Chapter III: Mathematical model and numerical method	64
III.1. Introduction	64
III.2. General equations	64
III .2.1. Continuity equation	64
III .2.2. The momentum conservation equation	65
III .2.3. Energy conservation equation	65
III.3. Boussinesq approximation	66
III.4. Mathematical model for the Applications studied	66
III.4. 1.The thermo-physical properties of the nanofluids used in the applications studied	66
III.4.2.Simplifying hypothesis for the applications studied	68
III.4.2.1. Simplifying hypothesis for the applications N° 1	68
III.4.2.2. Simplifying hypothesis for the applications N° 2	68
III.4.2.3. Simplifying hypothesis for the applications N° 3 and N°4	68
III.4.2.4. Simplifying hypothesis for the applications N° 5	68
III.4.2.5. Simplifying hypothesis for the applications N° 6	69
III.4.3. Mathematical model for the application N°1 studied: Numerical study of the thermal transfer in different geometries of the mini-channels	69
III.4.3.1 Geometries of the problems considered	69
III.4.3.2 Boundary conditions	70
III.4.3.3. Equations of the problem	70
III.4.4. Mathematical model for the application N°2 studied: Numerical study of the influence of nanofluids on thermal exchange in mini-channels	72
III.4.4.1. Geometries of the problems considered	72
III 4.4.2. Mathematical formulation	73
III.4.5. Mathematical model for the application N°3 studied: Study of thermal exchanges in different geometry sections of mini-channels of a cooler for cooling a chip using nanofluids	74
III.4.5.1. Geometries of the problems considered	74
III.4.5.2. Equations of the problem	76
III.4.5.3. Boundary conditions	78
III.4.6. Mathematical model for the application N°4 studied: Influence of types of nanoparticles, nanoparticles volume concentration and types of cooler metals on the heat transfer in a mini-channels cooler	80
III.4.6.1. Geometries of the problems considered	80

III.4.6.2. Boundary conditions	81
III.4.6.3. Equations of the problem	81
III.4.7. Mathematical model for the application N°5 studied: Study in three dimensions of influence of the fluids' nature and obstacle position on cooling of electronic component	81
III.4.7.1. Geometries of the problems considered	81
III.4.7.2. Boundary conditions	83
III.4.7.3. Equations of the problem	
III.4.7.4. dimensionless equations of the problem	84
III.4.8. Mathematical model for the application N°6 studied: A numerical study on the effect of the addition of the pie shape ribs and parallelogram ribs in micro-channels on thermal performance using Diamond - water fluid	85
III.4.8.1. Geometries of the problems considered	85
III.4.8.2. Boundary conditions	88
III.4.8.3. Equations of the problem	88
III.5. Numerical resolution using CFD codes	90
III.6. Numerical methods	90
III.7. Finite volume method	91
III.8. Mesh	92
III.9. Choice of mesh	93
III.10. Discretization of equations	95
III.11. Under-relaxation factors	98
III.12. Convergence criterion	98
III.13. Choice of the Pressure – velocity coupling method	99
III.14. Different steps to follow for numerical modeling	100
III.15. Steps of a CFD simulation using Fluent	102
III.15.1. Mesh	102
III.15.1.1. Choice of mesh type	102
III.15.1.2. General mesh	103
III.15.2. Simulation	106
III.15.2.1. Choice of solver	106
III.15.2.2. Definition of fluid characteristics	107
III.15.2.3. Operating conditions	107
III.15.2.4. Boundary conditions	107
III.15.2.5. Choice of convergence criteria	108
Chapter IV: Applications	109
Application N°1 : Numerical study of the thermal transfer in different geometries of the mini-channels	109
IV.1.1. Introduction	109
IV.1.2. Effect of the mesh on numerical solutions	109

IV.1.3. Results and interpretations	110
IV.1.4. Conclusion (Application N°1)	112
Application 2: Numerical study of the influence of nanofluids on thermal exchange in mini-channels	112
IV.2.1. Introduction	112
IV.2.2. Effect of the mesh on Numerical solutions	112
IV.2.3. Results and interpretations:	113
IV.2.4. Conclusion (Application N°2)	114
Application N°3 : A study of thermal exchanges in different geometry sections of mini-channels of a cooler for cooling a chip using nanofluids	115
IV.3.1. Introduction	115
IV.3.2. Effect of the mesh on numerical solutions	115
IV.3.3. Validation of the results	116
IV.3.4. Results and discussions	117
IV.3.4.1. Evolution of the temperature of the upper surface of the mini-channel cooler for all cases	117
IV.3.4.2. Evolution of the junction temperature value of the chip in function of the Reynolds number	118
IV.3.4.3. Distribution of the temperature in the surface of the chip for all cases	119
IV.3.4.4. Evolution of the average heat transfer for all cases	120
IV.3.4.5. Conclusion (Application 3)	122
Application N°4 : Influence of the types of nanoparticles, nanoparticles volume concentration and the types of cooler metals on the heat transfer in a mini-channels cooler	123
IV.4.1. Introduction	123
IV.4.2. Results and discussions	124
IV.4.2.1. Variation in the temperature of the mini-channels cooler with the three nano-fluids used and two metals of the cooler	125
IV.4.2.2. Effects of three different types of nano-particles on the temperature of the electronic component and the average heat transfer coefficient	125
IV.4.2.3. Evolution of the temperature of the electronic component for the two metals	126
IV.4.2.4. Distribution of the temperature of the mini channel with three nanofluid and tow metals of the cooler	127
IV.4.2.5. Conclusion (Application N°4)	129
Application N°5: Numerical study in three dimensions of the influence of the fluids' nature and obstacle position on cooling of electronic component	129
IV.5.1. Introduction	129
IV.5.2. Independence of the mesh	129
IV.5.3. Results and interpretations	130
IV.5.4 Conclusion (Application N°5)	135
Application N°6: A numerical study on the effect of the addition of the pie shape ribs and parallelogram ribs in micro- channels on thermal performance using Diamond - water nanofluid	135

IV.6.1. Introduction	135
IV.6.2. Independence of the mesh	136
IV.6.3. Validation of the results	137
IV.6.4. Results and discussions	137
IV.6.5. Conclusion (Application N°6)	146
Annex Annex :1 Publication proceeding from application N°1 Annex :2 Publication proceeding from application N°2	147
Annex Annex :3 Publication from application N°3 Annex :4 Publication from application N°4	147
Conclusion and recommandations	150
Bibliographic references	153

NOMENCLATURE

A_c	Cross sectional area of micro channel, (m ²)
A_w	Inner wall or fluid contact surface area, (m ²)
b	Constant term in the discretization equation
C_p	Specific heat of the fluid, (Jkg ⁻¹ K ⁻¹)
D_h	Hydraulic diameter of channel, $D_h=4*A_c/P_c$ (m)
$F_{in,\phi}$	The total flow at the input of the variable ϕ
F_d	The skewness factor
g	The acceleration of gravity, (ms ⁻²)
H	Height, (m)
H_c	Mini / micro channel height, (m)
h_{av}	Average heat transfer coefficient, (W m ⁻² K ⁻¹)
h	Convective exchange coefficient, (W m ⁻² K ⁻¹)
k	Thermal conductivity, (Wm ⁻¹ K ⁻¹)
L	Mini /micro channel length, (m)
N	Number of micro-channels
Nu	Nombre de Nusselt local
Nu_{av}	Nombre de Nusselt moyen
P_c	Wetted perimeter, (m)
p	pressure, (Pa)
P	Dimensionless pressure
Pr	Number of Prandtl, (ρ_f/α_f)
Q	Heat flux dissipated in the chip, (W)
q	Power density dissipated, (W/m ²)
q_v	Volumetric heat (W /m ³)
Re	Reynolds number, $Re = \rho w D_h/\mu$
R_\emptyset	The absolute sum of the residuals
Ra	Rayleigh number
S_ϕ	Source term
T	Temperature, (K)
T_0	The temperature at the entrance of the channel, (K)
T_m	Mass-average temperature of the coolant, (K)

T_w	Area-weighted temperature of the channel wall surface, (K)
T_{max}	Maximum temperature on the bottom wall, (K)
X, Y, Z	Dimensionless coordinates, (x/L , y/L , z/L)
x, y, z	Cartesian coordinate, (m)
U, V, W	Dimensionless components of velocity, (uL/ α_f , vL/ α_f , wL/ α_f)
u, v, w	Velocity components in three directions x, y and z , (m s ⁻¹)
W_c	Mini /micro channel width, (m)
Greek letters:	
α	Thermal diffusivity, (m ² .s ⁻¹)
φ	Volume fraction of solid, (%)
ϕ	general dependent variable
μ	Dynamic viscosity of coolant, (kg/m.s)
ρ	Coolant density, (kg/m ³)
β	Thermal expansion coefficient, (K ⁻¹)
θ	The dimensionless temperature,
Π	The intrinsic viscosity,
ϑ	Kinematic viscosity, (m ² /s)
v_T	Total volume, (m ³)
v_s	Volume of solid (nanoparticles)
δ	The under-relaxation factor
Γ	The diffusion coefficient
Indices	
av	Average
f	Base fluid (water)
in	Inlet
n	Outer normal coordinate at interface between the wall and fluid
nf	Nanofluid
out	Outlet
s	Solid

List of figures

Figure (I. 1):	(a) Nanofluids-related publication in the past decade (b) Projections of maximum heat flux and power dissipation for microprocessor chips	22
Figure (I.2) :	Schematic of the microfluidic heat sink.	23
Figure (I.3) :	(a) The rectangular ribbed microchannel; (b) the triangular ribbed microchannel; (c) the semicircular ribbed microchannel; and (d) the conventional smooth microchannel.	23
Figure (I.4) :	Cross-flow micro heat exchangers	24
Figure (I.5) :	Diagram of a channel with ribs and grooves	25
Figure (I.6) :	Schematic of (a) microchannel heat sink geometry and (b) cross section of different microchannel with its dimensions	26
Figure (I.7) :	Schematic of straight and with notches microchannels	26
Figure (I.8) :	Characteristic parameters of the ribs and shapes considered.	28
Figure (I.9) :	Geometrical construction of the unit cell of straight microchannel heat sink	29
Figure (I.10) :	Geometrical construction of the unit cell of semi cylindrical projections microchannel heat sink	29
Figure (I.11) :	Diagram of the micro-channels studied.	30
Figure (I.12) :	Model used for simulation with (a) Elliptical fins (b) Circular fins (c) Hexagonal fins (d) Square fins	32
Figure (I.13) :	Schematic of computational domain	34
Figure (I.14) :	Schematic of the various pin-fin layouts on micro-channel	36
Figure (I.15) :	a) Schematic diagram, (b) detailed view, and (c) geometric parameters of the computational domain for fractal minichannel heat sink with hexagonal fins	37
Figure (I.16) :	(a) Mini-channel heat sink (b) Conventional inlet/outlet arrangement with rectangular headers (c) Proposed inlet/outlet arrangement with rectangular headers.	39
Figure (I.17) :	(a) Schematic and (b) Isometric view of computational domain	40
Figure (I.18) :	Schematic of a heat sink used for cooling electronic components	42
Figure (I.19) :	A cross-section of the heat sink and two-dimensional schematic of the problem	43
Figure (I.20) :	Schematic view of micro channel in the heat sink	44
Figure (I.21) :	Geometric model	45
Figure (II.1) :	Molecular structures of Graphite, diamond and a carbon nanotube	48
Figure (II.2) :	Preparation of nanofluid using one-step vapor deposition method	51
Figure (II.3) :	Schematic procedure of the two-step nanofluids preparation	51
Figure (II.4) :	The thermal conductivity of different base fluids and solids materials at 298,15 K	52
Figure (II.5) :	Nanofluid thermophysical properties	53
Figure (II.6) :	Some parameters influencing nanofluids thermal conductivity	59
Figure (II.7) :	Variation of Al ₂ O ₃ -Ethylene Glycol nanofluid thermal conductivity as a function of temperature, for 1% and 3%, with 11 nm diameter and 150 nm diameter particles	60
Figure (II.8) :	Variation of Au-water nanofluid thermal conductivity at room	60

	temperature as a function of nanoparticle size, for a nanoparticle volume concentration of 0.00026%	
Figure (II.9) :	Thermal conductivity ratio via volume fraction in various temperature	61
Figure (II.10) :	Effect of base fluid on thermal conductivity for different nanofluid types	62
Figure (II.11) :	Comparison of thermal conductivity enhancement of SiO ₂ /60EGW and SiO ₂ /40EGW nanofluids	62
Figure (II.12) :	Effect of nanoparticle shape on the thermal conductivity of TiO ₂ -water nanofluid at 2.5%, as a function of temperature	63
Figure (III.1) :	The different cases of the studied mini-channels	69
Figure (III.2) :	Schematic of the mini channels cooler studied and computational domain of mini channel heat sink	73
Figure (III.3):	CAD model of the mini-channels cooler	74
Figure (III.4):	Computational domain of mini-channels cooler	75
Figure (III.5):	Studied cases of the mini-channel coolers: (a) case 4, (b) case 5, (c) case 6, (d) case 7, (e) case 8, (f) case 9	75
Figure (III.6):	Geometrical dimension of the studied cases: (a) case 4, (b) case 5, (c) case 6, (d) case 7, (e) case 8, (f) case 9	75-76
Figure (III.7):	CAD model of the cooler mini channels.	80
Figure (III.8):	Four cases of studied mini-channels.	82
Figure (III.9) :	Studied cases of the micro-channel heat sink	82-83
Figure (III.10):	A cell or control volume in three dimensions	92
Figure (III.11):	(a)staggered mesh for u, (b) staggered mesh for v, (c) staggered mesh for w.	93
Figure (III.12):	Diagram of the mesh used .(case 1 of application N°3)	94
Figure (III.13):	Diagram of the mesh used .(case 4 of application N°5)	94
Figure (III.14):	Diagram of the mesh used .(case 2 of application N°6)	94
Figure (III.15):	The SIMPLE algorithm	100
Figure (III.16):	Calculation organogram	101
Figure (III.17):	Structured and unstructured meshes (3D).	102
Figure (III.18):	Hybrid mesh (a) in 3D (b) in 2D	103
Figure (III.19):	Definition of skewness based on (a) equilateral volume (b) angular deviation	104
Figure (III.20):	Refinement of the mesh in regions of strong gradient	105
Figure (III.21):	Evolution of the size of the elements.	105
Figure (III.22) :	Mesh convergence test.	106
Figure (III.23) :	Choice of reference pressure	107
Figure (III.24) :	Choice of convergence criteria (residuals)	108
Figure (IV.1):	Influence of the mesh on the temperature of the upper surface of the mini channel cooler of the 2nd case	110
Figure (IV.2):	The temperature according to the power dissipated in the chip	110
Figure (IV.3):	The value of the maximum temperature of the junction of the electronic component obtained by simulations for a volume concentration of Cu- water nano-fluid of 0.05	111
Figure (IV.4):	The average heat transfer coefficients as a function of the Reynolds number for a volume fraction of 0.05	111
Figure (IV.5) :	Grid independence examination	113

Figure (IV.6):	The variation of the temperature of the electronic component according to the number of Reynolds	113
Figure (IV.7):	The distribution of the temperature in outlet of mini channel for diamond -water	114
Figure (IV.8):	The average heat transfer coefficient calculated as a function of the Reynolds number at volume fraction =0.05	114
Figure (IV.9):	Influence of the mesh on the temperature of the upper surface of the cooler	116
Figure (IV.10):	Variation of the temperature for different values of power	116
Figure (IV.11):	Evolution of the temperature according to the power dissipated in the chip (Q is the power dissipated in the chip)	117
Figure (IV.12):	The temperature of the upper surface of cooler in 6 cases for Re= 500, the power is 130W. The inlet temperature is equal to 298.15 K and for Cu- water nanofluid	118
Figure (IV.13):	Variation of the maximum temperature obtained from the IGBT chip for a volume concentration equal to 0.02 for various types of nanofluids: (a) Diamond-water, (b) Cu-water, (c) Ag-water, and different cases: (d) case 5, (e) case 4,	119
Figure (IV.14):	Distribution of the temperature in the surface of the chip IGBT and in the surfaces of the mini channels of the cooler for Re=500 and for cu-water nanofluid (volume fraction $\phi=0.02$): (a) case 4, (b) case 5, (c) case 6, (d) case 7, (e) case 8, (f) case 9.	120
Figure (IV.15):	Average heat transfer coefficient for a volume concentration equal 0.02 for various types of nanofluids: (a),(b),(c) and different cases:(d),(e).	121
Figure (IV.16):	(a) Illustrates the variation of the average heat transfer coefficient as a function of the range of volume concentration varying from 0.01 to 0.04; (b) Average heat transfer coefficient Vs the nanoparticle diameter	122
Figure (IV.17):	Variation in the surface temperature for different values of mass flow	123
Figure (IV.18):	Comparison of the surface temperature within three cases.	124
Figure (IV.19):	Profiles of the temperatures of the three nano-fluids and the two cooler metals at Re = 1414 and $\phi= 0,02$.	125
Figure (IV.20):	Variation of the maximum temperature vs. the volume fraction	126
Figure (IV.21):	Variation of the average heat transfer coefficient vs. the volume fraction.	126
Figure (IV.22):	Variation of the maximum temperature vs. the volume fraction	127
Figure (IV.23):	Distribution of the temperature in the surfaces of the mini-channel for Re = 1414 and three different nano-fluids (volume fraction = 0.06).	128
Figure (IV.24):	Influence of the number of cells on the temperature of the component for the first case (Re = 500 and $\phi= 0.05$).	130
Figure (IV.25):	The variation in the temperature of the electronic component according to the number of Reynolds.	131
Figure (IV.26):	Isotherms at the electronic component and in the middle of the mini channel corresponding to Re =500, volume fraction= 0,05 in four cases.	132
Figure (IV.27):	Velocity contour of Al ₂ O ₃ -water nanofluid flow in mini-channel	133

	corresponding to $Re = 500$, volume fraction = 0,05 in four cases.	
Figure (IV.28):	The values of the component temperature according to Re for four cases.	134
Figure (IV.29):	Meshing of microchannel of case 1	136
Figure (IV.30):	Grid independence examination at $Re = 200$ and the heat flux is 100 W/cm^2	136
Figure (IV.31):	Comparison of numerical results of Nusselt number vs Re with resultants of ref [139] for the smooth micro channel	137
Figure (IV.32):	Comparisons of temperature profiles on the heated bottom wall for all cases at $Re= 600$ and the heat flux is 100W/cm^2	138
Figure (IV.33):	The two-dimensional of the temperature distribution on the bottom wall in four cases (a: case 14, b: case 15, c: case 16 and d: case 17), at $Re=600$ and $\phi=0.05$, the unit of temperature is Kelvin	138
Figure (IV.34):	The maximum temperature on the heated bottom wall with the inlet Reynolds number ranging from 200 to 600 for all cases.	139
Figure (IV.35):	Evolution of the maximum temperature on the bottom wall in function with Re and with the geometric parameter in three cases	139 140
Figure (IV.36):	Evolution of the Nusselt number in function with the number of Reynolds and with the geometric parameter.	141
Figure (IV.37):	Static temperature contours for plane $y = 0.25 \text{ mm}$ along the length of the microchannel for different cases at Reynolds number of 600 and volume fraction equal 0.05	142
Figure (IV.38):	Thermal resistance of micro channel heat sinks with the inlet Reynolds number in four cases.	143
Figure (IV.39):	The variation between pressure drop and inlet Reynolds number in all cases	143
Figure (IV.40):	Average heat transfer coefficient of micro channel heat sinks with the Reynolds number in four cases	144
Figure (IV.41):	Variation of Nusselt number with Reynolds number in all cases	145
Figure (IV.42):	Average friction factor of all cases with Reynolds number for $q=100 \text{ W/cm}^2$	145

Liste of table

Table (II.1) :	Results concerning the improvement of the thermal conductivity of nanofluids	50
Table (II.2) :	Abstract of presented correlations for the thermal conductivity of nanofluids	57
Table (III.1) :	Thermo-physical properties of the water and nanoparticles used in each application	67
Table (III.2) :	Hydrodynamic and thermal boundary conditions in the form dimensionless	72
Table (III.3) :	Dimension of the studied cases in this application.	76
Table (III.4) :	Hydrodynamic and thermal boundary conditions	78
Table (III.5) :	Dimensions of unit cell of cooler mini channels.	81
Table (III.6) :	The dimensions of mini channel and obstacles studied in this application	83
Table (III.7):	Geometrical dimension of the studied cases	87
Table (III.8):	Different terms of the transport equation. (Application N°1 and N°2)	96
Table (III.9):	Different terms of the transport equation. (Application N°3 and N°4)	96
Table (III.10):	Different terms of the transport equation. (Application N°5)	97
Table (III.11):	Different terms of the transport equation. (Application N°6)	97
Table (III.12):	Default values of under-relaxation factors	98

General introduction

Heat transfer is a process of great importance in several areas, including technology and industry. Although it manifests itself in various forms (radiation, conduction and convection), the latter is the most targeted in most fields of industry. Convection can be natural, forced or mixed.

This transfer mode concerns fluids (liquids and gases). The movement of the fluid can result from variations in density of this same fluid due to the temperature differences induced by the transfer of heat between the fluid and the wall. If the movement of the fluid is caused by the action of external forces (pumps, fans), it will be forced convection.

The convection heat transfer can be improved in a specific engineering by several methods, including adjusting the geometry, adding the fins, using the surface roughness as well as changing the physical properties of a liquid used in the cooling process. In recent years, nano-fluids have attracted a lot of attention because of their use for cooling in various industrial applications, such as cooling of electronic components, cooling of vehicles, cooling of transformers, in applications of nuclear reactors, solar applications etc...

Nano-fluids consist of solid nano-particles suspended in a basic liquid (such as: water - oil...) and are also called colloidal solutions, a promising new technology in the context of heat transfer, especially in the field of cooling electronic devices, which is known to develop continuously, this led to reducing its size and increased operating rate has led to problems with its high temperature. To ameliorate this temperature, it is necessary to ameliorate the heat transfer and find appropriate ways to cool the electronic components. The latter is our goal in this study.

Objective of study

The aim of this doctoral thesis is to model and to study the heat exchange of the channels in order to better cool the electronic components using nano-fluids.

In our study, our effort focused on clarifying the effect of the parameters; such as the solid volume fraction, type of nano-particles and the geometry of mini-channel, on the cooling of electronic chips. The study assessed the importance of adding solid particles to the pure fluid in improving the cooling efficiency of hot surfaces as well as the effect of the shapes of channels and the nature of the coolant (nano-fluid), on the junction temperature of the electronic components.

We also studied the numerical modeling of heat transfer in microchannels and mini channels by adding obstacles and ribs using nano-fluid. The objective of this section is to find the optimal position of obstacle placement inside the channels as well as to find a suitable shape for the fins using nano-fluid in order to save the temperature of the electronic chips and in order to improve the heat exchange between the coolant (nano-fluid) and the walls of the channels.

Organization of the thesis

The thesis reporting the work accomplished within the framework of this Doctorate in Sciences consists of 4 chapters and a general conclusion.

The first chapter contains the results of bibliographic research on improving heat transfer in mini channels and microchannels using nanofluids

The second chapter presents reminders on the thermophysical properties of nano-fluids.

The third chapter contains the mathematical modeling of heat transfer. There is a presentation of the equations of fluid flows accompanied by thermal transfer (the continuity equation, momentum equation, energy conservation equation and the equation of the solid) as well as the hypotheses associated with this model. In this chapter, we present the numerical method chosen for the simulation (Finite volume method). At the end of the chapter, we briefly describe the ANSYS WORKBENCHE FLUENT trade codes used in the calculations of the numerical simulation.

The fourth chapter contains the results of a study divided into six parts (applications), the first part in which we studied numerically the thermal transfer in different geometries of the mini-channels, as for the second part, we studied numerically the influence of nano-fluids on thermal exchange in mini-channels.

The mathematical model, the numerical method, the geometry for this study are given in chapter III (In section III.4.3 and section III.4.4). In section IV.1.2 of part one and section IV.2.2 of the second part, we present the results of the mesh independence tests. Section IV.1.3 and section IV.2.3 contain the results in graphical form and their discussion. The first and second parts are ends with a conclusion bringing together the various observations.

The third part of this chapter contains the results of a numerical study of the thermal exchanges in different geometry sections of mini-channels of a cooler for cooling a chip using nano-fluids. In section IV.3.2 and IV.3.3 of this part of this chapter, we present the results of the mesh independence tests and the validation of the results. Section IV.3.4 contains the results in graphical form and their discussion. The fourth part is closed with a conclusion (section IV.3.4.5). As for the fourth part, we studied the influence of types of nano-particles, nano-

particles volume concentration, and types of cooler metals on the heat transfer in a mini-channels cooler.

The fifth part of this chapter presents the results of a numerical study in three dimensions of the influence of the fluids' nature and obstacle position on cooling of electronic component. This part is closed with a conclusion.

The sixth part (application) of this chapter presents the results of a numerical study of the effect of the addition of the pie shape ribs and Parallelogram ribs in micro-channels on thermal performance using Diamond - water nanofluid. The results of this chapter have been validated and mesh independence tested. This part ends with a conclusion.

Finally, the thesis is closed with the general conclusions drawn from the cases studied and the perspectives for the rest of the work.

Bibliographic review

In the last part of the twentieth century, interest in the field of nanofluids by researchers appeared and this is evident from the increase in the number of studies related to nanofluids that are published annually (Figure (I.1.a)) [1] nanofluid have good physical properties which is a mixture of metallic nanoparticles and between a basic liquid such as water or oil. These nanoparticles can be in different shapes, as a circular or cylindrical shape, and the ratio of particles in the basal liquid controls the physical properties of the nanofluid. It has the ability to improve heat exchange despite the fact that there are some disadvantages. It is used in several fields especially the one related to refrigeration high-power electronic components (such as processors, transistors, integrated circuits... etc) that emit high heat during operation [2]. This high temperature makes the electronic components not work properly and may be damaged by overheating especially with the increased energy dissipation of the electronic components. It is expected that the maximum power dissipation and heat flux from the high performance microprocessor chips was projected to reach about 360 W and 190 W/cm², respectively by the year 2020 (Figure (I.1.b)) [3].

Therefore, the heat generated must be removed by designing a suitable thermal management system for reliable operation of the electronic device using the nanofluids. Besides, the design of a thermal management system can contain micro channels, which are cooling elements that can provide and reduce the temperatures of electronic components due to their performance in dissipating large amounts of heat,

The term micro-channel applies to channels with a hydraulic diameter of 10 to 100 micrometer. Micro-channels consist of a heat sink made of a solid with a high thermal conductivity such as silicon or copper with the micro-channels machined within the solid. A micro-channel heat sink generally contains a large number of parallel micro-channels. The coolant is forced to pass through these channels to remove the heat generated in the hot surface in contact with the heat sink wall.

The improvement of the heat exchange between the cooling liquid and the cooler walls contributes in improving the cooling process of the hot surfaces and the improvement of the heat

exchange is mainly related to the improvement of the physical properties of the cooling fluids, and also it is related to the improvement of the geometrical shape of the cooler, for example, by adding fins and barriers inside the micro channels ... etc. To dissipate heat, where we find many published studies of researchers in the field of improving heat exchange, among them

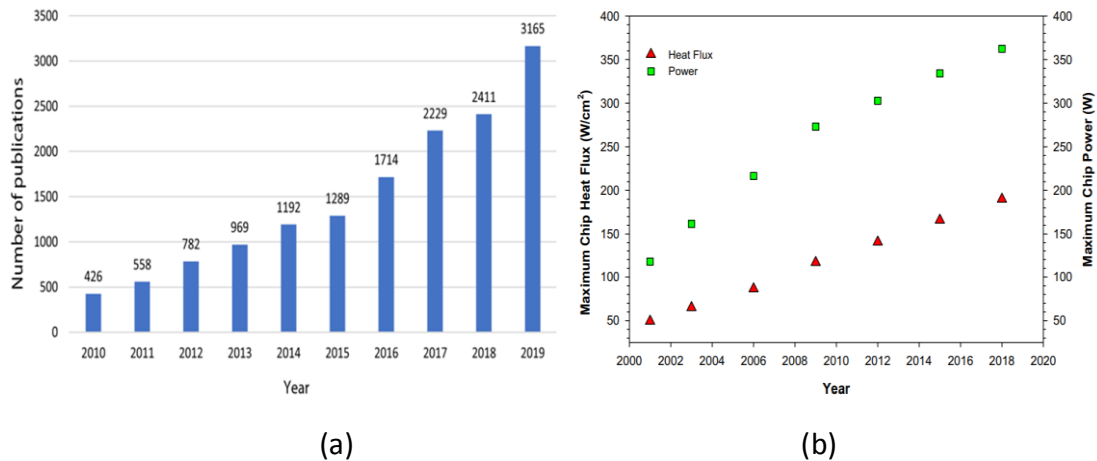


Figure (I.1): (a) Nanofluids-related publication in the past decade [1].
 (b) Projections of maximum heat flux and power dissipation for microprocessor chips [3]

Chavda (2015) [4] studied experimentally the effect of various concentrations (0,003%, 0,002% and 0,004%) of nano-particle (CuO) mixed in base fluid (water) on heat exchange performance of double pipe thermal exchanger for counter and parallel liquid flow arrangement. The results show that the heat transfer coefficient increases with the increases of the volume fraction of CuO nanoparticle.

Esfe et al. (2015) [5] studied the laminar mixed convection of nanofluid in a horizontal channel provided with two sources of thermal at constant temperature mounted on the bottom wall. In this study, they used a Al₂O₃/water nanofluid. They also used the limited volume method to solve the governing equations where they chose three thermal models for the study. Their study showed that the average Nusselt number increases by less than 10% over the obstacles, with the fraction of nanoparticles increasing from 0% to 5%. They found that and the difference between the average number of Nusselt figures and three thermal models does not exceed 3%.

Gui-Fu Ding et al. (2015) [6] investigated experimentally and numerically the heat exchange and friction characteristics with rectangular, triangular and semicircular ribs on the sidewalls of microfluidic channels by a surface-micromachining micro-electro-mechanical system to ameliorate the heat exchange rate of the microfluidic heat sink. They indicated that the using of micro-ribs provides a preferable thermal exchange rate, but also increases the pressure drop

penalty for microchannels. Furthermore, they found that the heat exchange and friction characteristics of the microchannels are strongly influenced by the rib form and the triangular ribbed microchannel possesses the biggest Nusselt number and friction factor between the three rib forms.

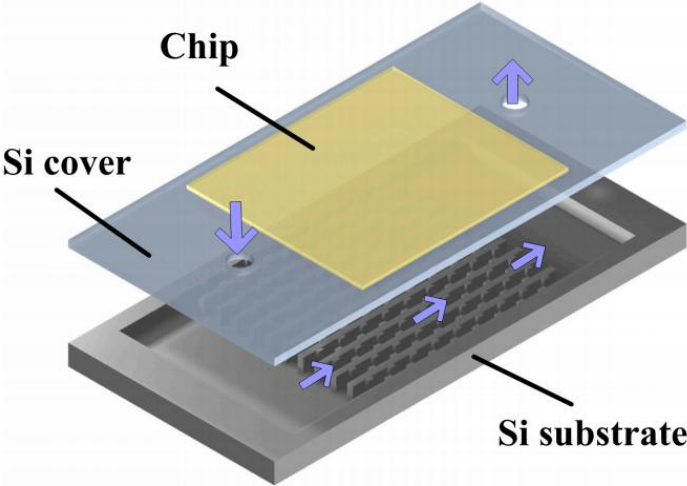


Figure (I.2): Schematic of the microfluidic heat sink. [6]

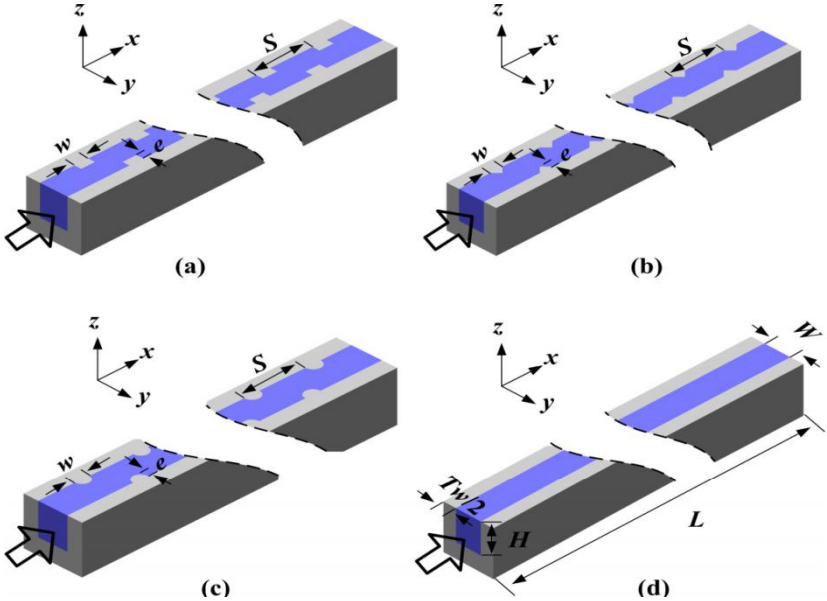


Figure (I.3): (a) The rectangular ribbed microchannel; (b) the triangular ribbed microchannel; (c) the semicircular ribbed microchannel; and (d) the conventional smooth microchannel. [6]

Also, on the other hand, **Nonino et al. (2015)** [7] developed an analytical study of the conjugate conduction/convection heat transfer in cross-liquid micro heat exchangers. It was showed that the increase of the microchannels number per layer yields increases relative pressure drop increments that are larger than those displayed by the relative heat flow rates.

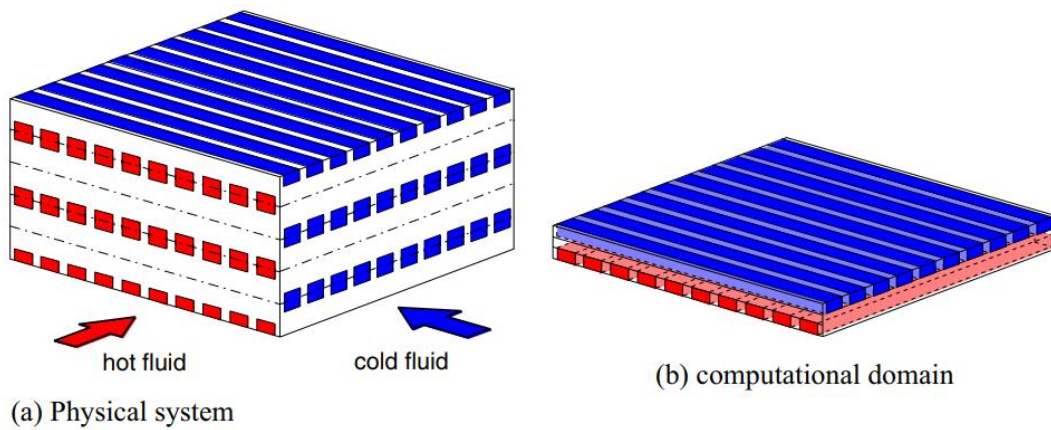


Figure (I.4): Cross-flow micro heat exchangers [7]

Ciloglu et al. (2015) [8] studied experimentally the effect of nanoparticles types (silica SiO_2 , alumina Al_2O_3 , titania TiO_2 and copper oxide CuO) on the quenching process with 0.1% particle of volume concentration. They mentioned that the type of nanoparticle used in nano-fluids substantially influenced the cooling, particularly with SiO_2 nanoparticles.

On the other hand **Navaei et al. [9]** studied numerically the influence of geometric parameters and four types of nanoparticles (Al_2O_3 , CuO , ZnO and SiO_2) on the thermal performance of grooved and ribbed channels with uniform heat flux. The study was carried out for three forms of ribs (rectangular, semi-circular and trapezoidal) with a Reynolds number which varies between 5,000 and 25,000, the volumetric fraction of nanoparticles vary between 1 and 4%, and the diameter of nanoparticles varies between 20 nm and 60 nm. They indicated that the semicircular rib has the highest Nusselt number, in the case of the use of nanofluids by modifying parameters such as the diameter of the nanoparticles.

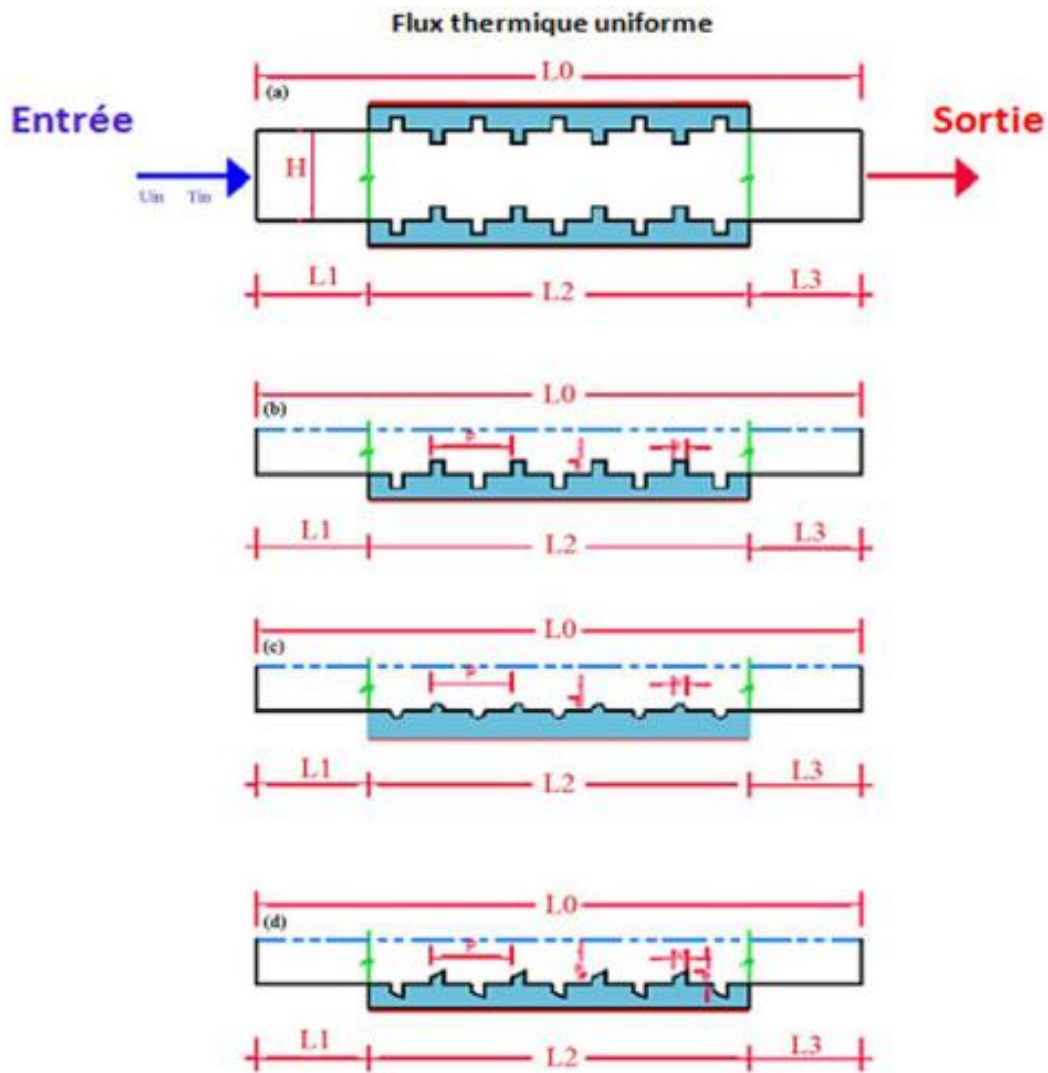


Figure (I.5): Diagram of a channel with ribs and grooves [9].

Hongtao et al. (2016) [10] studied numerically the influence of the geometric parameters on heat exchange performance and flow of the rectangular, trapezoidal and triangular cross-sectional formed microchannel heat sink. The results confirmed that the shape and geometric parameters of microchannel have a remarkable impact on the flow and heat transfer characteristics of the microchannel heat sink. For the rectangular microchannel, it has the best performance with the aspect ratio among 8.9–11.4. Also the channel number impacts the thermal resistance (The increase of channel number decrease the thermal resistance).

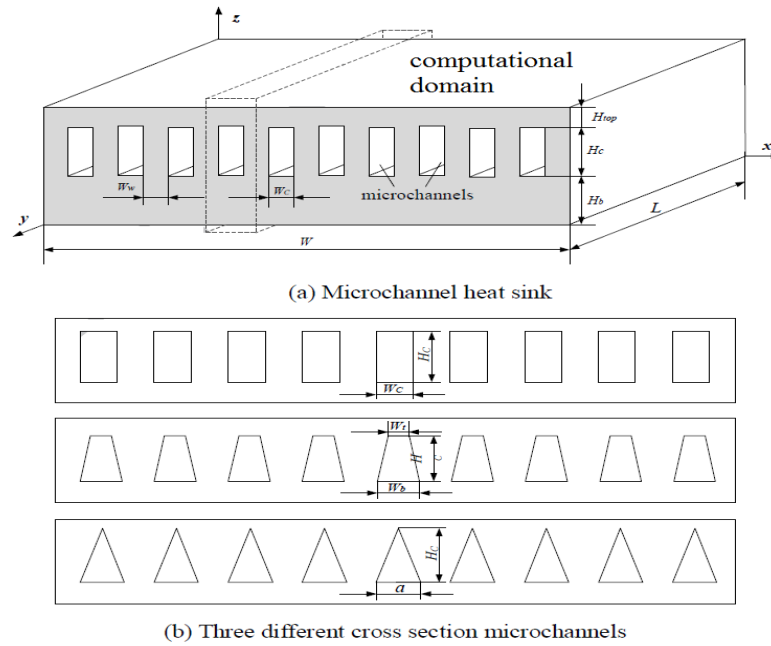
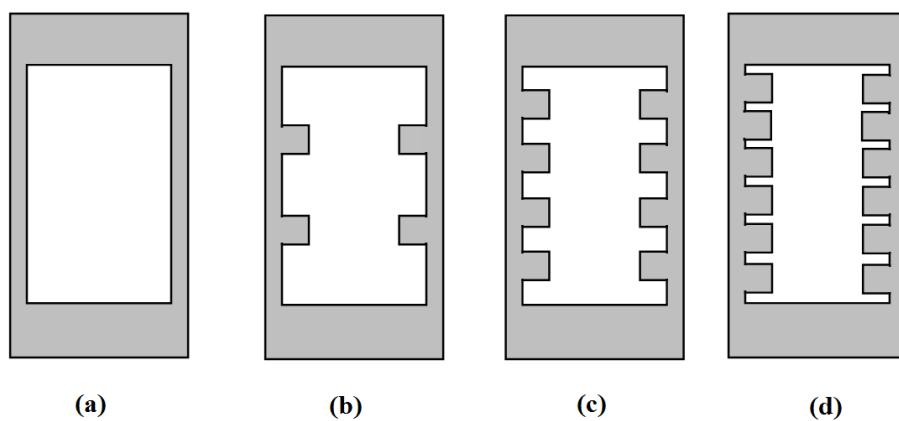


Figure (I.6): Schematic of (a) microchannel heat sink geometry and (b) cross section of different microchannel with its dimensions. [10]

Also, **Abed Ammar et al. (2016) [11]** studied the heat transfer and liquid flow in different forms of micro-channels. They concluded that the Nusselt number and convective heat transfer coefficient increase with the increase of the Reynolds number. They also confirmed that the micro-channels with two notches form present the convective heat transfer coefficient and Nusselt number (Nu) with the highest value, compared to the micro-channels with straight rectangular form and micro-channels with six and four notches form.



- (a) microchannel without notches
- (b) Microchannel with two Notches
- (c) Microchannel with four Notches
- (d) Microchannel with six Notches

Figure (I.7): Schematic of straight and with notches microchannels

Lei C. et al. (2016) [12] numerically investigated the characteristics of laminar flow and heat transfer in the MCHS with offset ribs on the sidewalls. The study is carried out for five different shapes of offset ribs that are designed, including rectangular, isosceles triangular, backward triangular, semicircular and forward triangular. Besides, in this study, Reynolds number is between 190 and 838. The results presented in this article show that the offset ribs result in significant heat transfer enhancement and rise pressure drop. This higher pressure drop, the microchannel heat sink with offset ribs progressively loses its advantage as an effective thermal exchange enhancement method at rise Reynolds number values.

Also, **Sharma et al. (2016) [13]** have experimentally studied the fluid flow and heat transfer with micro-channels. The material used for MCHS is copper and utilizing water as a cooling agent. They studied the evolution of heat transfer rates, the impact of friction factor, and the impact of pressure drop and evolution in temperature distribution. They concluded that the mass flow rate and the friction factor are reduced by a decrease in velocity of flowing fluid. Decreasing pressure increases with increased fluid velocity and heat removal rate. The heat transfer rate increases with MCHS, with an increase in the flow rate of the mass.

In this context **Togun (2016) [14]** investigated numerically the CuO-H₂O nano-fluid and heat transfer in the four configurations of backward facing step with and without obstacle. The Reynolds number (Re) in this study varied from 75 to 225 with volume fraction on CuO nanoparticles varied from 1 to 4 % at constant heat flux. I also use the finite volume method in two dimensions, where I tried four different configurations (without obstacle, with obstacle of 1.5 mm, with obstacle of 3 mm, with obstacle of 4.5 mm) to improve thermal performance. He observed that there is an increase of the vortex zone along with an increase in the obstacle height of the wall channel has remarkable effect on thermal performance.

Chemloul and Belmiloud (2016) [15] studied the influence of the nature of the nanofluid, the variation of the Rayleigh number and the volume concentration of the nanoparticles (TiO₂, Cu and Al₂O₃) on the convective heat transfer performance in a square cavity whose lower horizontal wall and right vertical wall are heated to a constant temperature. They used in this study volumetric fraction of the nanoparticles between 0-0,15. And the Rayleigh number is between 10³ and 10⁶, and the Prandtl number at Pr=6.2. They concluded that the thermal exchange increases with the Rayleigh number and the volume concentration. Also, they confirmed that improvement of the heat exchange is achieved by using Cu nanoparticles.

Andreozzi et al. [16] studied numerically the turbulent forced convection of a nanofluid ($\text{Al}_2\text{O}_3 / \text{H}_2\text{O}$) in a two-dimensional channel heated outside for different shapes of ribs (triangular, rectangular and trapezoidal). In this study, they used the finite volume method which is used to solve the equations of the model. They chose the volumetric concentration of nanoparticles that is varied between 0% and 4% and Reynolds number between 20,000 and 60,000. They noticed that the triangular ribs have higher thermal performance than the trapezoids and also the presence of nanoparticles increases the mean Nusselt number compared to the pure base fluid, and that the average Nusselt number increases by increasing the Reynolds number. They concluded that the mean Nusselt values for the triangular ribs are higher than for the trapezoidal ribs.

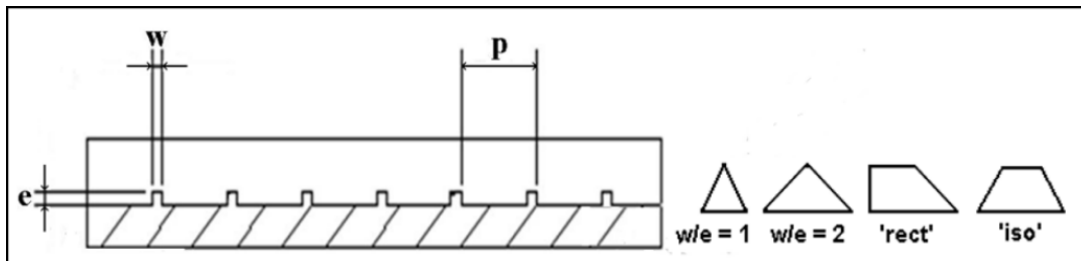
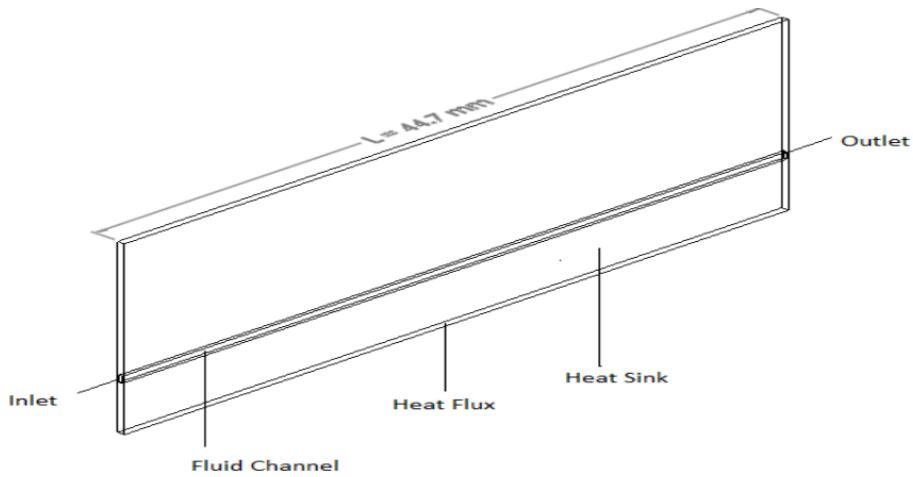


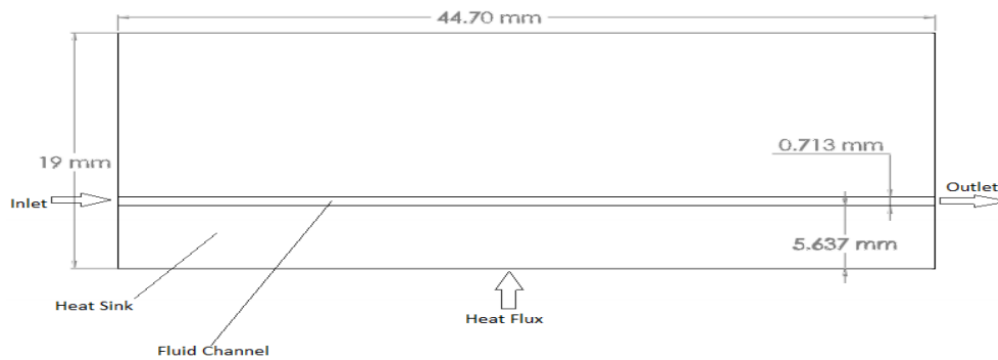
Figure (I.8): Characteristic parameters of the ribs and shapes considered.

Kumar et al. (2016) [17] conducted a comprehensive review of the physical-thermodynamic properties of nanofluids such as the convective heat transfer coefficient for laminar and turbulent region, thermal conductivity, viscosity and specific heat capacity as they also talked about how to prepare and maintain nanofluid stability.

Zunaid et al. (2017) [18] have numerically investigated the heat exchange and pressure drop characteristics of semi cylindrical and a straight rectangular projections microchannel heat sink made of copper. In this study they used water as a coolant for Reynolds number ranging between 200 to 1000 with constant heat flow of $10^6 \text{ W} / \text{m}^2$, They compared the pressure drop and heat transfer between rectangular and semi cylindrical projections microchannel. The results show that thermal exchange raises with the use of semi cylindrical projections micro channel heat sink.



(a) Isometric view



(b) Front view

Figure (I.9): Geometrical construction of the unit cell of straight microchannel heat sink. [18]

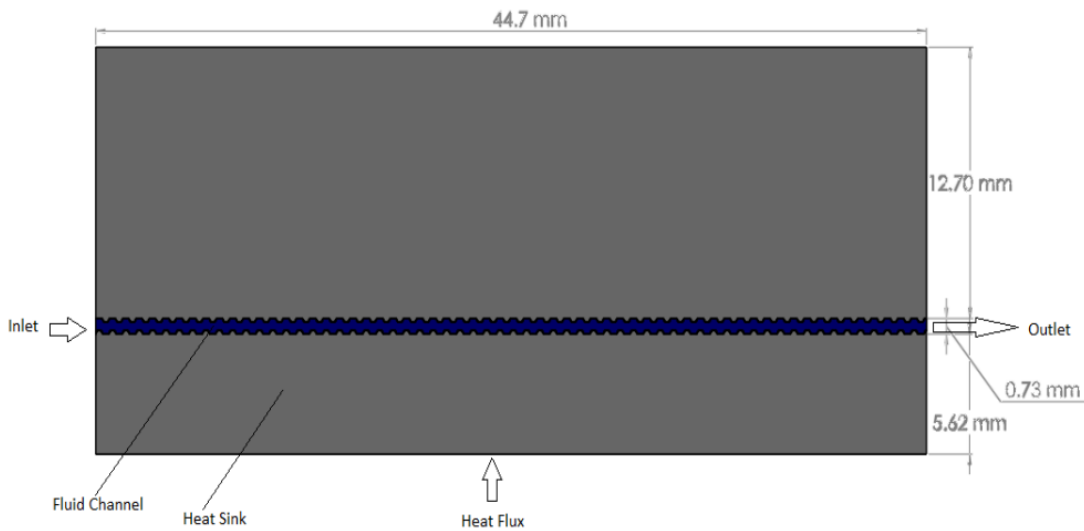


Figure (I.10): Geometrical construction of the unit cell of semi cylindrical projections microchannel heat sink. [18]

Behnampour et al. (2017) [19] studied numerically the effect of rectangular, triangular and trapezoidal ribs on the laminar heat transfer in a channel under a constant heat flux. In this study

they used water-Ag nanofluid as a coolant and also chose the Reynolds number of 1, 5 and 100 (laminar flow) and volume fractions of nanoparticles Ag of 0, 2% and 4%. The results indicate that the triangular shape has the best criteria for evaluating thermal performance to the laminar flow and for high Reynolds numbers, trapezoidal ribs are recommended.

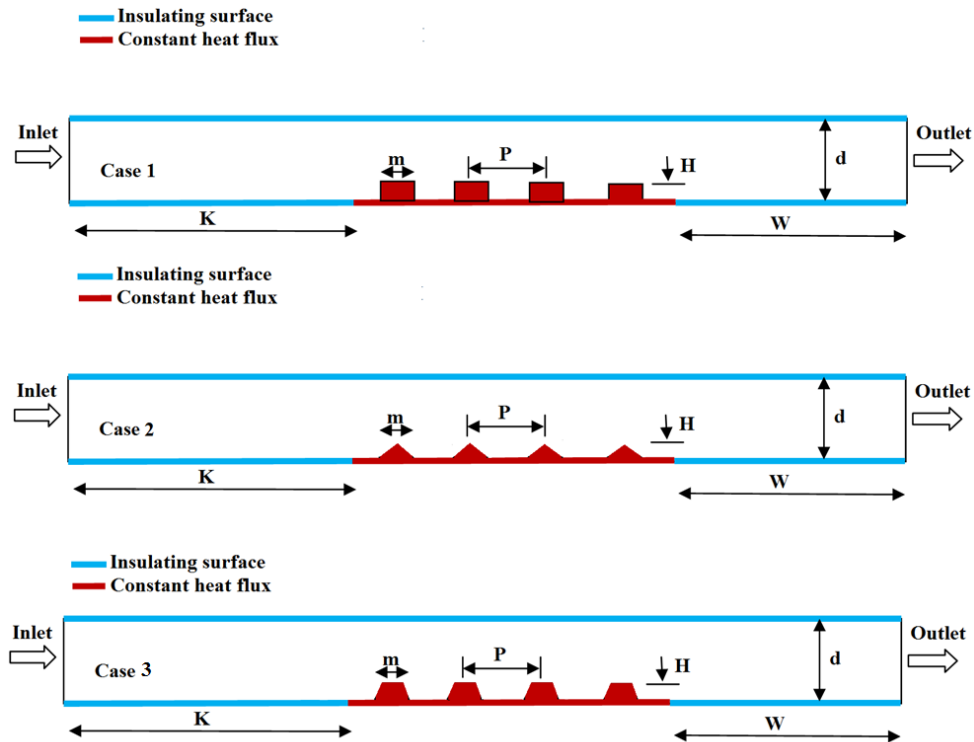


Figure (I.11): Diagram of the micro-channels studied.

Abd Elazem et al. (2017) [20] studied the effect of partial slip boundary condition on the mass transfer and heat of the Ag-water and Cu-water nanofluids over a stretching sheet in the presence of radiation and magnetic field.

TiO₂-water nanofluid was used by **Qi et al. (2017) [21]** with different volume fractions to investigate the stabilities of the natural convective heat transfer characteristics and thermo physical properties. They proved that the heat transfer can be enhanced by 34.2% with the increase of the mass concentration of nanoparticle at the largest cavity ratio and the lowest heating power. They also indicated that the thermal conductivities of TiO₂-H₂O nanofluids can be improved by 5.23%.

Mohebbi (2017) [22] studied the effect of location of a heat source on natural convection in a C-formed enclosure. They used water-Al₂O₃ nanofluid with different solid volume fractions (0-

0.05) and with different Rayleigh numbers (10^3 - 10^6). According to the results, they found that the biggest value of Nusselt number is achieved when the heat source is located within the horizontal cavity, they also found that the heat source locations inside the vertical cavity give the best offspring numbers at higher Rayleigh number. On the other hand **Ghasemi et al. (2017) [23]** numerically investigated the effect of using nanofluids on heat transfer and fluid flow characteristics in triangular shaped minichannel heat sink. In this study they used alumina-water (Al_2O_3 - H_2O) nanofluid as a coolant with different volume fractions. They concluded that the use of nanofluid as a coolant leads to enhanced heat transfer performance by increasing the volume fraction of nanoparticles, also concluded that the heat transfer coefficient and friction factor are increased, the thermal resistance of the heat sink decreases.

Colangelo et al. (2017) [24] analyzed the application of a new generation of heat transfer fluids and nanofluids, to electronic devices. They mentioned that the heat performance of the heat sink in general is not only depended on the properties of nanofluids, but also depended on engineering design.

They also mentioned that the most used nanoparticles are Al_2O_3 , due to their good thermo physical properties and also their cheap price on the market. They also spoke about a The blockage problem that can be a big problem, especially for high concentration (> 1.0% volume) for nanofluids, this should be taken into account with the narrow volume of micro channels in the heat sinks and review the thermal design of cooling systems for electronic equipment according to the nature and concentration of nanofluids.

Mangalkar et al. (2017) [25] presented a review in heat transfer enhancement using nanofluid for cooling of electronic components. One of their most important conclusions is that the heat transfer rate improves with the high thermal conductivity of nanoparticles as well as with the small diameter of nanoparticles and their increased concentration in the base liquid.

Sohel Murshed et al (2017) [3] reviewed and analyzed heat transfer properties and the performance of potential new refrigerants such as nanofluids with superior thermal properties in meeting the cooling requirements of high temperature electronic devices. They also talked about the technology of cooling electronic devices using micro- channels and nanofluids.

Munish et al. (2017) [26] summarized the important results regarding the improvement in the physical and thermodynamic properties of nanofluids and the effect of particles (loading,

material, size, and shape), base fluid type, temperature, and pH value on thermophysical properties of nanofluids.

Also on the other hand, **Sharad D. Patil and Sagar C. Wangdare (2018) [27]** studied heat transfer enhancement in plain MCHS six different types of offset ribs are added on sidewall such as rectangular, backward triangular, forward triangular, mix of forward isosceles and semicircular in forms at Reynolds number (Re) between 200 and 800. They find that mix of forward and backward offset ribs MCHS gives better results as compared to other types of channel. Also they found that with the increase in Re the Nu increases and friction factor decreases for selected MCHS.

Jadhav et al. (2018) [28] performed a numerical investigation of the effect of different pin fin shapes (ellipse, circle, square and hexagon) on micro channel. They concluded that for fin pins at larger height and at high flow coolant inlet velocities, the values of Nusselt number increases. They found that the square pin fins are the best among the studied pin fin shapes in terms of thermal performance.

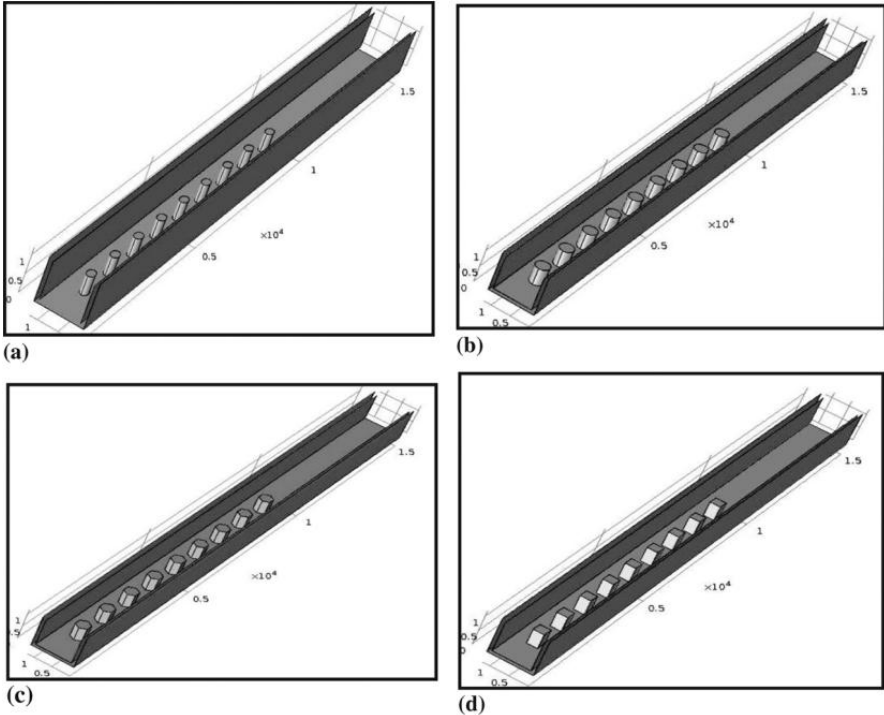


Figure (I.12): Model used for simulation with (a) Elliptical fins (b) Circular fins (c) Hexagonal fins (d) Square fins

Sohel Murshed et al. (2018) [29] studied the convection cooling for nanoparticle loaded liquids in micro channel systems. They also analyzed the research findings on the direct application of these new liquids (nanofluids) to electronic devices' cooling systems. Among their findings that the nanofluids possess a much higher thermal conductivity compared to conventional basic fluids and contribute to a better cooling of modern electronic devices. They also demonstrated the performance of convection heat exchange of nanofluids in micro and mini channels that they can be used in miniature devices such as modern electronics to improve cooling.

Mjallal et al. (2018) [30] simulated the distribution of heat on the heat sink using the Ansys fluent to study the effect of incorporating phase change materials into the heat sink in order to improve cooling electronic chips.

Saeed et al. (2018) [31] reviewed some studies conducted on the use of nanofluids in the cooling of electronics taking into account several aspects such as the type of liquid mass, the numerical approach, energy consumption, nanoparticles materials, and the second law of thermodynamics. They introduced some aspects of the use of nanofluids to cool electronic components as new coolants in various liquid blocks and heat pipes.

Also, **Rezazadeh et al. (2018) [32]** studied the effect of attack angles, height and Reynolds number and also the rib's arrangement on the performance of mini channel. They concluded that a raise for heat exchange ameliorates with the increase of rib's height and the Reynolds number, as well the arrangements with the attack angles of 60° have a better heat exchange performance. They also concluded that mini channels with both trapezoidal and rectangular ribs have best results for thermal exchange and fluid performance in comparison to a mini channel with rectangular ribs only.

A numerical research **(2018) [33]** studied numerically by using the commercial CFD package of ADINA R&D, Inc. 9.1. The heat transfer characteristics of the laminar flow inside a rectangular 2D microchannel of height H , which includes a slim micro obstacle of height h and width w placed on the lower wall of the channel. In this study they used two different types of slender barriers (triangle and rectangular) and three different values of height h for Reynolds number (Re) between 20 and 200.

They obtained that the increase of Reynolds number (Re) values raise the length of vortex zone, particularly behind the rectangular obstacle.

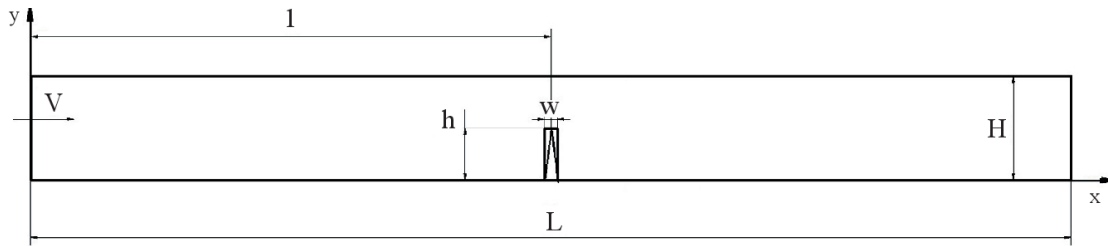


Figure (I.13): Schematic of computational domain

Abdollahi et al. (2018) [34] examined the thermal and hydraulic properties of laminar nanofluid flow in the square micro-channel contains four rectangular fins installed on the inner walls. Using four different types of nanoparticles (SiO_2 , Al_2O_3 , CuO and ZnO) dispersed in pure water base liquid with different volume parts ranging from 1 to 2% and different nanoparticle diameters from 30 to 60 nm. The outer walls of the micro channel are heated at a continuous thermal flow. Their results showed that there is an increase in the number of Nusselt (Nu) when the size of the solid nanoparticles increase, and while reducing the diameter of the nanoparticles, the friction factor remains constant does not change. Also, among the results they found that the SiO_2 nanoparticle has the highest rate of heat transfer from among the tested nanofluids and also that nanoparticles can enhance the performance of the channel with rectangular fins.

Also, **Kangude et al. (2018) [35]** studied experimentally the effect of nanoparticles on a single bubble-based nucleate pool boiling. They used water-silica nanofluids with different concentrations of nanoparticles (0,005% and 0,01%). Among the experimental results, they found out that the nanoparticles suspended tend to spread the strength of temperature gradients. **Fernando et al. (2018) [36]** proposed two computational fluid dynamics models for a rotor-stator cavity operating at $\text{Re}\omega = 1.0 \times 10^5$ and filled with a fluid that consists of different volume fractions of Al_2O_3 nanoparticles. The first model: the nanofluid mixture using a single phase transport and the second model using a two phase transport for the relative velocity between the particle and fluid phases. They used the finite volume method of solving governom equations alongside the OpenFOAM tool they found that the higher volume concentrations of Al_2O_3 nanoparticles can achieve higher heat transfer rates.

Belahmadi et al (2018) [37] studied numerically by using ANSYS Fluent software and a simple algorithm the entropy generation and the heat exchange of a $\text{Cu-H}_2\text{O}$ nano-fluid in a vertical channel. Their results proved that the increase of Reynolds numbers (Re) and Grashof and volume fraction of nanoparticles decreases the entropy generation and improves the heat exchange.

Saeed and Kim (2018) [38] investigated numerically and experimentally the heat transfer enhancement characteristics using four different channel configurations of mini-channel heat sink, and with three different volume fractions of nanoparticles Al_2O_3 in base fluid (water). They observed an enhancement of 24,9%, 27,6% and 31,1% in the heat transfer coefficient of the heat sink with fin spacing of 1,5 mm, 1 mm and 0,5 mm respectively. They also observed that enhancement factor increases by decreasing the fin spacing of the flow channel at the same value of volume fraction and rate of coolant flow.

Bakhshi et al. (2018) [39] studied numerically the effect of changes in geometric parameters of a laminar flow through the trapezoidal micro-channels on heat transfer and fluid flow. Also, they studied the heat flux rate with hydraulic diameter changes. They concluded that the minimum and maximum heat exchange rate occurs in a trapezoidal micro-channel with 30° and 75° internal's, respectively.

Naser et al. (2018) [40] made an important summary among of the aspects dealt with concerning the progress made in studying nanofluids as well as the procedures for manufacturing and marketing nanofluids, as well as measures to enhance stability in order to preserve their thermophysical properties.

Wang et al. (2018) [41] studied numerically the heat transfer of miniature loop heat pipe by using water-copper nanofluid with different volume concentrations. It was found that, the temperature differences of miniature loop heat pipe using nanofluid are always lower than those of miniature loop heat pipe using de-ionized water for an input power of 25 W.

Also **Khanlari et al. (2018) [42]** studied experimentally and numerically the heat exchange characteristics in the plate type thermal exchangers (PHE) with small size using TiO_2 /water nanofluid. They used the Flint 16 program in numerical simulation. And to facilitate the experiment, they added Triton X-100 to the mixture to improve the solubility of the nanoparticles TiO_2 . The results showed that the $\text{TiO}_2/\text{H}_2\text{O}$ nanofluid improved the heat transfer coefficient averagely by 6%.

Khan et al. (2018) [43] presented an analytical study of thermal exchange between the nanofluid and the vertical wall using two types of nanoparticles, silver (Ag) and copper (Cu), suspended in water. They used the Laplace transformation method to find the analytic solutions for the temperature and velocity fields. Their results show that thermal exchange decreases with

an increasing solid volume fraction of nanoparticles. They also found that the Hartman number and porosity have opposite impacts on fluid motion.

Rudyak et al. (2018) [44] studied experimental and molecular dynamics for the thermophysical properties of nanofluids (thermal conductivity, viscosity). They noticed that the transfer coefficients for nanofluids depend on the concentration of particle size and on its size and material, also the particle size decreases as the viscosity increases, while the thermal conductivity of the nanofluids increases in parallel with the particle size. They also observed in the laminar flow that the heat transfer coefficient of nanofluids is much more than the basic fluids, and that the use of nanofluids in turbulent conditions depends on the thermal conductivity of nanofluids and their viscosity.

Jadhav et al. (2019) [45] conducted a numerical analysis of the effect of the various pin-fin layouts on micro-channel heat sinks using the conjugate heat transfer module of COMSOL Multiphysics software. They compared the performance of microscopic channels with three different pinworm layouts for different fluid flow speeds, with constant channel dimensions and with elliptical pin fins of 500 μm fin height. They finally concluded that directing the pinworm fin intertwined into the micro-channel improves thermal performance and makes it better.

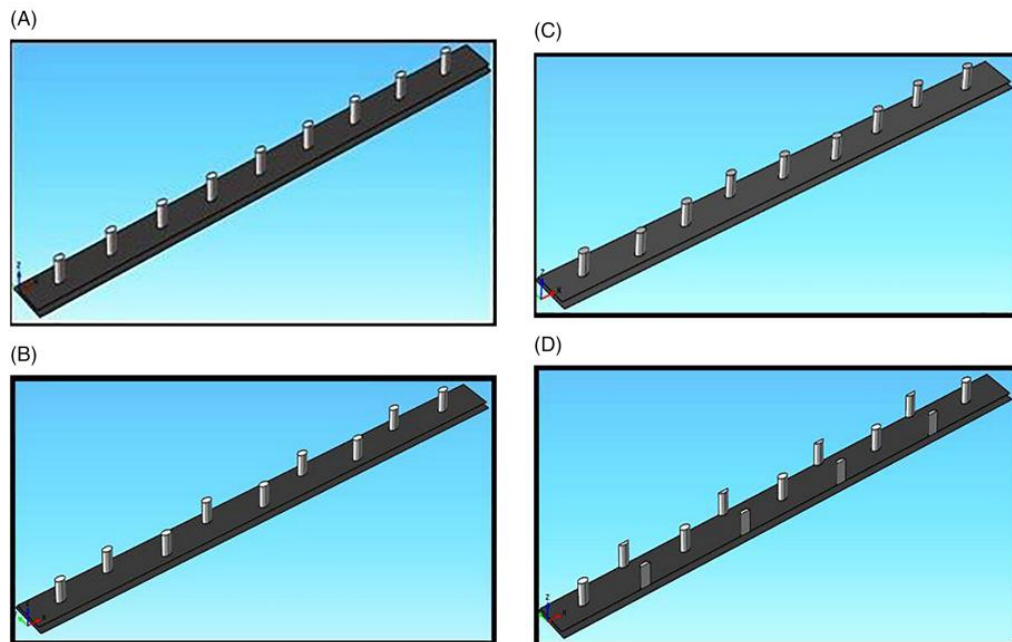


Figure (I.14): Schematic of the various pin-fin layouts on micro-channel. [45]

Yang et al. (2019) [46] numerically investigated for Reynolds number ranged from 50 to 550. The laminar convective heat transfer in fractal minichannels with hexagonal fins. Their results show a reduced temperature and more uniform temperature distribution on the base surface, and

they also noted that the variation of the branching angle possesses little effect on the maximum temperature, and that among the tested formations they studied. They noticed that the best performance was at the angle of the branch of 60 degrees and relative hexagonal side length of 1.50.

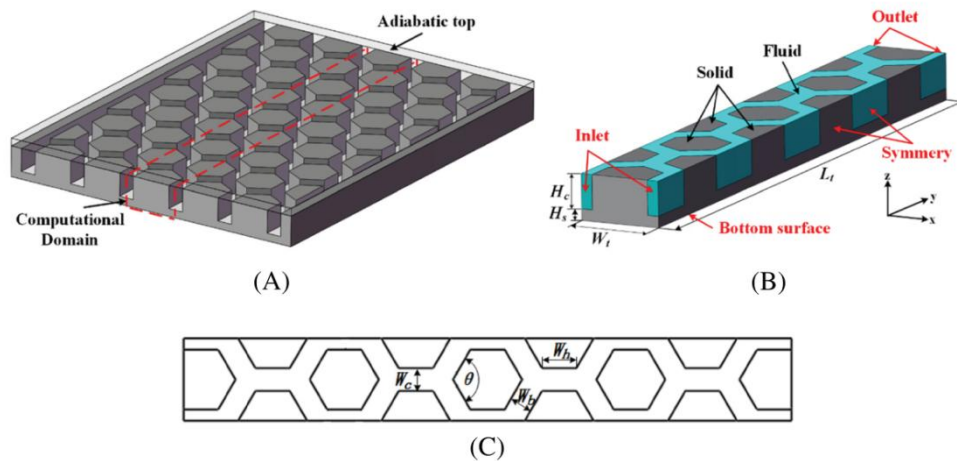


Figure (I.15): (A) Schematic diagram, (B) detailed view, and (C) geometric parameters of the computational domain for fractal minichannel heat sink with hexagonal fins. [46]

Moreover, **Gülbanu et al. (2019)** [47] numerically investigated convective heat transfer of two different nanofluids (Al_2O_3 -water and TiO_2 -water nanofluids) through square cross-sectional duct under constant heat flux ($500 \cdot 10^3 \text{ W/m}^2$) in Reynolds number between $\text{Re}=3,000$ and $100,000$. It was concluded that increasing in Reynolds number and the solid volume fraction increases the Nusselt number and pressure drop. In this context,

Fateh Mebarek et al. (2019) [48] studied numerically the natural convection of Cu-water nanofluid with volume concentration ranging from 0 to 0.1 in a vertical cylindrical annulus enclosure with two heat sources of diverse lengths, while the outer wall is kept at a lower temperature. The upper and lower walls are thermally insulated. They used the finite volume method using the SIMPLER algorithm. They found that the temperature and heat transfer of heaters depend on the length of heaters, the Rayleigh number and the volume fraction of nanoparticles copper.

Ahad et al. (2019) [49] numerically investigated the mixed convection of different nanofluids (Al_2O_3 -water, TiO_2 -water, Cu-water and Silver-water nanofluids) in horizontal annulus. They studied the effect of different parameters such as Richardson, Rayleigh, the volume fraction of nanoparticles and Reynolds number on heat transfer. They indicated that

the thermo-physical properties of nanoparticles has a direct effect in the heat transfer. It is clear from this study that the use of nanoparticles is critical to enhancing heat exchange properties.

Moreover, **Fateh Mebarek (2019) [50]** investigated numerically the hydrodynamic and thermal characteristics of titanium nanofluids of different base fluids in the cylindrical annulus with discrete heat source. In this research, he used three base fluids (water, ethylene glycol and engine oil) and also used the Maxwell model for convective heat transfer in nanofluids and the finite volume coupled method to solve equations (the continuity, momentum, and energy equations) with the SIMPLER algorithm. He pointed out that the base fluid and nanoparticle volume fraction have an impact on the local Nusselt number.

Another study investigated **(2019) [51]** the space effect and thermal dependent heat source on nanofluid flow near an infinite disk which stretches in the radial direction in the presence of thermal based heat source (THS) and exponential space-based heat source (ESHS). They concluded that as the thermal domain increases, the exponential space-based heat source and thermal-based heat source parameters increase.

Mohebbi et al. (2019) [52] investigated numerically to estimate the nanofluid thermogravitational convection within a Γ -formed enclosure that consists of a local heater by the lattice Boltzmann method, they used in this study solid volume fraction (0-0.05), cavity's aspect ratio (0.2 – 0.6) and the Rayleigh number (10^3 – 10^6). Among their results, they found that the average Nusselt number increases in parallel with the nanoparticles concentration and the Rayleigh number increases and also increases when the heater is located on the left border and that when increasing the obstruction height.

Rehena et al. (2019) [53] studied numerically in three-dimensional the effect of nanofluids on heat transfer and cooling system of the photovoltaic thermal (PVT) performance. Among the nanofluids used in this research Ag-water, Cu-water, Al-water. They concluded that photovoltaic thermal system worked by nanofluid is more effective than water-based photovoltaic thermal system. Especially with solid concentration equal to 2 %.

Among recent studies in the field of improved heat transfer, **Kumar and Pawan Kumar Singh (2019) [54]** improved the heat performance of a mini-channel using a new inlet-outlet approach arrangement with different flow inlet angle such as ($\theta = 90^\circ$, $\theta = 105^\circ$, and $\theta = 120^\circ$). Among their observations, inlet-outlet arrangement with inflow angle equal to 105° has the smallest value of maldistribution factor whereas conventional inlet-outlet arrangement has the

biggest value of maldistribution factor. Also, they founded that the maximum heat sink base temperature has been observed in the conventional arrangement. Indeed, the lowest heat sink base temperature has been founded in the proposed arrangement with inflow angle equal to 105° . Also, a temperature drop of 2°C has been observed with the proposed flow arrangement. Then, they concluded that the thermal resistance decreases with the rate of the fluid flow for all arrangements.

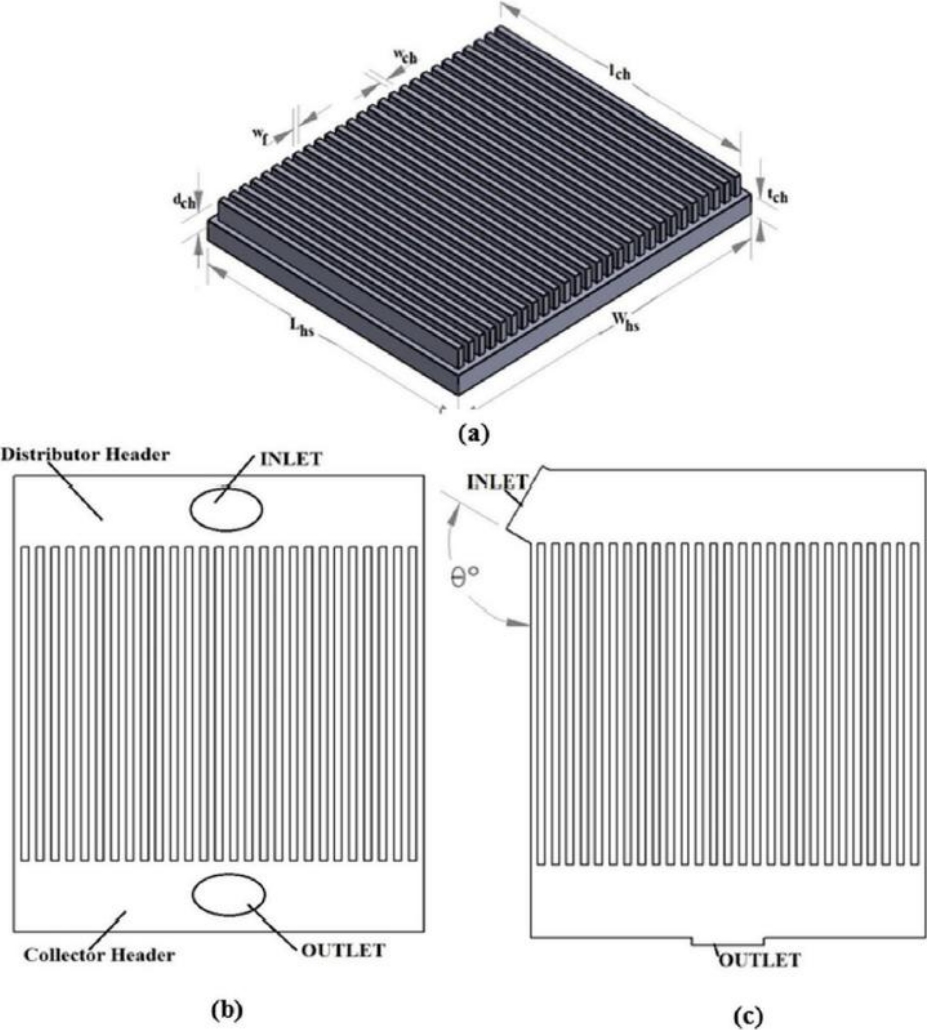


Figure (I.16): (a) Mini-channel heat sink (b) Conventional inlet/outlet arrangement with rectangular headers (c) Proposed inlet/outlet arrangement with rectangular headers. [54]

Bezaatpour and Goharkhah (2019) [55] studied numerically the effect of porous media on the convective heat transfer and pressure loss of magnetite-water nanofluid in rectangular and circular channel heat sinks. They found that, without porous media, the thermal transfer is lower for the circular channel heat sink than the rectangular channel heat sink. While, the thermal transfer from the circular channel overtake that of the rectangular channel in the presence of

porous media. Also, the thermal transfer with respect to the liquid flow in clear heat sinks increases with the volume concentration and decreases with the rate of liquid flow and porosity.

Yogesh K. Prajapati (2019) [56] studied numerically the heat transfer and fluid flow in rectangular parallel microchannel heat sinks, he investigated seven configurations of heat sink depending on the variable height of the fin (0,4 to 1,0 mm) for the Reynolds number range of 100–400 and for heat flux range of 100–500 kW/m², six heat sink configurations hold open space between fin top surfaces and cover wall as for the remaining heat sink, in case of complete closure. He noticed that heat transfer and pressure drop increases with increasing fin height, also found that heat sink of fin height 0,8 mm exhibits maximum heat transfer which is even higher than fin heights of 0,9 mm and 1,0 mm (completely closed heat sink).

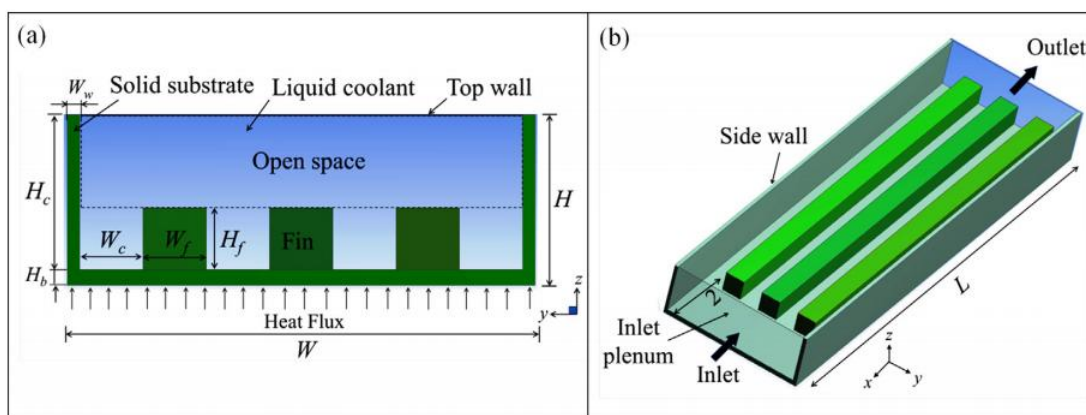


Figure (I.17): (a) Schematic and (b) Isometric view of computational domain. [56]

Deriszadeh et al. (2019) [57] studied in 3D the properties of fluid flow and heat transfer of nanofluids as coolants for the cooling system of electric motors. They used a numerical analysis of the cooling system with spiral channels, and they used computational fluid dynamics and fluid motion analysis to solve the governing equations. The parameters they studied were the Reynolds number and turn-number of spiral channels. They also, studied the effect of the volume fraction of nanoparticles in the water on the heat transfer performance of the cooling system in a laminar flow. Finally, they concluded that increasing the fraction size of the nanoparticles improves the heat transfer performance of the cooling of electric motors system, with a decrease in the pressure drop of the coolant.

Krishna et al. (2019) [58] analysed of a rectangular microchannel heat sink which was done using water, Al₂O₃-water, and TiO₂-water nanofluids. They studied the hydrodynamic and thermal behavior of a microchannel, and also calculated variation wall temperature, pressure

drop in the channel and the heat exchange rate and also studied the impact of Reynolds number (Re) on heat exchange in the microchannel. They found that improvement in the heat transfer with microchannel heat sink due to decrease in convective heat transfer resistance as the size of the thermal boundary layer decreased with microscopic size of the channels. They also concluded that there was no extra pressure drop at low volume concentration of nanoparticles in the base liquid.

Bahiraei et al. (2019) [59] evaluated the thermo-hydraulic attributes of a hybrid nanofluid containing graphene–Ag nanoparticles in a microchannel equipped with the secondary channels and ribs and their results showed that namely using the secondary channels, ribs and nanofluid in the microchannel ameliorate the heat sink performance significantly, especially by increasing either concentration or Reynolds number. Additionally, the average convective heat transfer coefficient enhances with increasing the concentration and Reynolds number, such as the increase of the concentration from 0 to 0.1% at $Re = 100$, a 17% enhancement happens in the convective heat transfer coefficient, also results showed that the bottom surface temperature decreases with increment of the concentration such that a 3.42 K reduction occurs with increasing the volume fraction from 0 to 0.1% at $Re = 100$. While, the flow experiences a greater pumping power at higher Reynolds numbers.

Also, among recent studies in the field of improved heat transfer, we find recent numerical study of **Wang et al. (2020) [60]** who studied the heat transfer and flow characteristics of a microchannel heat sink with truncated ribs on the sidewall for Reynolds number between 100 and 1000. They found that the Truncated rib (TR) can ameliorate the heat transfer by lowering the pressure drop penalty and the increase in the flow area contributes to a decrease in the penalty for the pressure drop.

Moreover, among recent studies in the field of improved heat transfer, we find a recent numerical study of **Laouira et al. (2020) [61]** who studied numerically in two dimensional the heat exchange phenomena inside a horizontal channel with an open trapezoidal enclosure subjected to a heat source of diverse lengths. They used, in this study, the flow which is incompressible, laminar with a constant Reynolds number ($Re=100$) and $Pr=0.71$, they indicated that the distribution of the isotherms depends significantly on the length of the heat source. Also, they found that and the local and the average Nusselt numbers raise as the local heat source length increases.

Magneto magnetic fluid load for Cu-H₂O nanofluids was studied (2020) [62] in a cavity with chambers considered under the influence of a magnetic field, the equations of continuity, motion and energy are solved by applying COMSOL Multiphysics the results show that the effects of volume portion and magnetic force on various irreversibility are important.

On the other hand Huminic et al. (2020) [63] studied entropy generation macrochannel and entropy generation in cavities. In this research, impacts of concentration of nanoparticles, as well as streamwise, electromagnetic, the flow regime and the temperature on entropy generation were studied. They indicated that the application of hybrid nanofluids in microchannels, minichannels, and cavities may be an important alternative to the classic thermal systems.

Furthermore, Alsarraf et al. (2020) [64] numerically studied the impact of radiation of aluminum/water nano-fluid between two blades of a heat sink on natural-convective heat exchange, which is under the impact of a uniform magnetic-field. The space between two blades of the heat sink is considered as a 2D square enclosure. In this square there are four pipes with constant temperature with a circular cross section. Among their results, they found that the enhancement of the angle of the enclosure from 0 to 90 leads to a diminution in the average Nusselt number on the left wall by 22% and As they noticed An enhancement of average Nusselt number on the right wall that is more than that on the left wall, also that the optimal conditions for maximum heat exchange and minimum irreversibility generation correspond to a distance and that as the aspect ratio of constant temperature pipes intensifying, the heat exchange rate and irreversibility generation intensify.

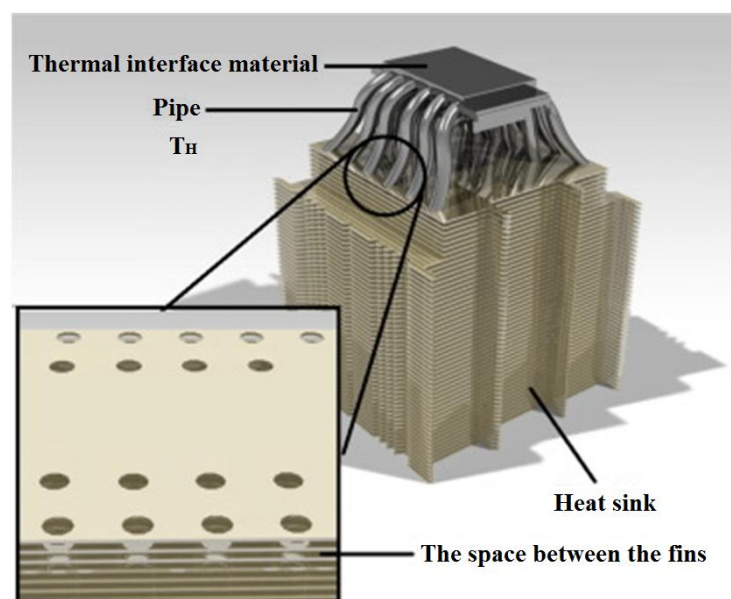


Figure (I.18): Schematic of a heat sink used for cooling electronic components.

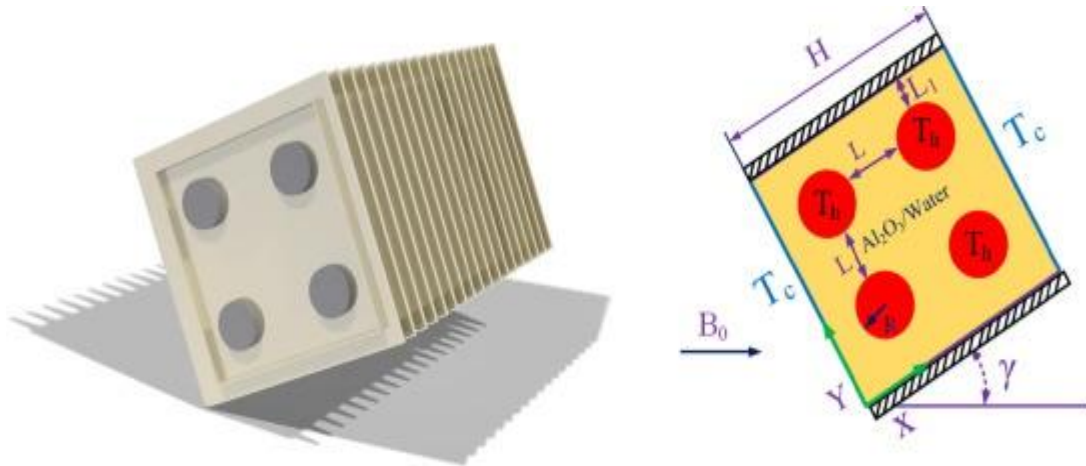
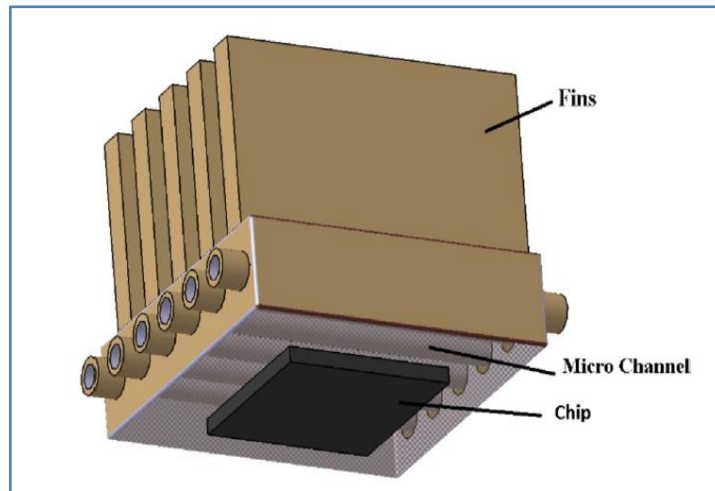


Figure (I.19): A cross-section of the heat sink and two-dimensional schematic of the problem. [64]

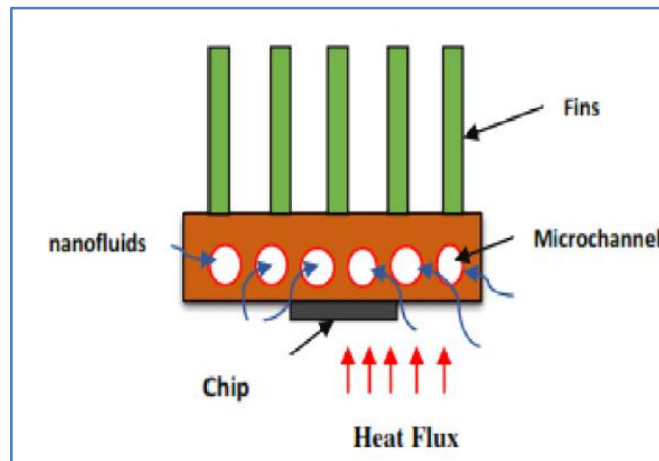
In contrast **Selimefendigil et al. (2020) [65]** studied numerically in 3D the natural convection of CNT-H₂O nanofluid in a cavity with an inner T-shaped adiabatic obstacle where they studied the impact ambient temperature, inclination of the side surface of 3D cavity, the size of the obstacle, inclination of the T-shaped obstacle and volume concentration (between 0 and 4%) on the natural convective heat exchange. They found that the heat transfer increase with CNT-nanoparticle is important and they achieved 128% amelioration in the average Nusselt number in the largest part of the volume of the nanoparticles.

Also among recent studies **Ait Hssain et al. (2020) [66]** studied numerically the cooling of heat sources at constant temperature in a horizontal channel by mixed convection of nanofluids, they found that the thermal exchange increases with the addition in the volume fraction of the nanoparticles and the Reynolds number and decreases with the raise of the separation distance between heated sources, they also showed that the heat exchange is improved by 20% at a volume fraction of 10% of Cu nanoparticles.

Kumar et al. (2020) [67] studied numerically in three dimensional the heat transfer rate, surface temperature, Nusselt number, thermal resistance, power consumption and reliability of electronic chip in the six circular channel heat sink with water and the Al₂O₃/water nanofluids as coolants, they observed that the Al₂O₃/water nanofluids decreases the surface temperature, the power consumption, and thermal resistance of electronic chip than water. In addition, they observed that the Nusselt number increases and the reliability of electronic chip using Al₂O₃/water nanofluids is 70% higher than water.



(a)



(b)

Figure (I.20): Schematic view of micro channel in the heat sink. [67]

Arshi Banu et al. (2020) [68] studied the Micro-Pin-Fin Heat Exchanger, with the water, Al_2O_3 -water and CuO -water nanofluids as coolants, Results demonstrate that as Reynolds number builds, the temperature difference diminished. Furthermore, the temperature difference increases with increase in volume fraction. Among the three working fluids, CuO -water pursued higher temperature difference compared to Al_2O_3 -water and pure water.

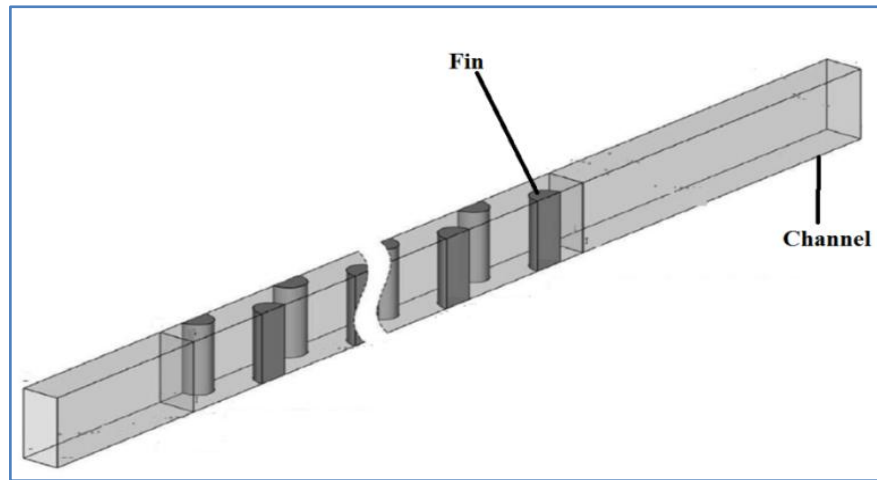


Figure (I.21): Geometric model

Abbas et al. (2020) [69] studied improvement of the physical properties of heat flux and heat transfer of unstable nanofluids after a mobile rotating plate in the presence of brown viscous dispersions and heat diffusion. Where they used three different types of nanoparticles copper, aluminum oxide and titanium dioxide were considered in different forms (spherical, cylindrical, and brick) and also used water as a basic liquid. They compared the previously published results with their results to validate them and found excellent agreement. They observed that the shape of nanoparticles plays a large role in determining the flow behavior significantly. They also found that using the shape of cylindrical nanoparticles improves heat transfer compared to the forms of nanoparticles they studied (spherical and brick).

Vicki et al. (2020) [70] studied the effect of the mixture of nanoparticles mixture and the temperature of the nanoparticle on the thermal conductivity of $\text{Al}_2\text{O}_3\text{-CuO}$ / water-EG hybrid nano-liquid. They prepared the stable suspension of $\text{Al}_2\text{O}_3\text{-CuO}$ hybrid nnaofluid at four different ratios of the nanoparticles from 20: 80 and 40: 60, 50:50 and 60:40 with a concentration of 1.0%. They obtained the highest thermal conductivity of $\text{Al}_2\text{O}_3\text{-CuO}$ nanoparticles for the ratio of 60:40 nanoparticles with a maximum increase of 12.33% relative to the base liquid. Besides, their results showed that the viscosity of the hybrid nanoparticle decreases with increasing temperature and that the hybrid nano liquid $\text{Al}_2\text{O}_3\text{-CuO}$ shows good thermal performance compared to the base liquid.

Chong et al. (2020) [71] investigated experimentally the effect of various concentrations of GOPs-water nanofluids in a pin-fin microchannel on heat transfer under pulsating inlet velocity. They chose the pulsating frequency ($f = 0, 1, 2, 3, 4, 5$), and mass fraction ($\varphi = 0.02\%, 0.05\%, 0.1\%, 0.15\%, 0.2\%$) and average Reynolds number $Re = 272, 407, 544$ Among their findings

that Heat transfer improves with increasing concentration of nanoparticles GOPs from 0.02% - 0.2% and also improves with the increase of average Reynolds number (272–544). Moreover, they observed that the low frequency pulsating flow has no significant impact on heat exchange enhancement of nanofluids compared to the steady flow.

The study made by the researchers (2020) [72] includes a critical and comparative review of all experimental, theoretical and numerical investigations on the effective thermal conductivity based on the particle size of nanofluids. This is to understand the effect of variation in the size of nanoparticles on the thermal performance of nanofluids in various nanoscale types.

Chapter II

Generality on the Thermal Properties of Nano-fluids

This chapter presents reminders on the thermal properties of nano-fluids and the parameters affecting thermal conductivity.

II. 1. Introduction

Nano-fluids are dispersion of particles of nano-metric size called nano-particles in a basic fluid to ameliorate certain properties. This type of nano-fluids provokes a big interest since the discovery of their particular thermal properties. As nano-particles contribute to improving heat transfer, particles with very high conductivity contribute in increasing the effective thermal conductivity of the mixture while the quality of the base liquid increases the thermal performance.

Despite these advantages, some nano-particles suffer from instability over time (Some nano-particles interact within the fluid Basic) and lead to the agglomeration of nano-particles, which leads to heterogeneity in the flow and sedimentation can occur, especially if the nano-particles are of large diameter.

II. 2. Types of nano-fluids

Different types of nano-materials have been used to make nano-fluids out of nano-particles of single element (e.g., Cu, Fe, and Ag), single element oxide (e.g., CuO, Al₂O₃, and TiO₂), multielement oxides (e.g., CuZnFe₄O₄, ZnFe₂O₄ and NiFe₂O₄), metal nitrides (e.g., AlN , TiN, and SiN), alloys (e.g., Ag-Cu , Fe-Ni and Cu-Zn), carbon materials (e.g.,diamond, graphite,

carbon nano-tubes) and metal carbides (e.g., ZrC , TiC and SiC), suspended in base fluid (e.g., water, oil, ethylene glycol).

We can generally distinguish two main categories:

II.2.1. Single material nano-fluids:

Single material nano-fluid was first proposed by Choi (1995), where a single kind of nano-particles is utilized to produce the suspension via several preparation methods [73]. We can find the single material nano-fluids in different types such as: pure metals, metal oxides, carbides, carbon materials, etc. Furthermore, carbon atoms can bond among themselves in a number of different ways to form a variety of carbon materials or allotropes of carbon. Typical carbon allotropes include amorphous carbon, graphite and diamond. Carbon allotropes can also have a variety of structures and morphologies such as crystalline (i.e., diamond, graphite sheets and carbon nano-tubes).

Carbon nano-tubes are a few nanometers in diameter and can reach several hundred micrometers. Nano-tubes can consist of a single coat of Graphene wrapped around itself and are called "single-walled nano-tube" (SWCNT). They can also consist of a winding of several layers of Graphene and are then called "Multi-walled carbon nano-tube" (MWCNT)

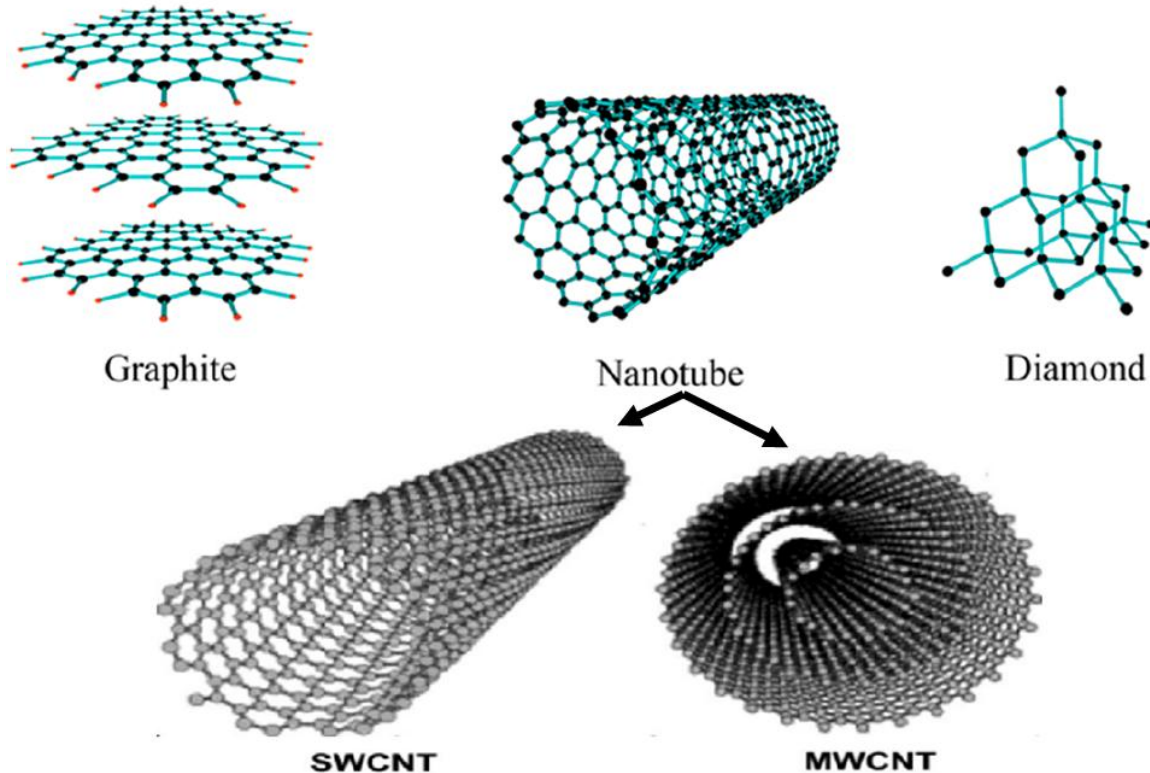


Figure (II.1): Molecular structures of Graphite, diamond and a carbon nano-tube [74]

There are several studies on nano-fluids based on carbon nano-tubes, some [75] have shown the highest raise in thermal conductivity in the order of 200% for a volume fractions of less than 1%. The main difficulty encountered during the preparation of nano-fluids based on carbon nano-tubes is the non-uniform dispersion and its damage during high temperature processing in a reactive environment. [76]. to remedy this dispersion problem, a surface functionalization of the nano-tubes is carried out. However, the nano-tubes of carbon introduce the highest thermal conductivity: $k \approx 6600\text{W/mK}$ for an isolated nano-tube at ambient temperature [77].

II.2.2 hybrid nano-fluids:

Hybrid nano fluids was first studied by Jana et al. (2007), in order to improve the fluid thermal conductivity beyond that of a conventional single material kind nano-fluid [78]. Hybrid nano-fluids are a developed category of nano-fluids which are made of a consolidation of more than one type of nano-particles (which combines two or more types of nano-particles) suspended in a base fluid. We can find examples such as: Ag-MgO/H₂O hybrid nano-fluid, Alumina-graphene/water hybrid nano-fluids... etc

Hybrid nano-particles could be synthesized either by chemical or by physical methods.

In their study (Jana et al.(2007)) [78], they examined Cu nano-particles, carbon nano-tubes (CNT), and Au nano-particles dispersed in water, as well as their hybrids (CNT–Cu/H₂O and CNT–Au/H₂O) The results showed that the thermal conductivity of Cu/H₂O nano-fluid was the highest among the tested samples and increased linearly with the rise of particle concentration.

Nevertheless, the stability of the CNT–Cu/water nano-fluid achieved longer settling time than the other types of nano-fluids before degrading.

Also, other theoretical approaches have emerged to try to describe the increases in thermal conductivity of nano-fluids. Phenomena such as the contribution of Brownian motion [79] or the exchange of phonons [80] between particles have been studied. However, none of these theories can correctly describe all the behaviours observed experimentally. Table (II.1) shows the most significant results concerning the improvement of the thermal conductivity of nano-fluids.

<i>Fluid</i>	<i>Nano-particle</i>	<i>volume fraction of solid (in %)</i>	<i>Relative gain (in %)</i>
Ethylene glycol. EG	<i>CuO, 18.6 nm</i>	4	20
water	<i>CuO, 18.6 nm</i>	4.3	10
water	<i>TiO₂, 27 nm</i>	4.35	10.6
water	<i>TiO₂, 15 nm</i>	4	33
Pump oil	<i>Cu, 35 nm</i>	0.055	45
water	<i>Cu, 100 nm</i>	7.5	75
Transformer oil	<i>Cu, 100 nm</i>	7.5	45
Ethylene glycol. EG	<i>Cu, 10 nm</i>	0.2	40
water	<i>Au, 15 nm</i>	0.00026	8.3
water	<i>Al₂O₃, 60 nm</i>	5	20
Ethylene glycol. EG	<i>Al₂O₃, 60 nm</i>	5	30
Pump oil	<i>Al₂O₃, 60 nm</i>	5	40
water	<i>Al₂O₃, 60 nm</i>	0.5	100
water	<i>Al₂O₃, 60 nm</i>	1	16

Table (II.1): Results concerning the improvement of the thermal conductivity of nano-fluids [75].

II.3. Nano-fluid preparation:

Nano-fluids can be unstable. Therefore, the preparation technique used is extremely important to produce stable nano-fluids. Different methods have been used to avoid nano-particle agglomeration and improve the stability of nano-fluids, such as pH control, ultrasonic agitation, surfactant addition, magnetic stirring and high-pressure homogenization [81]. According to Yu and Xie [81], there are three main methods used for nano-fluids preparation: one-step chemical technique (such as pyrolysis or chemical precipitation), one-step physical technique (such as mechanical grinding.) and two-step technique.

II.3.1 one-step method:

It is about producing the nano-particles in the base fluid, this method helps in preventing the agglomeration and oxidation of the nano-particles. An example, when a thin film of the base liquid forms on the vessel and this is due to under the centrifugal force of the rotating disk, Raw material is evaporated in a crucible by the heating process, the vapor is condensed into nano-particles when it contacts the cold base fluid film, and nano fluid is formed (Figure (II.2)).

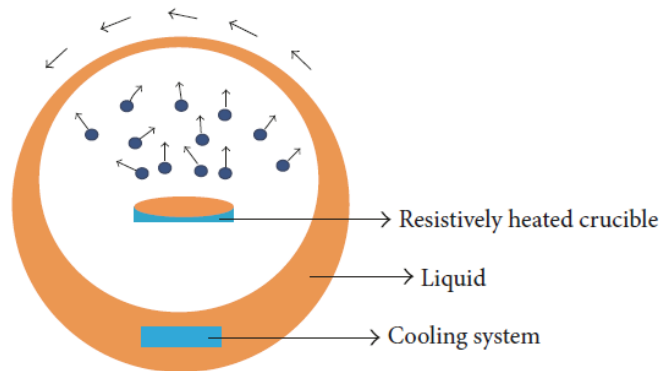


Figure (II.2): Preparation of nano-fluid using one-step vapor deposition method [82].

II.3.2 Two-step method:

The first step is to make the nano-particles, and in the second step the nano-particles are dispersed in a base fluid. Figure (II.3) demonstrates an example of the schematic procedure of the two-step approach used for synthesising nano-fluid, to allow perfect dispersion. Among the utilized equipment for dispersing nanoparticles in the base liquid is ultrasonic bath, magnetic stirrers, high-shear mixers. In addition, to avoid agglomeration due to attractive forces between particles, electrostatic repulsive forces are used by charging the surface of the particles through the adjustment of the pH.

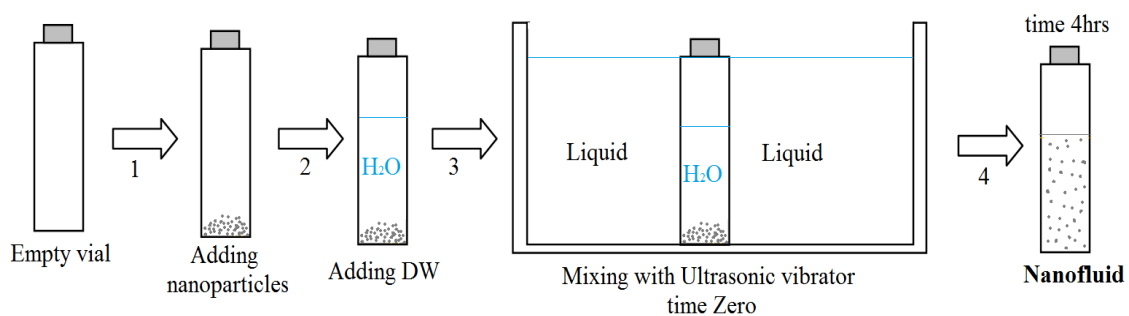


Figure (II.3): Schematic procedure of the two-step nano-fluids preparation.

II. 4. Thermophysical properties of nano-fluids

Conventional heat transfer fluids such as engine oils, water and ethylene glycol have some limitations as their thermal properties are quite low when compared to those of solids, as shown in Figure (II.4). It compares thermal conductivities of several base fluids and solids. It also, explains the benefits of a particulate diamond nano-fluid over other nano-fluids making it of particular interest. Diamond itself has the highest thermal conductivity of any material because of low phonon scattering and strong carbon-carbon (C-C) covalent bonding [83], while metallic particles such as silver (Ag) have a rise thermal conductivity, their electrical conductivity can render it unusable in several applications. Nevertheless, the thermal conductivity of smaller volume (size) diamonds may vary in host fluids or compounds [84].

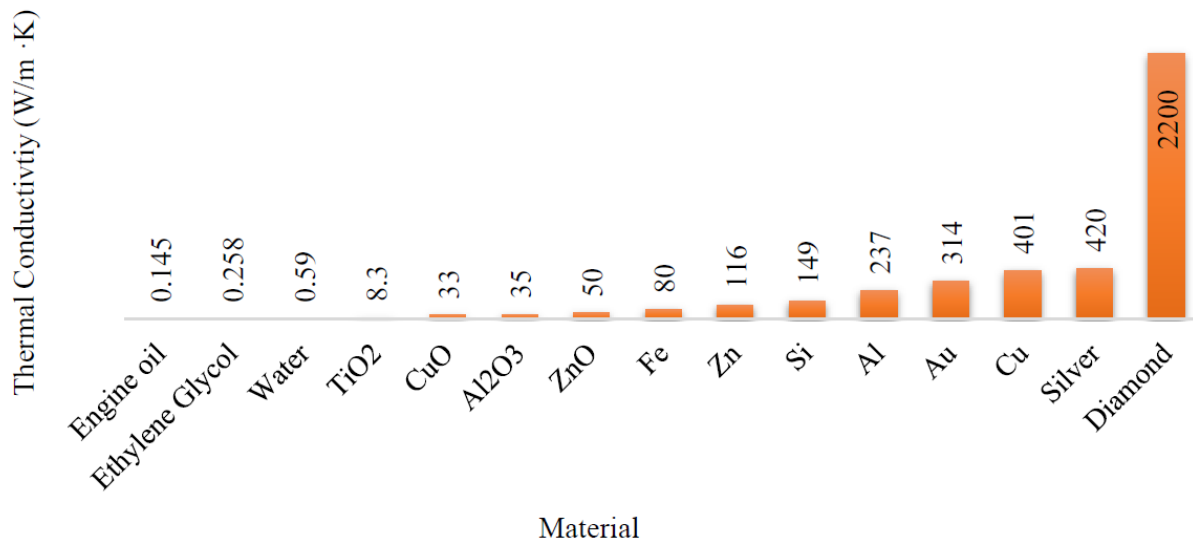


Figure (II.4): The thermal conductivity of different base fluids and solids materials at 298,15 K [84].

II. 4. 1. The volume fraction (ϕ):

The volume fraction is the most important property for the nano-fluid, since the calculations of all the other properties are based on the volume fraction of the nano-fluid. Nonetheless, we can define the volume fraction as the volume of solid or particle (nano-particles) over the total volume (nano-particles + base fluid). The value of the volume fraction is varied between 0 (pure base fluid) and 1. The volume fraction is given by the following relation:

$$\phi = \frac{v_s}{v_T} \quad (\text{II.1})$$

v_s : volume of solid (nano-particles).

v_T : total volume.

The physical-thermodynamic properties of nano-fluids depend mainly on the quality of the base fluid and the quality of the dissolved nano-particles in the basic liquid. Among the parameters that control the determination of the properties of the nano-particle: thermal conductivity, dynamic and kinematic viscosity, specific heat capacity, etc. In addition to that the shape, diameter of nano-particles, the concentration of suspended particles and the temperature of the nano-fluids also influence the physical properties of the nano-fluids.

Figure (II. 5) demonstrates the thermophysical properties of nano-fluids which are discussed in more detail below.

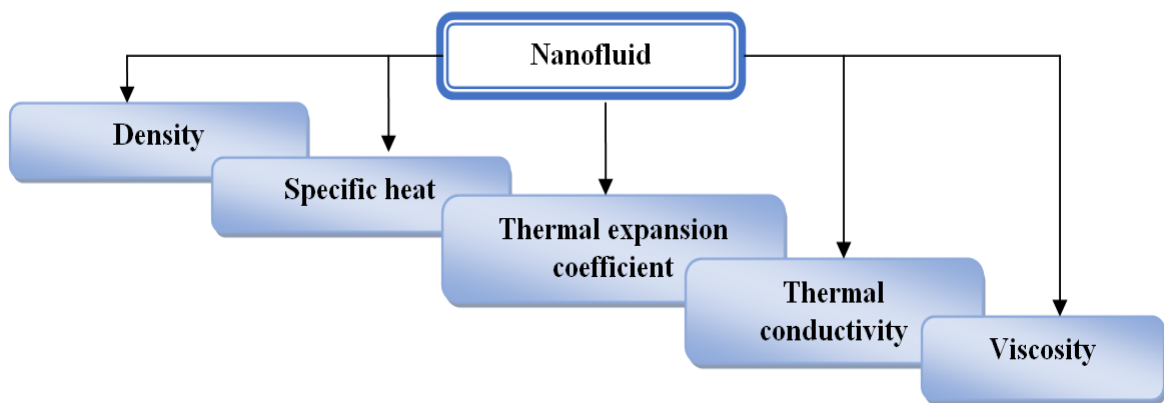


Figure (II.5): Nano-fluid Thermophysical properties

II. 4. 2. The density:

The density of a perfectly homogeneous nano-fluid is determined (good dispersion of the nano-particles in the fluid) as a function of the volume fraction φ at a given temperature T, is made from the definition of the density of a mixture.

We then deduce the density of the nano-fluid:

$$\rho_{nf} = (1 - \varphi)\rho_f + \varphi\rho_s \quad (\text{II.2})$$

Where

ρ_{nf} : The density of the nano-fluid

ρ_f : The density of the base fluid

ρ_s : The density of solid nano-particles.

II. 4. 3. Specific heat

Specific heat is the calorific capacity per unit of mass of a homogeneous system or a substance. The specific heat corresponds to the heat input necessary to raise the temperature of the substance unit by 1 K during the considered transformation. For the determination of the specific heat of a nano-fluid, the following relationships are found:

Many authors including Pak and Cho. [85] used:

$$(C_P)_{nf} = (1 - \varphi)(C_P)_f + \varphi(C_P)_s \quad (\text{II.3})$$

Some others including Xuan and Roetzel [86] used:

$$(\rho C_P)_{nf} = (1 - \varphi)(\rho C_P)_f + \varphi(\rho C_P)_s \quad (\text{II.4})$$

$(C_P)_{nf}$, $(C_P)_f$, $(C_P)_s$ the specific heats of the nano-fluid, the base fluid and the nano-particles, respectively.

It is this last relation that we keep in the rest of our work.

II. 4. 4. The thermal expansion coefficient

In the context of our study, we are only interested in incompressible fluids (density independent of pressure). This variation in density under the action of temperature is characterized by the coefficient of thermal expansion, also called the coefficient of expansion (Bejan, [87])

To calculate the value of this coefficient for nano-fluids, we use this expression:

$$\rho_{nf} \beta_{nf} = (1 - \varphi) \rho_f \beta_f + \varphi \rho_s \beta_s \quad (\text{II.5})$$

Kim et al. [88] assumed that the coefficient of thermal expansion of the fluid (β_s) is much greater than that of solid nano-particles (β_s). They reduced equation (II.5) to the following simplified form

$$\rho_{nf} \beta_{nf} = (1 - \varphi) \rho_f \beta_f \quad (\text{II.6})$$

II. 4. 5. The thermal conductivity of nano-fluids

The thermal conductivity is generally an important property, mainly because it plays a very important role in the phenomenon of heat transfer. It can clearly indicate the efficiency of the heat transfer of the fluid or the solid, the conductivity depends on the temperature.

In addition to its variation as a function of temperature, the thermal conductivity of the nano-fluid also varies as a function of the volume fraction, the thermal conductivity of a nano-fluid is calculated according to the following models:

II. 4. 5. 1. Maxwell model [89]

Maxwell model is interested in calculating the thermal conductivity of a fluid containing spherical particles in suspension. To arrive at the estimation of this last, he assumed that the fluid contains several spherical particles of the same diameter.

Maxwell's formula is given by:

$$k_{nf} = \frac{k_s + 2k_f - 2\phi(k_f - k_s)}{k_s + 2k_f + \phi(k_f - k_s)} k_f \quad (\text{II.7})$$

k_{nf} , k_f and k_s : the thermal conductivities of the nano-fluid, the base fluid and the solid particles, respectively .

Maxwell's model is satisfactory for suspensions containing spherical particles with relatively small volume concentrations but does not take into account the effect of the size or the shape of the particles.

It should also be noted that the effect of inter-particle interactions is neglected in this model.

II. 4. 5. 2. Hamilton-Crosser Model [90]

The Hamilton and Crosser model was established to resolve the Maxwell model limit. Since the latter is valid only in the case of spherical particles, one thing which makes the model not efficient for the description of the phenomenon studied. For this model was developed to make the calculation of thermal conductivity nano-fluid more efficient whatever the form of the nano-particle, and that by introducing the notion of the geometric factor called sphericity (ψ). This factor is defined as the ratio of the surface of the sphere having the same volume as the nano-particles on the surface of a nano-particle.

The thermal conductivity in this model given by the following expression:

$$k_{nf} = \frac{k_s + (n-1)k_f - (n-1)\phi(k_f - k_s)}{k_s + (n-1)k_f + \phi(k_f - k_s)} k_f \quad (\text{II.8})$$

Where n is an empirical form factor given by: $n = \frac{3}{\psi}$

$n = 3$ for spherical particles et $n = 6$ for cylindrical particles.

for $\psi=1$ (spherical particles), the Hamilton-Crosser model is identical to the Maxwell model.

II. 4. 5. 3. Yu et Choi Model [91]

Another expression for calculating thermal conductivity was introduced by Yu and Choi. They proposed model nano-fluids as a basic liquid and solid particles separated by a nano-metric layer, this layer acts as a thermal bridge between the fluid and the nano-particles. In addition, they assumed that the thermal conductivity of the nano-metric layer is greater than the thermal conductivity of liquid,

$$k_{nf} = \frac{k_S + 2k_f + 2\varphi(k_S - k_f)(1 + \beta)^3}{k_S + 2k_f - \varphi(k_S - k_f)(1 + \beta)^3} k_f \quad (\text{II.9})$$

Where (β) is the ratio of the thickness of the nano-metric layer to the radius of the particles.

II. 4. 5. 4. Bruggeman Model [92]

The model proposed by Bruggeman seems to better approximate certain experimental results compared to other models for the case of spherical nano-particles with no limitation concerning the concentrations of nano-particles,

$$k_{nf} = \frac{(3\varphi - 1) \frac{k_S}{k_f} + \left[3((1 - \varphi) + \sqrt{\Delta}) \right]}{4} k_f \quad (\text{II.10})$$

With

$$k_{nf} = \left[(3\varphi - 1) \left(\frac{k_S}{k_f} \right)^2 + (2 - 3\varphi)^2 + 2(2 + 9\varphi - 9\varphi^2) \left(\frac{k_S}{k_f} \right) \right]$$

Providing mathematical correlations is selected as a method to model the thermal conductivity behaviour. Table (II.2) lists some of the presented mathematical correlations for thermal conductivity of nano-fluids.

Nano-fluid	Correlation	References
<i>MgO/water-EG</i>	$\frac{k_{nf}}{k_f} = 0.4 + 0.0332\varphi + 0.00101T + 0.000619\varphi T + 0.0687\varphi^3 + 0.0148\varphi^5 - 0.00218\varphi^6 - 0.0419\varphi^4 - 0.0604\varphi^2$	Hemmat Esfe et al. [93]
<i>MgO/EG</i>	$\frac{k_{nf}}{k_f} = 1.00475 + 2.26216 \varphi + 1.57146T \varphi^2 + 481.646 \varphi^2 EXP(-66.7522 \varphi) - 0.0100301 T \varphi \cos(\frac{1560.99\varphi}{T})$	Hemmat Esfe et al. [94]
<i>Al₂O₃/water</i>	$\frac{k_{nf}}{k_f} = 0.991 + 0.267T\varphi + 77.6\varphi^2 + 3641.231\varphi^2 T + \frac{0.00217}{\sin(\frac{\varphi}{T - \varphi})} - 6.01 \times 10^{-6} T^2 - 3647.099T\varphi \sin(\frac{\varphi}{T})$	Hemmat Esfe et al. [95]
<i>Al₂O₃/methanol</i>	$\frac{k_{nf}}{k_f} = 1.0712 + 1.546\varphi$	Mostafizur et al. [96]
<i>SiO₂/methanol</i>	$\frac{k_{nf}}{k_f} = 1.0405 + 1.3342\varphi$	Mostafizur et al. [96]
<i>TiO₂/ methanol</i>	$\frac{k_{nf}}{k_f} = 1.0514 + 1.3317\varphi$	Mostafizur et al. [96]
<i>MWCNT/water</i>	$\frac{k_{nf}}{k_f} = 0.9396 + 0.9997\varphi + 0.0003T$	Xing et al. [97]
<i>SiC/EG</i>	$\frac{k_{nf}}{k_f} = 4.583 + 12.71\varphi$	Li et al. [98]

Table (II.2): Abstract of presented: correlations for the thermal conductivity (K_{nf}) of nano-fluids

II. 4. 6. Dynamic viscosity

Viscosity can be defined as a property of a fluid so that it resists deformation when it is set in motion. We can therefore speak of viscosity as a measure of the internal friction of a fluid. A very viscous liquid is a liquid that has high internal friction.

The dynamic viscosity of the nano-fluid greatly influenced by the quality of the dispersion of the nano-particle in the base fluid and the temperature, this dynamic viscosity can be calculated from the dynamic viscosity of the base fluid and the volume fraction of the nano-fluid.

II. 4. 6. 1. Einstein Model [99]

The dynamic viscosity of a nano-fluid is given by Einstein's model for a mixture containing dilute suspensions of rigid fine particles

$$\mu_{nf} = (1 - 2.5\varphi)\mu_f \quad (II.11)$$

Einstein's formula has since been verified experimentally and is considered satisfactory for very dilute suspensions of spherical particles (Brownian or non-Brownian), typically for volume

concentrations of less than 1%. Note that this model does not take into account the effects of particle size and interparticle interactions.

II. 4. 6. 2. Batchelor Model [100]

In fact, the flow around each particle is influenced by the possible presence of other particles nearby and by collisions between particles. So this translates into taking into account a term (φ^2) in Batchelor's model

$$\mu_{nf} = (1 + \Pi\varphi + k_H\varphi^2) \quad (\text{II.12})$$

Where Π is the intrinsic viscosity and k_H is the Huggins coefficient. The value of Π and k_H are 2.5 and 6.5 respectively for spherical particles.

II. 4. 6. 3. Brinkman Model [101]

Brinkman's formula completes Einstein's model up to a volume concentration of less than 4%,

$$\mu_{nf} = \frac{\mu_f}{(1 - \varphi)^{2.5}} \quad (\text{II.13})$$

It is noted that this relation describes a nonlinear evolution of the dynamic viscosity with the volume concentration but does not take account of the collision between the particles.

II. 4. 6. 4. Pack and Cho Model [85]

Pack and Cho proposed a correlation for the Al_2O_3 nano-particles dispersed in the water given by:

$$\mu_{nf} = (533.9\varphi^2 + 39.11\varphi + 1)\mu_f \quad (\text{II.14})$$

II. 4. 6. 5. Maiga et al. Model [102]

Other relationships have been proposed in the literature limited to very specific applications. Maiga et al. from measurement results proposed the correlation.

$$\mu_{nf} = (123\varphi^2 + 7.3\varphi + 1)\mu_f \quad (\text{II.15})$$

By comparing this correlation to Einstein and Brinkman models, we find that these last two approaches underestimate the experimental values of the viscosity of nano-fluids.

II. 4. 7. The parameters affecting thermal conductivity

In this section, we have briefly presented some parameters that affect the thermal conductivity shown in the Figure (II.6).

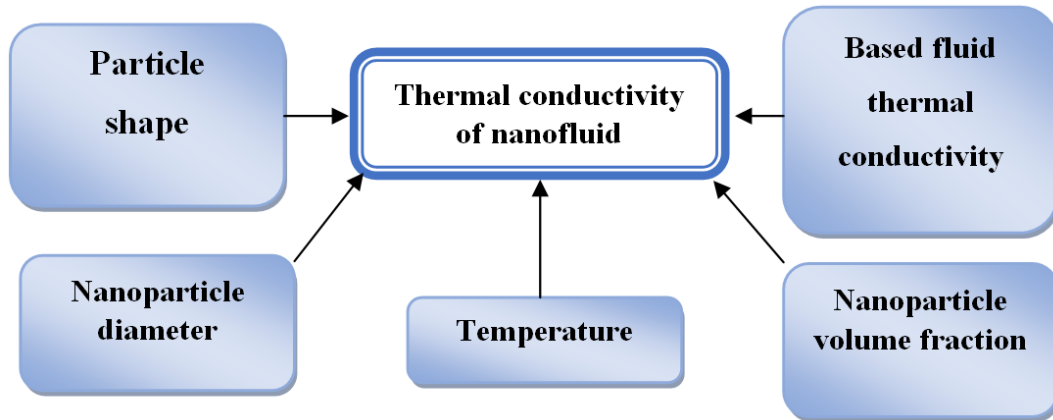


Figure (II.6): Some parameters influencing nano-fluids thermal conductivity.

II. 4. 7. 1. Effect of temperature and nano-particle size on thermal conductivity

Temperature is an important factor that affects the enhancement of the thermal conductivity of nano-fluids. Where Patel et al. [103] studied the different thermal conductivity of ethylene glycol dioxide Al_2O_3 as a function in the temperature, for volume fraction = 1% and 3%, and for diameter of particle equal 11 nm and 150 nm. As shown in Figure (II. 7), which indicated an increase in thermal conductivity with increasing temperature and also, with the decrease of nanoparticle size due to the increase in surface area to volume ratio, with low nano-particle size, which allows more efficient heat transfer to the base liquid. Also, increased Brownian motion with smaller nano-particles has resulted in an increase in thermal conductivity.

We also find that Chun et al. [104] measured the thermal conductivity of $\text{Al}_2\text{O}_3\text{-H}_2\text{O}$ nano liquids between 294 K and 344 K and reported an increasing trend with increasing temperature, Paul et al. [105] studied the variation of $\text{Au-H}_2\text{O}$ nano-fluid thermal conductivity at room temperature as a function of nano-particle size, for a nano-particle volume fraction of 0.00026%. They found that the thermal conductivity increased with the decrease of nano-particle size, which is shown in Figure (II.8). They concluded that this increase was a result of increased Brownian motion and greater surface area to volume ratio for smaller nano-particles.

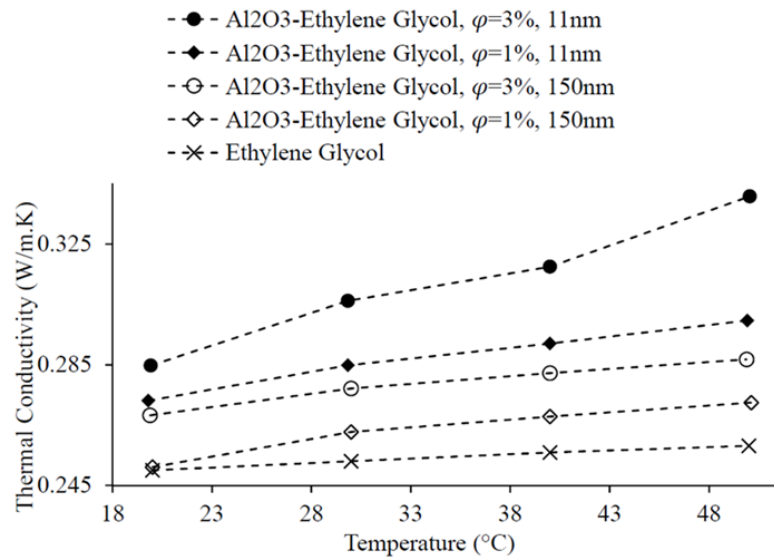


Figure (II.7): Variation of Al₂O₃-Ethylene Glycol nano-fluid thermal conductivity as a function of temperature, 150 nm diameter particles [106].

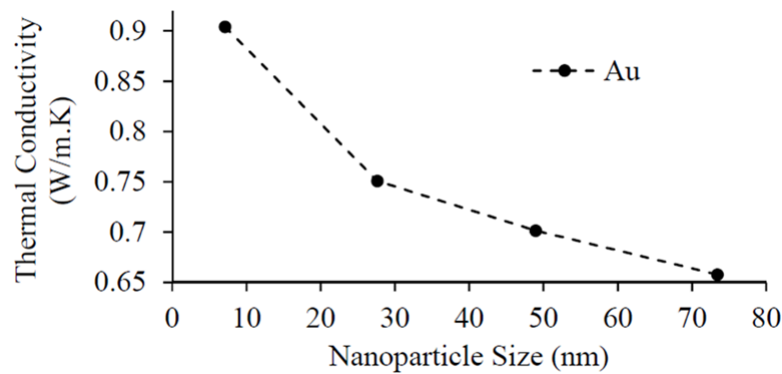


Figure (II.8): Variation of Au-H₂O nano-fluid thermal conductivity at room temperature as a function of nano-particle size [106].

II. 4. 7. 2. Effect of nano-particle volume fraction on thermal conductivity

Various scientists have studied the impact of the nano-particle volume fraction on the thermal conductivity of various nano-fluids. Figure (II.9) shows the variation in the thermal conductivity ratio with the volume concentration for different temperatures of nano-fluid. The majority of the research studies highlighted that increases in the fraction of solid nano-particles cause an increase in the thermal conductivity of nano-fluids. While most researchers found the relationship to be linear, some researchers found it to be nonlinear. This phenomenon can be associated with the accumulation of nano-particles in liquids, as mentioned in [107] or the interactions between the particles in the system (Choi *et al* [108]).

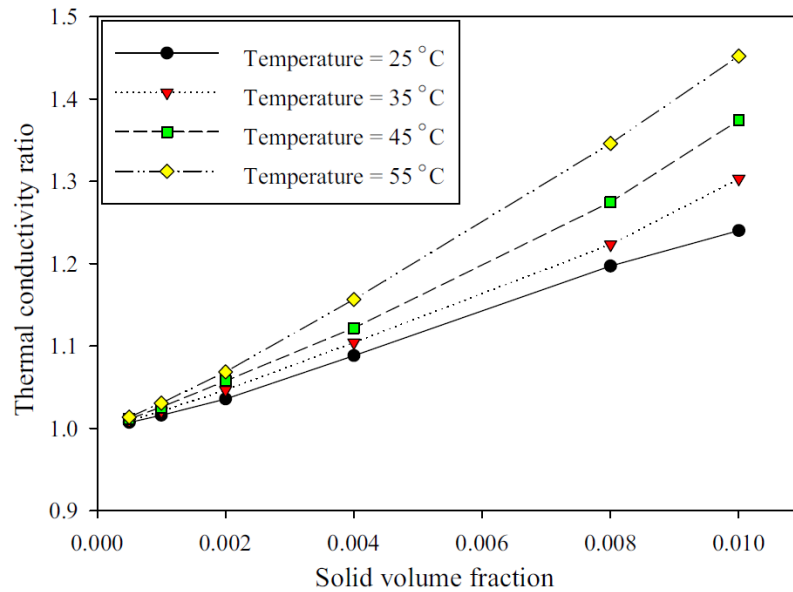


Figure (II.9): Thermal conductivity ratio via volume concentration in various temperatures [109].

II. 4. 7. 3. Effect of the base liquid on thermal conductivity

There are several studies concerned with studying the impact of basic fluids on nano-particles, but the results of some studies differed from others. Some researchers that the thermal conductivity betterment was found to be inversely proportional to the base fluid thermal conductivity [110, 111, 112], Wang et al. [113] studied the thermal conductivity of suspensions of Al₂O₃ and CuO nano-particles in several base liquids such as ethylene glycol, water, engine oil and vacuum pump oil, the highest thermal conductivity ratio was observed when ethylene glycol was used as the base liquid, which has a relatively low thermal conductivity compared to other basic liquids. They found that the thermal conductivity of nanofluids increases when the thermal conductivity of the basic liquid decreases, while other authors reported an opposite finding [114], Chopkar et al. [115] contradicts the above results as it was concluded to improve the thermal conductivity of nano-fluids. It adopts the high conductivity of basic fluids. Moreover, in a recent study conducted by [116] aims to find the best basic fluids for use in solar PV / T applications, where they chose three nano-fluids for their experiment, namely (water /0.5% SiC), 35% ethylene glycol /0.5% SiC and 35% propylene glycol / 0.5% SiC. These liquids were experimented at a temperature between 25 and 60°C. Finally, they did not notice any significant difference in the thermal conductivity of the three nano-particles (see figure (II.10)).

In another study [117] studied experimentally the impact of base fluids on thermo - physical properties of SiO₂ nano-fluids. The ratio was considered as 40:40 and 60:40 by volume in ethylene glycol and water, respectively. They prepared nano-fluids by dispersing SiO₂ nano-

particles in EG and "water" (W) mixed in "60:40" (60EGW) and "40:60" (40EGW) ratio by volume.

They studied the stability of nano-fluids through pH values, electrical conductivity, or the potential of zeta. Their experimental results showed, SiO₂ molecules achieved increased a 34% and 32% in thermal conductivity with the two base fluids. They also noticed that 40EGW-based nano-fluids have a higher thermal conductivity value (see figure (II.11)).

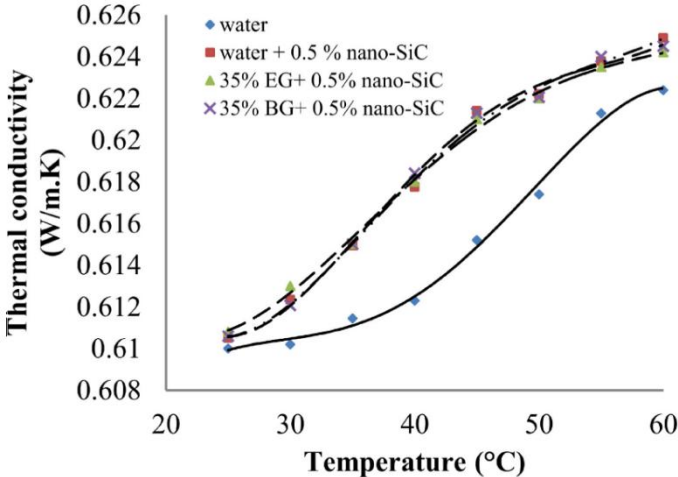


Figure (II. 10): impact of base liquid on thermal conductivity for different nano-fluid types [116].

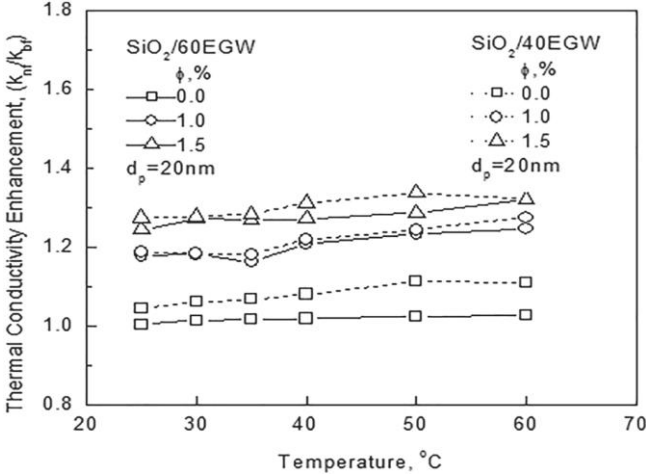


Figure (II.11): Comparison of thermal conductivity enhancement of SiO₂/60EGW and SiO₂/40EGW nano-fluids [117]

II. 4. 7. 4. Effect of particle shape on thermal conductivity

Researchers studied the impact of nano-particle shapes on thermal conductivity, and they noticed that nano-fluids with nano-particles have a greater surface area while volume ratios have

a higher thermal conductivity. Maheshwari et al. [118] studied the thermal conductivity of TiO_2 – H_2O nano-fluid using cubic nano-particles (51.87 nm), spherical nano-particles (22.9 nm) and rod nano-particles (43.08 nm). They observed that the nano-fluid containing cubic nano-particles had the highest thermal conductivity and that containing spherical nano-particles had the lowest thermal conductivity, shown in Figure (II.12). They confirmed that the use of spherical nano-particles, It helps to stabilize the particles and reduces the blockage problem.

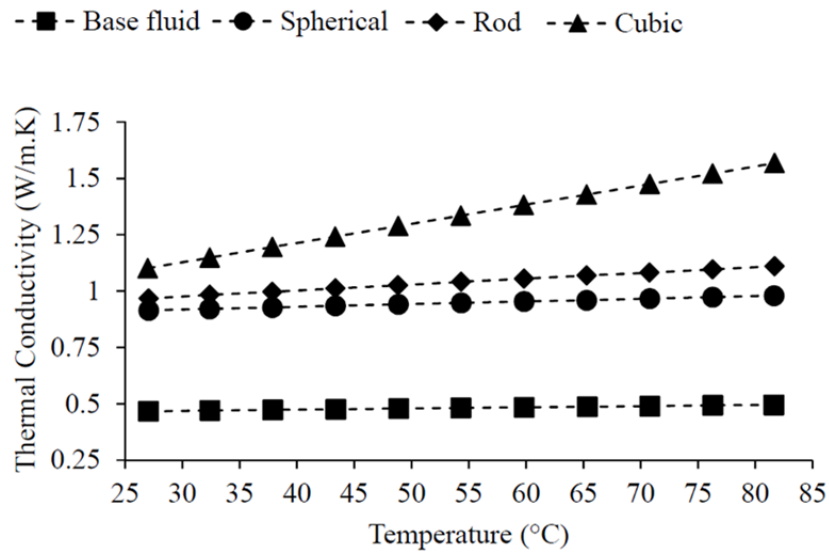


Figure (II.12): Effect of nano-particle shape on the thermal conductivity of TiO_2 –water nano-fluid at 2.5%, as a function of temperature [106].

Chapter III

Mathematical model and numerical method

III.1.Introduction

Convection is one of the three modes of heat transfer with conduction and radiation. The term convection refers to the heat transfers occurring between a surface and a moving fluid when these are at different temperatures. To study convection, there are several numerical and experimental methods, today numerical simulation still the cheapest method, and the most usable compared to experimental methods, where the numerical simulation made it possible to understand the different phenomena of thermal transfer and the coupling between them.

To formalize forced and natural convection, it is necessary to describe the coupling of the temperature, pressure and velocity fields from the conservation equations of momentum, mass and energy.

The objective of this chapter is devoted to the modeling equations of the cases treated in this thesis using the conservation equations of mass, momentum and energy then to present the numerical method used to solve these equations.

III.2. General equations

The mathematical formula for convective phenomena depends on equations that link the various parameters, namely: velocity, pressure and temperature. These equations are obtained as special cases from the following general equations (continuity equation, momentum conservation equation and energy conservation equation).

III .2.1. Continuity equation (laminar regime)

This is the equation which expresses the law of conservation of mass for a volume of material control. It is expressed mathematically in the following form:

$$\frac{\partial \rho}{\partial t} + \vec{\nabla}(\rho \cdot \vec{V}) = 0 \quad (\text{III. 1})$$

Where ρ is the density and V is the velocity vector.

III .2.2. The momentum conservation equation

The second law of dynamics indicates that the rate of variation in quantity of movement contained in the control volume D is equal to the sum of all external forces applied to it. It is written in the following form:

$$\frac{D}{Dt} \int_D \rho \vec{V} dV = \int_D \vec{F} dV + \int_S \rho \vec{\sigma} dS \quad (\text{III.2})$$

Where:

D, S and σ are control domain of volume (V) and surface of the continuous medium and the constraint vector, respectively.

The momentum conservation equation can be written as:

$$\frac{D(\rho \vec{V})}{Dt} = \rho \vec{F} - \nabla P + \frac{1}{3} \nabla \mu (\nabla \cdot \vec{V}) + \mu \nabla^2 \vec{V} \quad (\text{III.3})$$

Or

$$\underbrace{\frac{\partial(\rho \vec{V})}{\partial t} + \nabla \cdot \rho \vec{V}}_{\boxed{1}} = \underbrace{\rho \vec{F} - \nabla P}_{\boxed{2}} + \underbrace{\frac{1}{3} \nabla \mu (\nabla \cdot \vec{V})}_{\boxed{3}} + \underbrace{\mu \nabla^2 \vec{V}}_{\boxed{4}} \quad (\text{III.4})$$

- 1: The rate of variation and transport of quantity of movement.
- 2: Forces due to pressure
- 3: Brinkman's viscous term.
- 4: Viscosity forces.

Where: F and μ are a force per unit of volume and the dynamic viscosity, respectively.

III .2.3. Energy conservation equation

The energy conservation equation is obtained from the first principle of thermodynamics and it can be written as:

$$\underbrace{\frac{D(\rho c_p T)}{Dt}}_{\boxed{1}} = \underbrace{\Delta(kT)}_{\boxed{2}} + \underbrace{q + \beta T \frac{Dp}{Dt}}_{\boxed{3}} + \underbrace{\mu \phi}_{\boxed{4}} = 0 \quad (\text{III.5})$$

With:

- 1: The total variation of energy (by accumulation and convection).

2: The variation of energy by conduction.

q : Power density dissipated.

3: The energy variation due to compressibility.

4 : Irreversible dissipation due to viscous friction.

c_p , k , β are the heat capacity, the conductivity thermal and the isobaric coefficient of expansion of the fluid, respectively.

III.3. Boussinesq approximation

The approximation of Boussinesq indicates an approximation of equations of Navier-Stokes for incompressible flows with free surface in which exists a gradient of density vertical resulting in the absence of hydrostatic equilibrium. This approximation is attributed to Boussinesq [119], but it was presented for the first time by Oberbeck [120]

Boussinesq's approximation consists of assuming that all the thermo-physical characteristics of fluids are constant and uniform, except in the density, it is assumed to vary linearly with temperature. The relation can be written as follows.

$$\rho(T) = \rho_0[1 - \alpha(T - T_0)] \quad (\text{III.6})$$

This development in the first order is valid for many problems of natural and mixed convection since the temperature difference within the fluid always remains less than ten degrees, T represents the temperature of the fluid at a given point of the system, T_0 is the reference temperature which generally corresponds to the mean value of the temperature of the system (operating temperature), α is the coefficient of thermal expansion of the fluid and ρ_0 is constant density of the fluid.

III.4. Mathematical model for the applications studied

III.4.1. The thermo-physical properties of the nanofluids used in the applications studied

The calculation of the thermo-physical properties of the nanofluids used in my work are considered in this section

The thermal conductivity of the nanofluid is approximated by the Maxwell–Garnetts model [121]:

$$k_{nf} = \frac{k_s + 2k_f - 2\varphi(k_f - k_s)}{k_s + 2k_f + \varphi(k_f - k_s)} k_f \quad (\text{III.7})$$

Where φ is the volume fraction, k_s is the thermal conductivity of the nanoparticles, and k_f and k_{nf} represent the thermal conductivity of the base fluid (water) and nanofluid.

The dynamic viscosity of the nanofluid is given as[121]:

$$\mu_{nf} = \frac{\mu_f}{(1 - \varphi)^{2.5}} \quad (\text{III.8})$$

Where μ_f is the dynamic viscosity of the water

The density of the nanofluid is given as[86]:

$$\rho_{nf} = (1 - \varphi)\rho_f + \varphi\rho_s \quad (\text{III. 9})$$

Where ρ_f is the density of the water, ρ_s is the density of the nanoparticles

The heat capacity of the nanofluid is expressed as the following by **Xuan and Roetzel [86]**:

$$(\rho C_p)_{nf} = (1 - \varphi)(\rho C_p)_f + \varphi(\rho C_p)_s \quad (\text{III.10})$$

Where C_{pf} is the heat capacity of the water, C_{ps} is the heat capacity of the nanoparticles.

Applications	Base fluid and Nanoparticles	ρ (kg/m ³)	C_p (J/kg K)	k (W/m K)	μ (kg/m s)
Application N°1	water	997	4187	0,613	0,00085
	Cu nanoparticles	8933	385	401	-
Applications N°2, N°3 and N°4	water	997	4187	0,613	0,00085
	Cu nanoparticles	8933	385	401	-
	Ag nanoparticles	10500	235	429	-
	Diamond nanoparticles	3500	509	2300	-
Application N°5	Pure water	998.2	4182	0,6	0,001003
	Al ₂ O ₃ nanoparticles	3970	765	40	/
	SiO ₂ nanoparticles	2200	703	1.2	/
	TiO ₂ nanoparticles	4250	686.2	8.95	/
Application N°6	Pure water	998.2	4182	0,6	0,001003
	Diamond nanoparticles	3500	509	2300	-

Table (III.1): Thermo-physical properties of the water and nanoparticles used in each application

III.4.2.Simplifying hypothesis for the applications studied

III.4.2.1. Simplifying hypothesis for the applications N° 1

In this research, we assumed that the flow is stationary. The base fluid is supposed to be Newtonian. The nano-fluid Cu-water is supposed to be incompressible and the thermo physical properties of nanofluids are constant. The heat transfer by radiation is considered negligible.

- The effect of body force and viscosity dissipation is neglected
- The thermo-physical characteristics of nano-fluid are constant.

III.4.2.2. Simplifying hypothesis for the applications N° 2

In this study, we assumed that the flow is stationary. The base fluid is supposed to be Newtonian and incompressible. The thermo physical properties of the nano-fluids are taken as constant. The radiation heat transfer is negligible.

The effect of body force and viscosity dissipation is neglected.

III.4.2.3. Simplifying hypothesis for the applications N°3 and N°4

- The base fluid is supposed to be Newtonian.
- Nano-fluids are supposed to be incompressible and the thermo-physical characteristics of nano-fluids are constant, except for the variation of the density, which is estimated by the Boussinesq hypothesis.
- The heat transfer by radiation is considered negligible.
- The flow is stationary.
- The impact of the body force and the viscosity dissipation is neglected.

III.4.2.4. Simplifying hypothesis for the applications N°5

- The flow is stationary.
- The walls of mini channels are assumed to be adiabatic.
- The power of the electronic component is constant
- The thermo-physical characteristics of nano-fluids are constant, except for the variation of the density, which is estimated by the Boussinesq hypothesis.
- The base fluid is supposed to be Newtonian.
- The heat transfer by radiation is considered negligible.
- The impact of the body force and the viscosity dissipation is neglected.

III.4.2.5. Simplifying hypothesis for the applications N° 6

In this study, we assumed that the flow is stationary. The diamond-water nano fluid considered is supposed to be Newtonian, laminar and incompressible. The thermo physical properties of nano fluid are constant. The heat transfer by radiation is considered negligible

- No-slip boundary conditions are applied to all micro channel walls
- The top wall of micro channels is assumed to be adiabatic.
- The impact of the body force and the viscosity dissipation is neglected.
- A constant heat flux is applied to the bottom wall.

III.4.3 Mathematical model for the application N° 1 studied: Numerical study of the thermal transfer in different geometries of the mini-channels

III.4.3.1 Geometries of the problems considered:

The geometry of the mini channel of the cooler is represented by Figure (III.1) three different shapes using a fluent software.15 have been studied. The dimensions of the cooler are in the order of $21 \times 21\text{mm}^2$ with a thickness of 3.5 mm. This cooler is composed of 10 channels and 11 fins, The inlet temperature of the nanofluid in the three cases of the mini channels is set at 298.15K. For reasons of symmetry, only half of the cooler have been simulated.

Three different shapes have been considered to cool an electronic component of dimensions $(10 \times 10 \times 0.25 \text{ mm}^3)$ using a nanofluid (Cu-water) as a coolant.

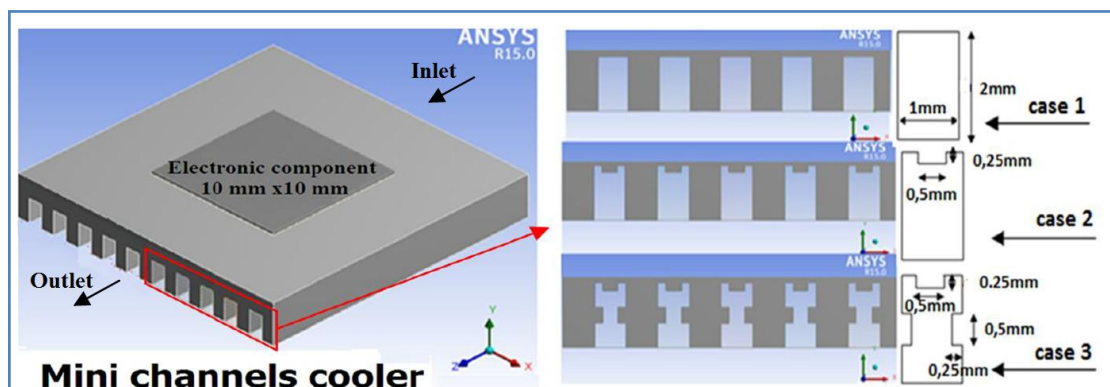


Figure (III.1): The different cases of the studied mini-channels

III.4.3.2 Boundary conditions:

The boundary conditions in this application are:

- At the inlet, the velocity w_{in} and temperature are constant.
- The maximum flux of the electronic component is constant with thermal insulation on all external faces of the cooler
- Zero pressure at the outlet of the mini channels
- A non-slip boundary condition is specified for the fluid at the level of the wall of the channel $u = v = w = 0$
- At the solid/nano-fluid interface, the continuity of the flux can be written as follows:

$$k_s \frac{\partial T}{\partial n} \Big|_{wall} = k_{nf} \frac{\partial T}{\partial n} \Big|_{wall} \quad (III.11)$$

III.4.3.3. Equations of the problem

The different equations necessary for the resolution of the problem are considered in this study (application 1) as follows:

- The continuity equation is written as follows:

$$\frac{\partial u}{\partial x} + \frac{\partial v}{\partial y} + \frac{\partial w}{\partial z} = 0. \quad (III.12)$$

Where u , v and w are the velocities in three directions x , y and z

- The momentum equations:

The x-axis:

$$u \frac{\partial u}{\partial x} + v \frac{\partial u}{\partial y} + w \frac{\partial u}{\partial z} = \frac{1}{\rho_{nf}} \left[-\frac{\partial p}{\partial x} + \mu_{nf} \left(\frac{\partial^2 u}{\partial x^2} + \frac{\partial^2 u}{\partial y^2} + \frac{\partial^2 u}{\partial z^2} \right) \right]. \quad (III.13)$$

The y-axis:

$$u \frac{\partial v}{\partial x} + v \frac{\partial v}{\partial y} + w \frac{\partial v}{\partial z} = \frac{1}{\rho_{nf}} \left[-\frac{\partial p}{\partial y} + \mu_{nf} \left(\frac{\partial^2 v}{\partial x^2} + \frac{\partial^2 v}{\partial y^2} + \frac{\partial^2 v}{\partial z^2} \right) \right]. \quad (III.14)$$

The z-axis:

$$u \frac{\partial w}{\partial x} + v \frac{\partial w}{\partial y} + w \frac{\partial w}{\partial z} = \frac{1}{\rho_{nf}} \left[-\frac{\partial p}{\partial z} + \mu_{nf} \left(\frac{\partial^2 w}{\partial x^2} + \frac{\partial^2 w}{\partial y^2} + \frac{\partial^2 w}{\partial z^2} \right) \right]. \quad (III.15)$$

Where p is the pressure.

- The equation of energy:

$$u \frac{\partial T}{\partial x} + v \frac{\partial T}{\partial y} + w \frac{\partial T}{\partial z} = \alpha_{nf} \left(\frac{\partial^2 T}{\partial x^2} + \frac{\partial^2 T}{\partial y^2} + \frac{\partial^2 T}{\partial z^2} \right). \quad (\text{III.16})$$

Where α_{nf} is the thermal diffusivity of nanofluids,

The heat conduction through the solid wall can be written as follows:

$$\left(\frac{\partial^2 T}{\partial x^2} + \frac{\partial^2 T}{\partial y^2} + \frac{\partial^2 T}{\partial z^2} \right) = 0 \quad (\text{III.17})$$

The following dimensionless variables are used to dimensionnalize the problem:

L Length of the mini channel for lengths

$$X = \frac{x}{L}; \quad Y = \frac{y}{L}; \quad Z = \frac{z}{L}$$

The dimensionless temperature is defined by $\theta = \frac{T-T_m}{\Delta T}$

Where ΔT is a temperature difference characteristic of our problem

For the velocity :

$$U = \frac{uL}{\alpha_f}; \quad V = \frac{vL}{\alpha_f}; \quad W = \frac{wL}{\alpha_f}$$

For the pressure:

$$P = \frac{\rho L^2}{\rho_{nf} \alpha_f^2}$$

By introducing the dimensionless greatness into the mass conservation equations (III.12), momentum equations (III.13-III.15) and energy (III.16- III.17), we obtain respectively:

The continuity equation:

$$\frac{\partial U}{\partial X} + \frac{\partial V}{\partial Y} + \frac{\partial W}{\partial Z} = 0 \quad (\text{III.18})$$

The momentum equations are written as follows:

$$U \frac{\partial U}{\partial X} + V \frac{\partial U}{\partial Y} + W \frac{\partial U}{\partial Z} = \left[-\frac{\partial P}{\partial X} + \frac{\mu_{nf}}{\rho_{nf} \alpha_f} \left(\frac{\partial^2 U}{\partial X^2} + \frac{\partial^2 U}{\partial Y^2} + \frac{\partial^2 U}{\partial Z^2} \right) \right]. \quad (\text{III.19})$$

$$U \frac{\partial V}{\partial X} + V \frac{\partial V}{\partial Y} + W \frac{\partial V}{\partial Z} = \left[-\frac{\partial P}{\partial Y} + \frac{\mu_{nf}}{\rho_{nf} \alpha_f} \left(\frac{\partial^2 V}{\partial X^2} + \frac{\partial^2 V}{\partial Y^2} + \frac{\partial^2 V}{\partial Z^2} \right) \right]. \quad (\text{III.20})$$

$$U \frac{\partial W}{\partial X} + V \frac{\partial W}{\partial Y} + W \frac{\partial W}{\partial Z} = \left[-\frac{\partial P}{\partial Z} + \frac{\mu_{nf}}{\rho_{nf} \alpha_f} \left(\frac{\partial^2 W}{\partial X^2} + \frac{\partial^2 W}{\partial Y^2} + \frac{\partial^2 W}{\partial Z^2} \right) \right]. \quad (\text{III.21})$$

The equation of energy:

$$U \frac{\partial \theta}{\partial X} + V \frac{\partial \theta}{\partial Y} + W \frac{\partial \theta}{\partial Z} = \frac{\alpha_{nf}}{\alpha_f} \left(\frac{\partial^2 \theta}{\partial X^2} + \frac{\partial^2 \theta}{\partial Y^2} + \frac{\partial^2 \theta}{\partial Z^2} \right). \quad (\text{III.22})$$

The heat conduction through the solid wall can be written as follows:

$$\left(\frac{\partial^2 \theta}{\partial X^2} + \frac{\partial^2 \theta}{\partial Y^2} + \frac{\partial^2 \theta}{\partial Z^2} \right) = 0 \quad (\text{III.23})$$

The above equations were solved using the above boundary conditions and shown (the form dimensionless) in the following table.

limits	Hydrodynamic conditions	Thermal conditions
at the inlet of mini channels, $Z=0$	$U = V = 0$ $W = w_{in} \cdot L / \alpha_f$	$\theta = 0$
at the outlet of mini channels, $Z=1$	$\frac{\partial U}{\partial Z} = \frac{\partial V}{\partial Z} = \frac{\partial W}{\partial Z} = 0$	$\frac{\partial \theta}{\partial Z} = 0$
the axis of symmetry	$\frac{\partial U}{\partial X} = \frac{\partial V}{\partial X} = \frac{\partial W}{\partial X} = 0$	$\frac{\partial \theta}{\partial X} = 0$

Table (III.2): Hydrodynamic and thermal boundary conditions in the form dimensionless

III.4.4. Mathematical model for the application N°2 studied: Numerical study of the influence of different types of nanofluids on thermal exchange in mini-channels

III.4.4.1 Geometries of the problems considered:

Figure (III.2) shows the geometry of the studied silicon mini channels cooler, using fluent industrial software. The dimensions of the mini-channel cooler are of the order of 42 x 52 mm with a thickness of 6 mm. This cooler is formed of 13 channels. The power of the electronic component is equal to 200W

Due to symmetry, and in order to reduce the grid size and the computational time, only half of the mini channel has been modeled.

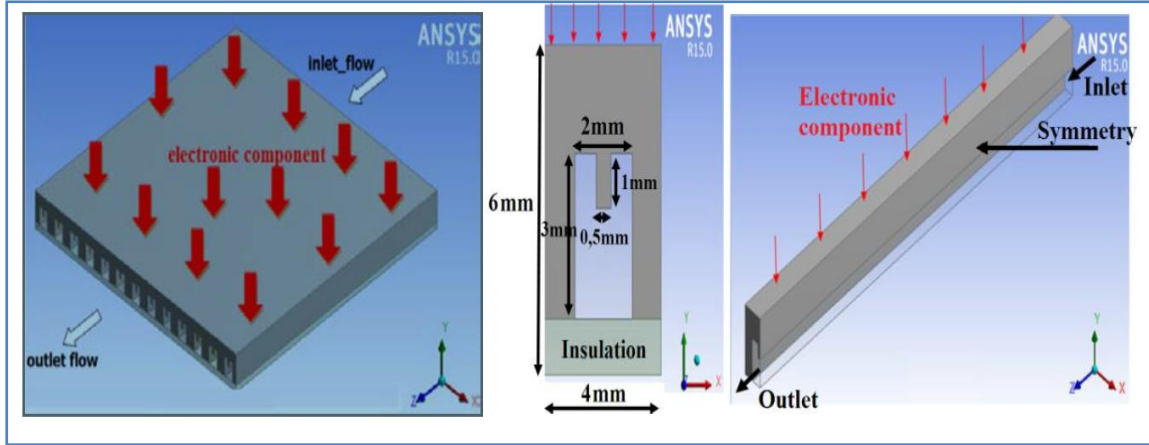


Figure (III.2): Schematic of the mini channels cooler studied and computational domain of mini channel heat sink

The boundary conditions are the same as those mentioned in the first problem (Application N°1).

III. 4.4.2 Mathematical formulation:

The governing equations are given in terms of mass conservation equation, momentum equation, energy conservation equation and solid equation as follows [122]:

The continuity equation is written as follows:

$$\frac{\partial u}{\partial x} + \frac{\partial v}{\partial y} + \frac{\partial w}{\partial z} = 0. \quad (\text{III.24})$$

Where V is the velocity

The momentum equations are written as follows:

The x-axis:

$$u \frac{\partial u}{\partial x} + v \frac{\partial u}{\partial y} + w \frac{\partial u}{\partial z} = \frac{1}{\rho_{nf}} \left[-\frac{\partial p}{\partial x} + \mu_{nf} \left(\frac{\partial^2 u}{\partial x^2} + \frac{\partial^2 u}{\partial y^2} + \frac{\partial^2 u}{\partial z^2} \right) \right]. \quad (\text{III.25})$$

The y-axis:

$$u \frac{\partial v}{\partial x} + v \frac{\partial v}{\partial y} + w \frac{\partial v}{\partial z} = \frac{1}{\rho_{nf}} \left[-\frac{\partial p}{\partial y} + \mu_{nf} \left(\frac{\partial^2 v}{\partial x^2} + \frac{\partial^2 v}{\partial y^2} + \frac{\partial^2 v}{\partial z^2} \right) \right]. \quad (\text{III.26})$$

The z-axis:

$$u \frac{\partial w}{\partial x} + v \frac{\partial w}{\partial y} + w \frac{\partial w}{\partial z} = \frac{1}{\rho_{nf}} \left[-\frac{\partial p}{\partial z} + \mu_{nf} \left(\frac{\partial^2 w}{\partial x^2} + \frac{\partial^2 w}{\partial y^2} + \frac{\partial^2 w}{\partial z^2} \right) \right]. \quad (\text{III.27})$$

Where p is the pressure

The energy equation is written as follows:

$$u \frac{\partial T}{\partial x} + v \frac{\partial T}{\partial y} + w \frac{\partial T}{\partial z} = \alpha_{nf} \left(\frac{\partial^2 T}{\partial x^2} + \frac{\partial^2 T}{\partial y^2} + \frac{\partial^2 T}{\partial z^2} \right) \quad (\text{III.28})$$

The heat conduction through the solid wall can be written as follows:

$$\left(\frac{\partial^2 T}{\partial x^2} + \frac{\partial^2 T}{\partial y^2} + \frac{\partial^2 T}{\partial z^2} \right) = 0 \quad (\text{III.29})$$

The same steps mentioned in the previous section (III.4.3.3) to determine the following dimensionless variables are used to dimensionnalize the problem.

III.4.5. Mathematical model for the application N°3 studied: Study of thermal exchanges in different geometry sections of mini-channels of a cooler for cooling a chip using nanofluids

III.4.5.1 Geometries of the problems considered:

The geometrical system is represented in Figure (III.3). It is based on the mini-channels cooler. Due to the symmetry configuration, we have considered only half of the cooler, as presented in Figure (III.4).

The geometry of the first case was used in an experimental and numerical study of a cooling system of electronic components by a liquid metal [127]. This cooler is formed of 10 channels and 11 fins. The power of the chip IGBT 1200 V 75 A is equal to 130 W with thermal insulation on all the outside faces of the cooler. The inlet temperature of the nano-fluid in the cooler in all cases is equal to $T = 298.15\text{K}$. In these simulations we consider the Cu-water, the Ag-water, and the Diamond-water as coolants with a volume fraction of 0.02.

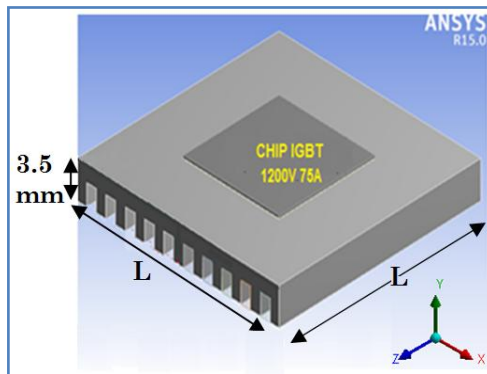


Figure (III.3): CAD model of the mini-channels cooler

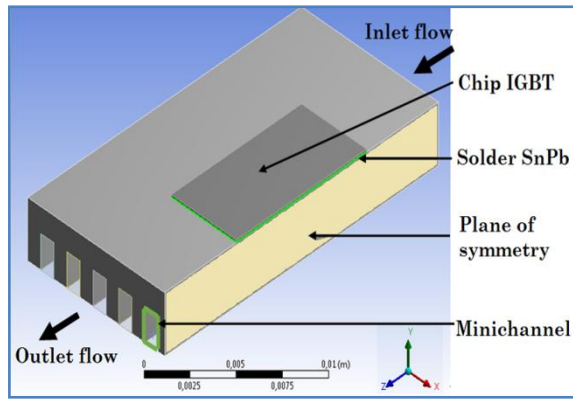


Figure (III. 4): Computational domain of mini-channels cooler

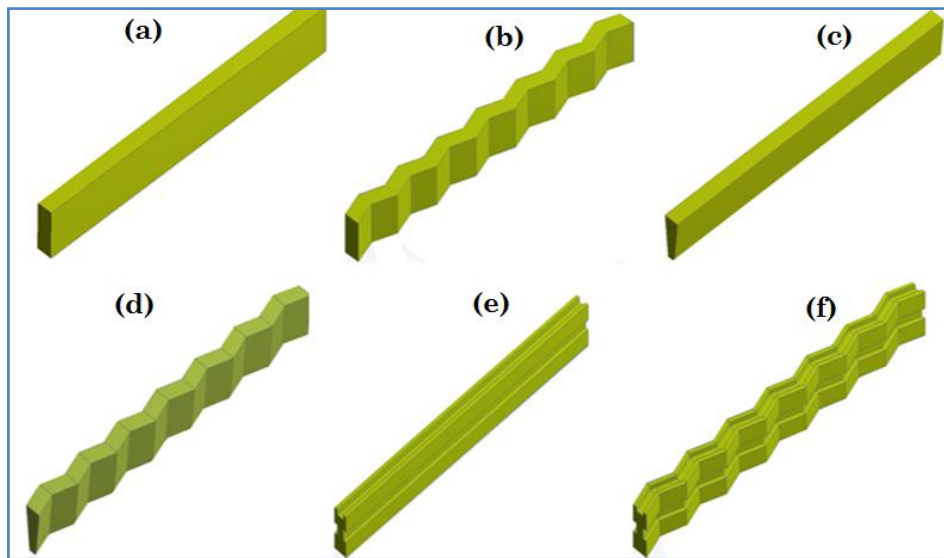
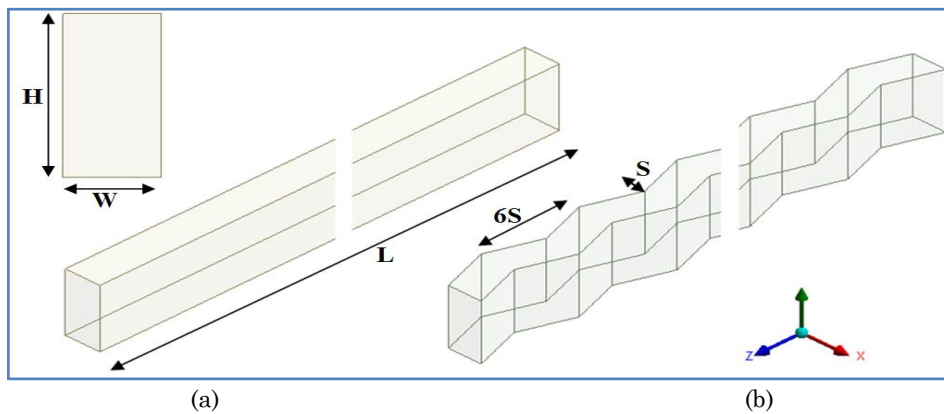


Figure (III. 5): Studied cases of the mini-channel coolers: (a) case 4, (b) case 5, (c) case 6, (d) case 7, (e) case 8, (f) case 9



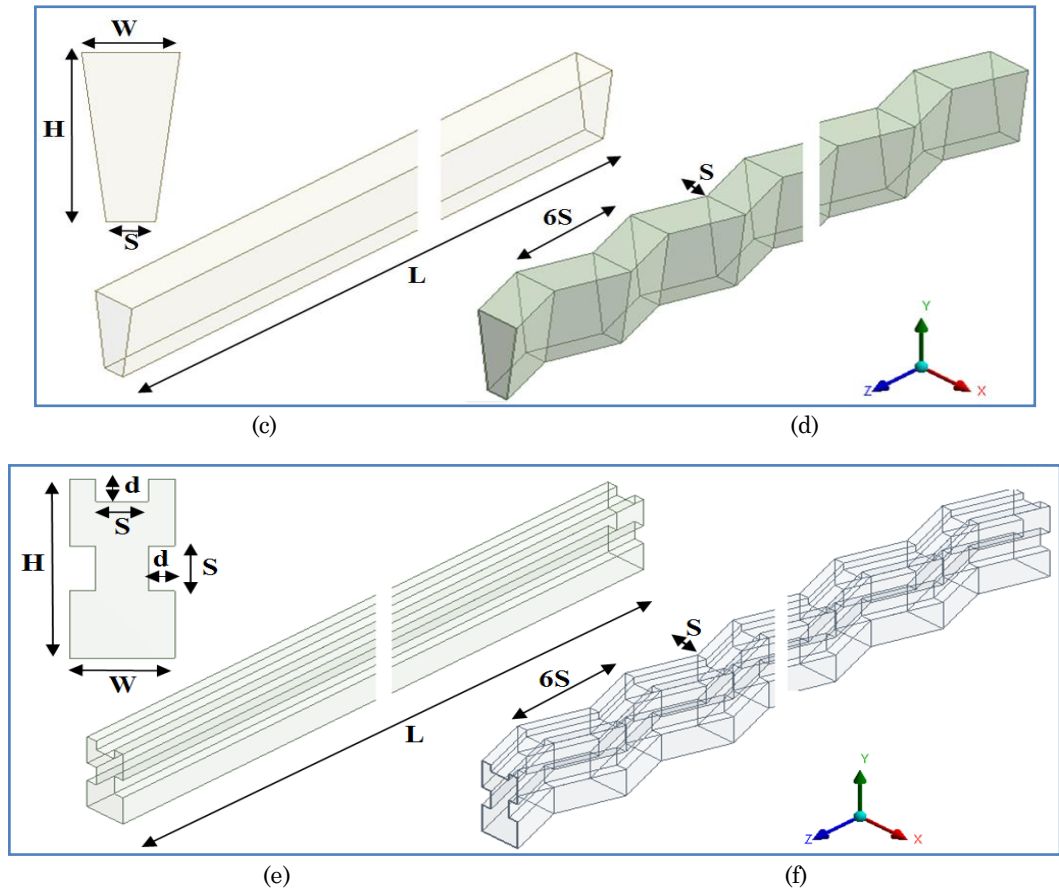


Figure (III.6): Geometrical dimension of the studied cases: (a) case 4, (b) case 5, (c) case 6, (d) case 7, (e) case 8, (f) case 9

Cases	H (mm)	W (mm)	L (mm)	S (mm)	d (mm)
Case 4 and case 5	2	1	21	/	/
Case 6 and case 7	2	1	21	0.50	/
Case 8 and case 9	2	1	21	0.50	0.25

Table (III.3). Dimension of the studied cases in this application.

III.4.5.2. Equations of the problem

The numerical model is governed by the equation of conservation of the mass, momentum equation, energy conservation equation and the equation of the solid.

The continuity equation is written as follows:

$$\frac{\partial u}{\partial x} + \frac{\partial v}{\partial y} + \frac{\partial w}{\partial z} = 0. \quad (\text{III.30})$$

Where u , v and w are the velocities in three directions x , y and z

The momentum equations:

The x-axis:

$$u \frac{\partial u}{\partial x} + v \frac{\partial u}{\partial y} + w \frac{\partial u}{\partial z} = \frac{I}{\rho_{nf}} \left[-\frac{\partial p}{\partial x} + \mu_{nf} \left(\frac{\partial^2 u}{\partial x^2} + \frac{\partial^2 u}{\partial y^2} + \frac{\partial^2 u}{\partial z^2} \right) \right]. \quad (\text{III.31})$$

Where p is the pressure.

The y-axis:

$$u \frac{\partial v}{\partial x} + v \frac{\partial v}{\partial y} + w \frac{\partial v}{\partial z} = \frac{I}{\rho_{nf}} \left[-\frac{\partial p}{\partial y} + \mu_{nf} \left(\frac{\partial^2 v}{\partial x^2} + \frac{\partial^2 v}{\partial y^2} + \frac{\partial^2 v}{\partial z^2} \right) + (\rho\beta)_{nf} g(T - T_0) \right]. \quad (\text{III.32})$$

Where T is the temperature, T_0 is the temperature at the entrance of the channel and g is the acceleration of gravity.

The z-axis:

$$u \frac{\partial w}{\partial x} + v \frac{\partial w}{\partial y} + w \frac{\partial w}{\partial z} = \frac{I}{\rho_{nf}} \left[-\frac{\partial p}{\partial z} + \mu_{nf} \left(\frac{\partial^2 w}{\partial x^2} + \frac{\partial^2 w}{\partial y^2} + \frac{\partial^2 w}{\partial z^2} \right) \right]. \quad (\text{III.33})$$

The equation of energy:

$$u \frac{\partial T}{\partial x} + v \frac{\partial T}{\partial y} + w \frac{\partial T}{\partial z} = \alpha_{nf} \left(\frac{\partial^2 T}{\partial x^2} + \frac{\partial^2 T}{\partial y^2} + \frac{\partial^2 T}{\partial z^2} \right). \quad (\text{III.34})$$

Where α is the thermal diffusivity,

The heat conduction through the solid wall can be written as follows:

$$\left(\frac{\partial^2 T}{\partial x^2} + \frac{\partial^2 T}{\partial y^2} + \frac{\partial^2 T}{\partial z^2} \right) = 0 \quad (\text{III.35})$$

The equations (III.29-III.34) can be changed to the form of dimensionless variables as follows:

$$X = \frac{x}{L}; \quad Y = \frac{y}{L}; \quad Z = \frac{z}{L}$$

The dimensionless temperature is defined by $\theta = \frac{T - T_m}{\Delta T}$

Where ΔT is a temperature difference characteristic of our problem

$$\text{For the velocity: } U = \frac{uL}{\alpha_f}; \quad V = \frac{vL}{\alpha_f}; \quad W = \frac{wL}{\alpha_f}$$

For the pressure:

$$P = \frac{pL^2}{\rho_{nf} \alpha_f^2}$$

The Rayleigh number Ra , and the Prandtl number Pr . These dimensionless numbers being defined by [123]:

$$Ra = \frac{g\beta_f L^4 q}{\vartheta_f \alpha_f k_f} \quad \text{and} \quad Pr = \frac{\vartheta_f}{\alpha_f}$$

By introducing the dimensionless greatness into the equations we obtain respectively:

The continuity equation:

$$\frac{\partial U}{\partial X} + \frac{\partial V}{\partial Y} + \frac{\partial W}{\partial Z} = 0 \quad (\text{III.36})$$

The momentum equations are written as follows:

$$U \frac{\partial U}{\partial X} + V \frac{\partial U}{\partial Y} + W \frac{\partial U}{\partial Z} = \left[-\frac{\partial P}{\partial X} + \frac{\mu_{nf}}{\rho_{nf}\alpha_f} \left(\frac{\partial^2 U}{\partial X^2} + \frac{\partial^2 U}{\partial Y^2} + \frac{\partial^2 U}{\partial Z^2} \right) \right] \quad (\text{III.37})$$

$$U \frac{\partial V}{\partial X} + V \frac{\partial V}{\partial Y} + W \frac{\partial V}{\partial Z} = \left[-\frac{\partial P}{\partial Y} + \frac{\mu_{nf}}{\rho_{nf}\alpha_f} \left(\frac{\partial^2 V}{\partial X^2} + \frac{\partial^2 V}{\partial Y^2} + \frac{\partial^2 V}{\partial Z^2} \right) \right] + \frac{(\rho\beta)_{nf}}{\rho_{nf}\beta_f} Ra.Pr \theta \quad (\text{III.38})$$

$$U \frac{\partial W}{\partial X} + V \frac{\partial W}{\partial Y} + W \frac{\partial W}{\partial Z} = \left[-\frac{\partial P}{\partial Z} + \frac{\mu_{nf}}{\rho_{nf}\alpha_f} \left(\frac{\partial^2 W}{\partial X^2} + \frac{\partial^2 W}{\partial Y^2} + \frac{\partial^2 W}{\partial Z^2} \right) \right] \quad (\text{III.39})$$

The equation of energy:

$$U \frac{\partial \theta}{\partial X} + V \frac{\partial \theta}{\partial Y} + W \frac{\partial \theta}{\partial Z} = \frac{\alpha_{nf}}{\alpha_f} \left(\frac{\partial^2 \theta}{\partial X^2} + \frac{\partial^2 \theta}{\partial Y^2} + \frac{\partial^2 \theta}{\partial Z^2} \right) \quad (\text{III.40})$$

The heat conduction through the solid wall can be written as follows:

$$\left(\frac{\partial^2 \theta}{\partial X^2} + \frac{\partial^2 \theta}{\partial Y^2} + \frac{\partial^2 \theta}{\partial Z^2} \right) = 0 \quad (\text{III.41})$$

III.4.5.3. Boundary conditions

The boundary conditions used for the configuration studied in this application (Figure (III.4)) are as follows:

limits	Hydrodynamic conditions	Thermal conditions
At the inlet of mini channels	$u = v = 0$ $w = w_{in} = constant$	$T = T_{in} = constant$
At the walls of the mini channel	$u = v = w = 0$	$T = T_{wall}$
At the outlet of mini channel (out flow)	$\frac{\partial u}{\partial z} = \frac{\partial v}{\partial z} = \frac{\partial w}{\partial z} = 0$	$\frac{\partial T}{\partial z} = 0$
the axis of symmetry	$\frac{\partial u}{\partial x} = \frac{\partial v}{\partial x} = \frac{\partial w}{\partial x} = 0$	$\frac{\partial T}{\partial x} = 0$

Table (III.4): Hydrodynamic and thermal boundary conditions

The above equations (dimensionless system) were solved using boundary conditions (see figure (III.4) and table (III.4)).

- **Heat transfer**

The rate of heat transfer by convection is described by the dimensional number called the Nusselt number, Nu which plays a particular role. This dimensional number represents the ratio of the convective heat flow of the pure diffusion heat flow. The convective flow is given by Newton's law:

$$Q_{conv} = hA_w \Delta T \quad (\text{III.42})$$

The conductive flux is given by the Fourier law:

$$Q_{cond} = kA_w \frac{\Delta T}{D_h} \quad (\text{III.43})$$

The hydraulic diameter (D_h) is calculated using [130]:

$$D_h = \frac{4.A_c}{P_c} \quad (\text{III.44})$$

Reynolds number is defined as [131]

$$Re = \frac{\rho_{nf} \cdot w \cdot D_h}{\mu_{nf}} \quad (\text{III.45})$$

So the Nusselt number is defined by [125]:

$$Nu = \frac{Q_{conv}}{Q_{cond}} = \frac{h.A_w.\Delta T}{k.A_w.\frac{\Delta T}{D_h}} = \frac{h.D_h}{k} \quad (\text{III.46})$$

Where D_h is the hydraulic diameter of the channel and k is the thermal conductivity of the fluid, h is the convective exchange coefficient.

Once the temperature field has been calculated, the local heat transfer coefficient $h(z)$ can be calculated through the back wall using the formula:

$$h(z) = \frac{q}{(T_s(z) - T_m)} \quad (\text{III.47})$$

When $T_s(z)$ is the local temperature of a point located on the heated surface. This value of $h(z)$ makes it possible to calculate the local Nusselt number by means of the formula:

$$Nu(z) = h(z) \frac{D_h}{k_f} \quad (\text{III.48})$$

The average Nusselt number Nu_{av} is determined by integration $Nu(z)$ along the active part of the hot wall.

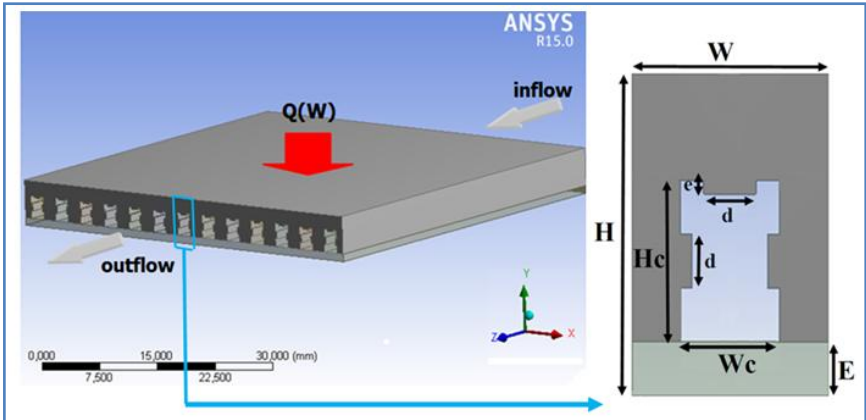
$$Nu_{av} = \frac{1}{L} \int_0^L Nu(z) dz \quad (\text{III.49})$$

III.4.6. Mathematical model for the application N°4 studied: Influence of the types of nanoparticles, nanoparticles volume concentration and types of cooler metals (copper cooler and aluminum cooler) on the heat transfer in a mini-channels cooler.

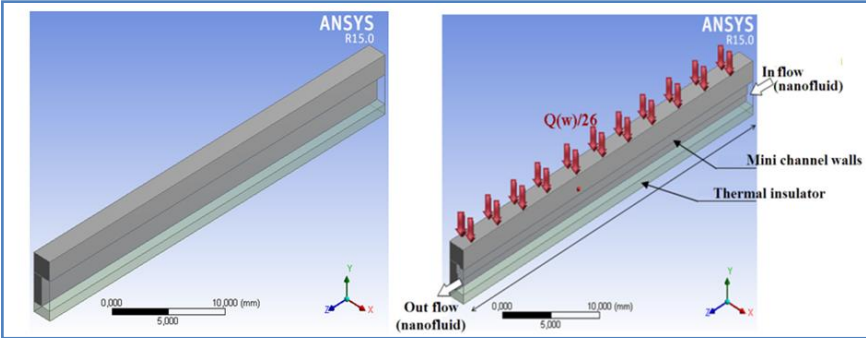
III.4.6.1 Geometries of the problems considered:

Figure (III.7) shows the geometry of the cooler mini channels. The dimensions of this cooler are the same that are considered by **Tawk *et al.* [126]**

The difference is in the dimensions and shape of mini channels. In fact, this cooler is formed by 13 channels and 12 fins. Indeed, we assume that the bottom of the cooler contains a thermal insulator and that the upper surface of the cooler has an electronic component with a constant value. In these conditions, the thermal insulation is considered upon all the outside faces of the cooler. At the superior face of the cooler, the power of electronic component is equal to 130 W, In these simulations we consider the Cu-water, the Ag-water, and the Diamond-water as coolants with a volume fraction of $\phi=0,02$. Due to the symmetry, we have considered only half of the fin and half of the mini-channel.



(a) Geometrical arrangements of a mini channel



(b) Half a mini channel.

(c) Boundary conditions

Figure (III.7): CAD model of the mini channels cooler.

III.4.6.2. Boundary Conditions

The boundary conditions at the inlet are written as follows:

$$u = v = 0 \quad ; \quad w = w_{in} = constant \quad ; \quad T = T_{in} = constant$$

At the outlet, we can write:

$$P = P_{out} = 0$$

A non-slip boundary condition is specified for the fluid at the level of the wall of the mini channel, we can write:

$$u = v = w = 0 \quad ; \quad T = T_{solid}$$

- The maximum flux of the electronic component is constant with thermal insulation on all external faces of the cooler

- At the solid/nano-fluid interface, the continuity of the flux can be written as follows:

$$k_s \frac{\partial T}{\partial n} \Big|_{wall} = k_{nf} \frac{\partial T}{\partial n} \Big|_{wall} \quad (III.50)$$

III.4.6.3. Equations of the problem:

Mathematical model for the equation of conservation of mass, momentum equation, energy conservation equation and equation of the solid in this section are the same ones mentioned in the previous section (section III.4.5.2)

The table (III.5) represents the dimensions of unit cell of mini channels we used in this application (application N°4).

H	W	L	E	H _c	W _c	d	e	D _h
6	4	42	1	3	2	1	0,25	1,826

Table (III.5) Dimensions of unit cell of mini channels. (Unit in mm)

III.4.7. the Mathematical model for the application N°5 studied: Study in three dimensions of the influence of the fluids' nature and obstacle position on the cooling of electronic component.

III.4.7.1 Geometries of the problems considered:

The configuration studied is shown schematically in Figure (III.8). It represents electronic component, mounted in a mini channel with the addition of obstacles in three cases, and one case does not contain the obstacles in mini channel. Within the mini-channel of dimensions (10 x 10 x 108 mm³) on the cooling of electronic component. The power of the electronic component is constant. In these simulations we consider the Al₂O₃-water, SiO₂-water and TiO₂-water as

coolants. The numerical results are obtained by choosing a Reynolds number (Re) between 300 and 500 and considering the flow regime to be stationary.

The maximum flux of the electronic component is constant; the inlet temperature of the nanofluid all cases of the mini channels is set at 293K.

The dimensions of the mini channel and the obstacles used in this application are shown in Table (III.6).

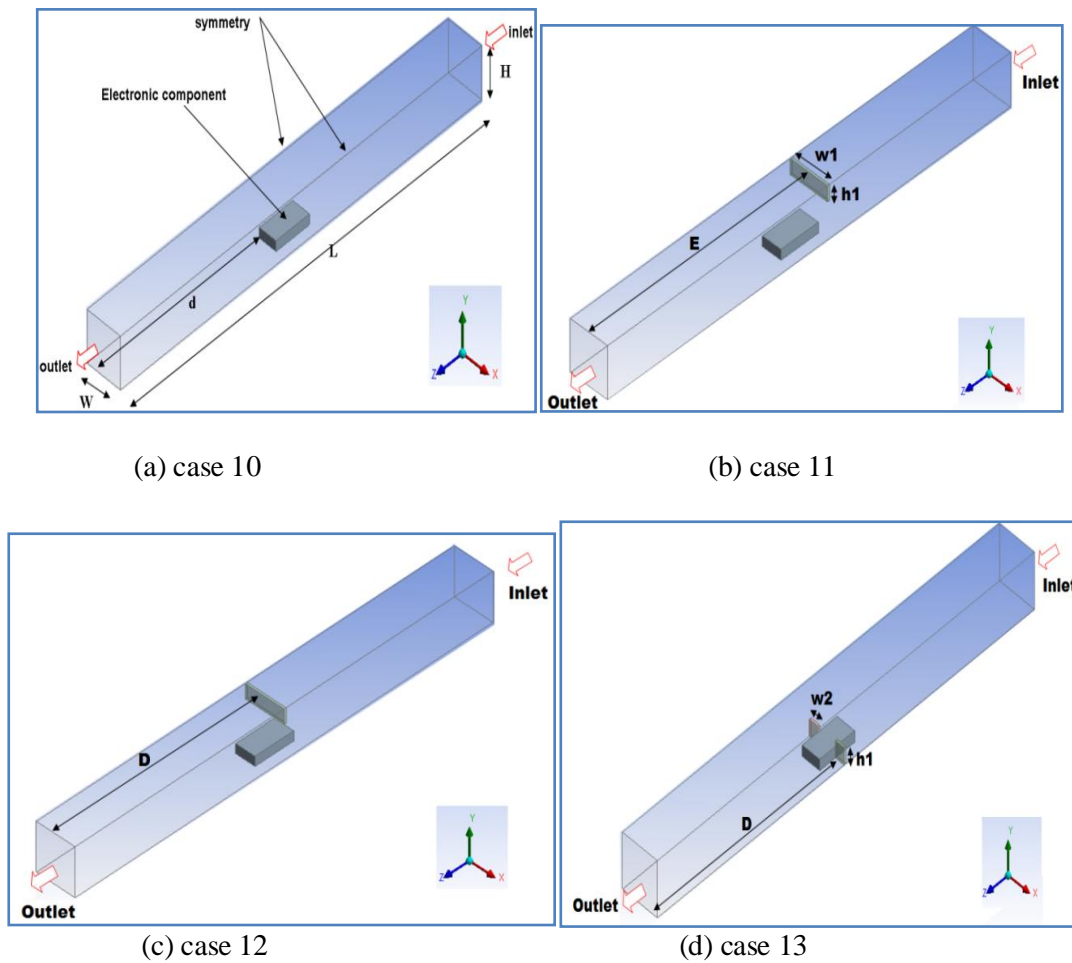


Figure. (III.8): Four cases of studied mini-channels.

Case 10: Minichannel containing electronic component without obstacle.

Case 11: Minichannel containing electronic component with an obstacle located on the upper wall of the channel and a distance of E from the outlet.

Case 12: Minichannel containing electronic component with an obstacle located on the upper wall of the channel and a distance of D from the outlet.

Case 13: Minichannel containing electronic component with an obstacle located on the sides of the electronic component built into the bottom wall of the channel and at a distance of D from the outlet.

Length L[mm]	Height of minichannel H[mm]	Width of minichannel W [mm]	D [mm]	E [mm]	w1 [mm]	w2 [mm]	h1 [mm]	d [mm]
108	10	10	54	59	10	2.5	3	49

Table (III.6): The dimensions of mini channel and obstacles studied in this application

The thermophysical properties of water and nanoparticles used in this application (application N°5) at T= 300K are grouped in Table (III.1) [127, 128, 129]

III.4.7.2. Boundary conditions

The boundary conditions at the inlet are written as follows:

$$u = v = 0$$

$$w = w_{in} = \text{constant}, \quad T = T_{in} = \text{constant}$$

- At the outlet, we can write: the gauge pressure is zero
- A non-slip boundary condition is specified for the fluid at the level of the wall of the mini channel, we can write:

$$u = v = w = 0, \quad T = T_{wall}$$

- At the fluid-solid interface, the continuity of the heat flux at the interface between the solid and the fluid is implemented using this formula:

$$k_s \frac{\partial T}{\partial n} \Big|_{wall} = k_{nf} \frac{\partial T}{\partial n} \Big|_{wall} \quad (\text{III.51})$$

III.4.7.3. Equations of the problem:

The continuity equation is written as follows:

$$\frac{\partial u}{\partial x} + \frac{\partial v}{\partial y} + \frac{\partial w}{\partial z} = 0. \quad (\text{III. 52})$$

Where u , v and w are the velocities in three directions x , y and z

The momentum equations:

The x-axis:

$$u \frac{\partial u}{\partial x} + v \frac{\partial u}{\partial y} + w \frac{\partial u}{\partial z} = \frac{1}{\rho_{nf}} \left[-\frac{\partial p}{\partial x} + \mu_{nf} \left(\frac{\partial^2 u}{\partial x^2} + \frac{\partial^2 u}{\partial y^2} + \frac{\partial^2 u}{\partial z^2} \right) \right]. \quad (\text{III.53})$$

Where P is the pressure.

The y-axis:

$$u \frac{\partial v}{\partial x} + v \frac{\partial v}{\partial y} + w \frac{\partial v}{\partial z} = \frac{1}{\rho_{nf}} \left[-\frac{\partial p}{\partial y} + \mu_{nf} \left(\frac{\partial^2 v}{\partial x^2} + \frac{\partial^2 v}{\partial y^2} + \frac{\partial^2 v}{\partial z^2} \right) + (\rho\beta)_{nf} g(T - T_0) \right]. \quad (\text{III.54})$$

Where T is the temperature, T_0 is the temperature at the entrance of the channel and g is the acceleration of gravity.

The z-axis:

$$u \frac{\partial w}{\partial x} + v \frac{\partial w}{\partial y} + w \frac{\partial w}{\partial z} = \frac{1}{\rho_{nf}} \left[-\frac{\partial p}{\partial z} + \mu_{nf} \left(\frac{\partial^2 w}{\partial x^2} + \frac{\partial^2 w}{\partial y^2} + \frac{\partial^2 w}{\partial z^2} \right) \right]. \quad (\text{III.55})$$

The equation of energy:

$$u \frac{\partial T}{\partial x} + v \frac{\partial T}{\partial y} + w \frac{\partial T}{\partial z} = \alpha_{nf} \left(\frac{\partial^2 T}{\partial x^2} + \frac{\partial^2 T}{\partial y^2} + \frac{\partial^2 T}{\partial z^2} \right) + \frac{q_v}{(\rho C_P)_{nf}}. \quad (\text{III.56})$$

Where α is the thermal diffusivity, q_v is volumetric heat.

III.4.7.4. dimensionless equations of the problem:

According to the dimensional equations mentioned in section (III.4.7.3), dimensionless variables can be written as follows:

$$X = \frac{x}{L}; \quad Y = \frac{y}{L}; \quad Z = \frac{z}{L}$$

The dimensionless temperature is defined by $\theta = \frac{T - T_m}{\Delta T}$

Where ΔT is a temperature difference characteristic of our problem

For the velocity:

$$U = \frac{uL}{\alpha_f}; \quad V = \frac{vL}{\alpha_f}; \quad W = \frac{wL}{\alpha_f}$$

For the pressure

$$P = \frac{pL^2}{\rho_{nf} \alpha_f^2}$$

By introducing the dimensionless greatness into the mass conservation equations (III.52), movement (III.53-III.55) and energy (III.56), we obtain respectively:

The continuity equation

$$\frac{\partial U}{\partial X} + \frac{\partial V}{\partial Y} + \frac{\partial W}{\partial Z} = 0. \quad (\text{III.57})$$

The momentum equations are written as follows:

$$U \frac{\partial U}{\partial X} + V \frac{\partial U}{\partial Y} + W \frac{\partial U}{\partial Z} = \left[-\frac{\partial P}{\partial X} + \frac{\mu_{nf}}{\rho_{nf} \alpha_f} \left(\frac{\partial^2 U}{\partial X^2} + \frac{\partial^2 U}{\partial Y^2} + \frac{\partial^2 U}{\partial Z^2} \right) \right]. \quad (\text{III.58})$$

$$U \frac{\partial V}{\partial X} + V \frac{\partial V}{\partial Y} + W \frac{\partial V}{\partial Z} = \left[-\frac{\partial P}{\partial Y} + \frac{\mu_{nf}}{\rho_{nf}\alpha_f} \left(\frac{\partial^2 V}{\partial X^2} + \frac{\partial^2 V}{\partial Y^2} + \frac{\partial^2 V}{\partial Z^2} \right) \right] + \frac{(\rho\beta)_{hf}}{\rho_{nf}\beta_f} Ra.Pr \theta \quad (III.59)$$

$$U \frac{\partial W}{\partial X} + V \frac{\partial W}{\partial Y} + W \frac{\partial W}{\partial Z} = \left[-\frac{\partial P}{\partial Z} + \frac{\mu_{nf}}{\rho_{nf}\alpha_f} \left(\frac{\partial^2 W}{\partial X^2} + \frac{\partial^2 W}{\partial Y^2} + \frac{\partial^2 W}{\partial Z^2} \right) \right]. \quad (III.60)$$

The equation of energy:

$$U \frac{\partial \theta}{\partial X} + V \frac{\partial \theta}{\partial Y} + W \frac{\partial \theta}{\partial Z} = \frac{\alpha_{nf}}{\alpha_f} \left(\frac{\partial^2 \theta}{\partial X^2} + \frac{\partial^2 \theta}{\partial Y^2} + \frac{\partial^2 \theta}{\partial Z^2} \right) + \frac{q_v.L^2}{(\rho C_p)_{hf}.\alpha_f.\Delta T}. \quad (III.61)$$

The heat conduction through the solid wall can be written as follows:

$$\left(\frac{\partial^2 \theta}{\partial X^2} + \frac{\partial^2 \theta}{\partial Y^2} + \frac{\partial^2 \theta}{\partial Z^2} \right) = 0 \quad (III.62)$$

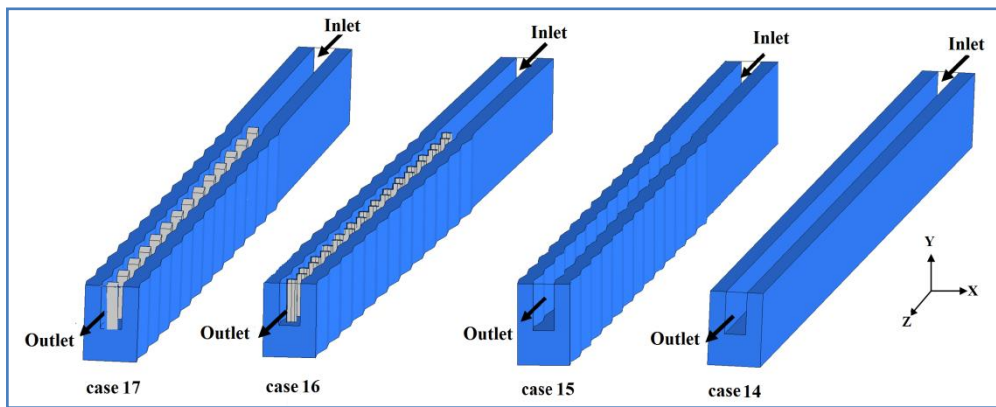
The dimensionless boundary conditions are:

- At the inlet of mini channels: $Z=0$; $U=0$; $V=0$; $W=w_{in} L/\alpha_f$; $\theta=0$
- At the outlet of mini channels: $Z=1$; $\frac{\partial U}{\partial Z} = \frac{\partial V}{\partial Z} = \frac{\partial W}{\partial Z} = 0$; $\frac{\partial \theta}{\partial Z} = 0$
- The walls adiabatic : $Y=0$; $0 \leq Z \leq 1$; $0 \leq X \leq W/L$; $U=0$; $V=0$; $W=0$; $\frac{\partial \theta}{\partial Y} = 0$
 $Y=H/L$; $0 \leq Z \leq 1$; $0 \leq X \leq W/L$; $U=0$; $V=0$; $W=0$; $\frac{\partial \theta}{\partial Y} = 0$
- The axis symmetry: $\frac{\partial U}{\partial X} = \frac{\partial V}{\partial X} = \frac{\partial W}{\partial X} = 0$; $\frac{\partial \theta}{\partial X} = 0$

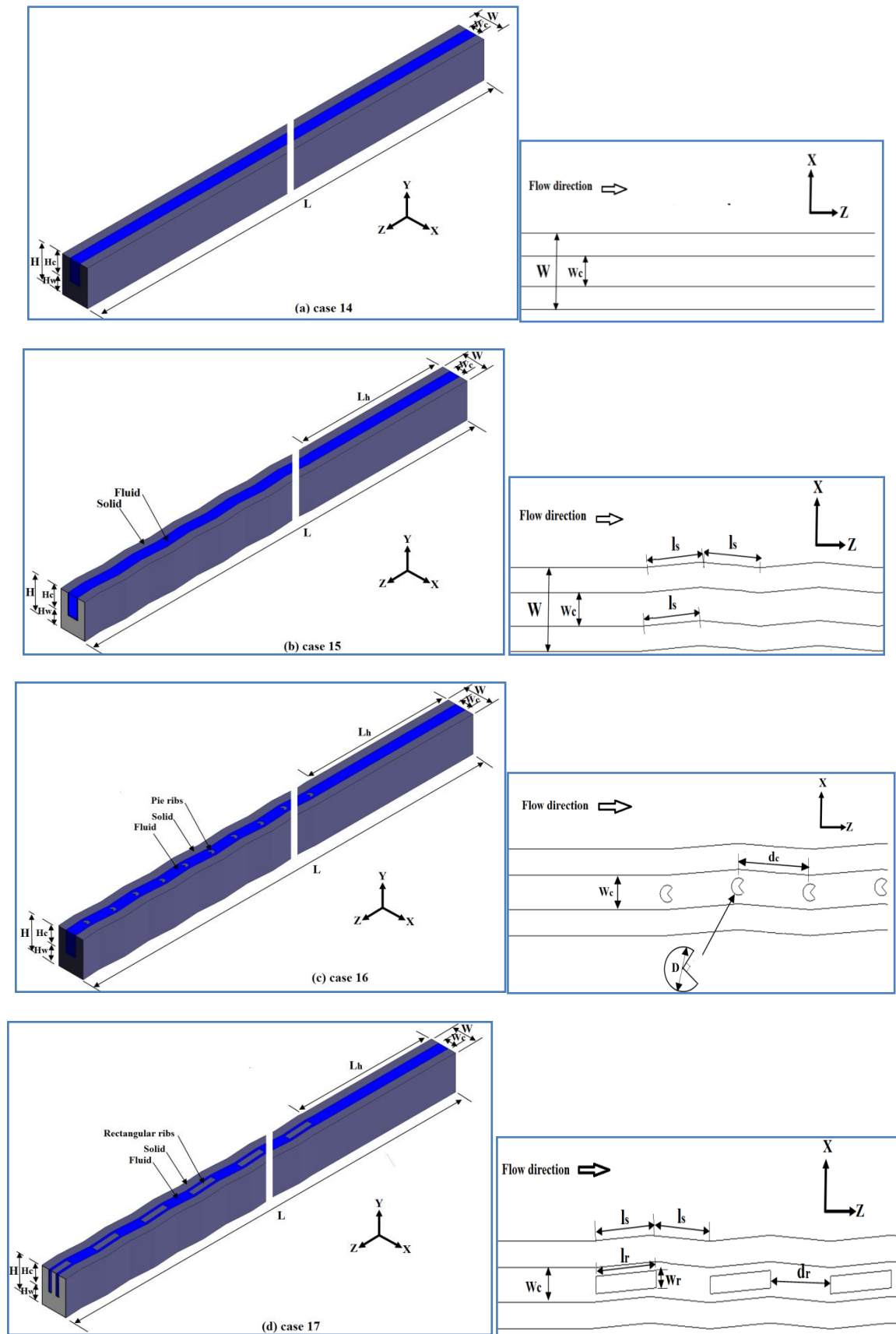
III.4.8. Mathematical model for the application N°6 studied:

A numerical study on the effect of the addition of the pie shape ribs and parallelogram ribs in micro- channels on thermal performance using Diamond - water nanofluid

III.4.8.1 Geometries of the problems considered:



(1.a) CAD model of the micro channel heat sink



(1.b) Schematic diagrams of four cases with the dimensions

Figure (III.9). Studied cases of the micro-channel heat sink

The geometries of the system are represented in Figure (III.9). It is based on the micro-channel heat sinks. The microchannel heat sinks of rectangular cross section consist of 20 microchannels. Each microchannel has a length L , a width W_c and a height H_c . The unvaried total area being cooled (bottom area) is 10 mm x 5 mm. Due to the symmetry, we have considered only the single of the micro channel each case as presented in Figure III.9(a). Heat is supplied to the silicon MCHS substrate through a bottom surface where the electronic chips are attached. The heat flux generated by the chips equal $q=100W/cm^2$ and thermal insulation on all the outside faces of the heat sinks are considered.

We have chosen silicon micro channel heat sinks for four cases, microchannels heat sinks and we used a nano fluid diamond-water with 0.05 volume concentration of diamond nanoparticle as a coolant.

- (a) Case 14: Single rectangular micro channel without ribs.
- (b) Case 15: A quarter of the length of the channel rectangular and the length the rest are wavy.
- (c) Case 16: The same is the second case with the addition of pie shape ribs at a distance $z=6.67$ mm from the micro channel exit.
- (d) Case 17: The same is the second case with the addition of parallelogram ribs at a distance $z=6.67$ mm from the micro channel exit.

The dimensions of the studied cases used in this application (application N°6) are given in table (III.7).

	Case 14	Case 15	Case 16	Case 17
L (mm) (base fluid)	10	10	10	10
H (mm)	0.35	0.35	0.35	0.35
W (mm)	0.25	0.25	0.25	0.25
Hc (mm)	0.20	0.20	0.20	0.20
Wc (mm)	0.10	0.10	0.10	0.10
Is (mm)	/	0.25	0.25	0.25
Ir (mm)	/	/	/	0.25
Lh (mm)	3.33	3.33	3.33	3.33
Hw (mm)	0.15	0.15	0.15	0.15
Wr (mm)	/	/	/	0.05
dr (mm)	/	/	/	0.25
dc (mm)	/	/	0.25	/
D (mm)	/	/	0.05	/

Table (III.7): Geometrical dimension of the studied cases.

III.4.8.2. Boundary conditions

- The boundary conditions at the inlet are written as follows:

$$u = v = 0$$

$$w = w_{in} = \text{constant}, \quad T = T_{in} = \text{constant}$$

- At the outlet, we can write: the gauge pressure is zero

-At the solid/nano-fluid interface, the continuity of the flux can be written as follows:

$$k_s \frac{\partial T}{\partial n} \Big|_{\text{wall}} = k_{nf} \frac{\partial T}{\partial n} \Big|_{\text{wall}}$$

- The velocity components of the fluid at the level of the channel wall are equal to zero.

- The maximum flux of the electronic component is constant.

III.4.8.3. Equations of the problem

Government's equations are governed by the equation of conservation of mass, momentum equation, energy conservation equation and the equation of the solid,

The continuity equation is written as follows:

$$\frac{\partial u}{\partial x} + \frac{\partial v}{\partial y} + \frac{\partial w}{\partial z} = 0 \quad (\text{III.63})$$

where u , v and w are the velocity components in x -axis, y -axis and the z -axis respectively.

The momentum equations along the x -axis, the y -axis and the z -axis are written as follows:

x -axis :

$$u \frac{\partial u}{\partial x} + v \frac{\partial u}{\partial y} + w \frac{\partial u}{\partial z} = \frac{1}{\rho_{nf}} \left[-\frac{\partial p}{\partial x} + \mu_{nf} \left(\frac{\partial^2 u}{\partial x^2} + \frac{\partial^2 u}{\partial y^2} + \frac{\partial^2 u}{\partial z^2} \right) \right] \quad (\text{III.64})$$

y -axis :

$$u \frac{\partial v}{\partial x} + v \frac{\partial v}{\partial y} + w \frac{\partial v}{\partial z} = \frac{1}{\rho_{nf}} \left[-\frac{\partial p}{\partial y} + \mu_{nf} \left(\frac{\partial^2 v}{\partial x^2} + \frac{\partial^2 v}{\partial y^2} + \frac{\partial^2 v}{\partial z^2} \right) \right] \quad (\text{III.65})$$

z -axis :

$$u \frac{\partial w}{\partial x} + v \frac{\partial w}{\partial y} + w \frac{\partial w}{\partial z} = \frac{1}{\rho_{nf}} \left[-\frac{\partial p}{\partial z} + \mu_{nf} \left(\frac{\partial^2 w}{\partial x^2} + \frac{\partial^2 w}{\partial y^2} + \frac{\partial^2 w}{\partial z^2} \right) \right] \quad (\text{III.66})$$

where ρ_{nf} , μ_{nf} and p are the density, dynamic viscosity and the pressure of the nanofluid, respectively

The energy equation is written as follows:

$$u \frac{\partial T}{\partial x} + v \frac{\partial T}{\partial y} + w \frac{\partial T}{\partial z} = \alpha_{nf} \left(\frac{\partial^2 T}{\partial x^2} + \frac{\partial^2 T}{\partial y^2} + \frac{\partial^2 T}{\partial z^2} \right) \quad (\text{III.67})$$

Where T is the temperature of the nanofluid, α_{nf} is thermal diffusivity of the nano fluid.

- The heat conduction through the solid wall

$$\frac{\partial^2 T_s}{\partial x^2} + \frac{\partial^2 T_s}{\partial y^2} + \frac{\partial^2 T_s}{\partial z^2} = 0 \quad (\text{III.68})$$

The same steps mentioned in the previous section (III.4.3.3) to determine the following dimensionless variables are used to dimensionnalize the problem.

The hydraulic diameter is defined as the ratio of cross sectional area over the wetted parameter and it is calculated using [130]:

$$D_h = \frac{4.A_c}{P_c} \quad (\text{III.69})$$

The average heat transfer coefficient of the micro channels is determined by the following [131, 124]:

$$h_{av} = \frac{Q}{NA_w(T_w - T_m)} \quad (\text{III.70})$$

$$Nu = \frac{h_{av} D_h}{k_{nf}} \quad (\text{III.71})$$

where A_w , T_w , N , k_{nf} , T_m are the convection heat transfer area, average temperature of the wall, number of micro-channels, fluid thermal conductivity and average temperature of fluid, respectively.

Reynolds number is defined as [131]

$$Re = \frac{\rho_{nf} \cdot w \cdot D_h}{\mu_{nf}} \quad (\text{III.72})$$

Average fanning friction factor are calculated by the following equation [132]

$$f = \frac{(P_{in} - P_{out}) D_h}{2 \rho_{nf} \cdot w^2 \cdot L} \quad (\text{III.73})$$

Where $(p_{in} - p_{out})$ and L are the difference between the inlet pressure and outlet pressure and the length of micro channel, respectively

The thermal resistance of the heat sink is calculated by [131]:

$$R_{th} = \frac{T_{max} - T_{in}}{Q} \quad (III.74)$$

Where T_{max} and T_{in} are maximum temperature on the bottom wall and fluid inlet temperature, respectively.

III.5. Numerical resolution using CFD code

Computational Fluid Dynamics or CFD is the analysis of systems that include fluid flow, heat transfer and associated phenomena such as chemical reactions using numerical methods via computer simulations which rely on powerful computers that have the ability to simulate and give satisfactory and acceptable solutions. The simulation technique using the computational fluid dynamics has wide spread or expansion in several fields especially in the field of industry. As this technique deals with relatively complex problems as it is much less expensive than experimental methods but it is not without some disadvantages, as computation time may extend for large models, and also possible uncertainties caused by too little computing values per cell and hence therefore resulting interpolation errors. Experimental methods are also often difficult to implement and it takes some time to solve the problem in addition to being expensive, but it is realistic and can be used as a confirmation of numerical results. In addition to that, there are analytical methods that rely on hypotheses, but they are limited and are not appropriate to complex phenomena.

III.6. Numerical methods

The objective of numerical methods is to provide a solution approach to the real behavior of physical phenomena. Among the most widely used numerical methods for solving partial differential equations numerically it can be mentioned as follows:

- to finite difference method (FDM).
- to finite elements method (FEM).
- to finite volumes method (FVM).

The finite difference method presents a technic to solve partial differential equations, with approximating derivatives by finite differences. This method consists of subdividing the domain of study into a determined number of nodes and in representing the function searched in each of the nodes of the domain by a taylor series expansion. Thus, the differential equation is transformed into an algebraic equation for each node. On the other hand, the finite difference

method (FDM) is simple and effective on structured grids and does not conserve momentum, energy, and mass on coarse grids.

As for finite element method consists of transforming the differential equations into integral forms based on the concept of minimization of a quantity (such as energy...), leading to the exact solution. In other term, it is about finding a global function representing the mathematical model in the studied domain.

The fundamental principle of this method is consisted of [133,134] - subdividing the field of study into elementary regions (Finis Elements) and build the integral forms and also minimize the integral, then a matrix organization of calculations, in the last a resolution of the algebraic system. This method that helps for the resolution of partial differential equations especially in complex geometries. Its implementation, on the other hand, the finite element method (FEM) is used in structural analysis of solids, but is also applicable to fluids. It is the highest accuracy on coarse grids. However, it is slow for large problems and not well suited for turbulent flow.

As for the finite volume method, it is widely used and is well suited to the resolution of conservation laws (mass, momentum, energy) also, it's a common approach used in CFD codes. One of its advantages is that the equations are calculated iteratively by imposing initial conditions and boundary conditions of the domain. The solver then seeks a solution of the fields of pressure, velocity, temperature, (...), This method can be discussed in the next title.

III.7. Finite volume method

The principle of the finite volume method is based on a discretization technique, whereby computation domain is divided into a finite number of elementary subdomains, called control volumes. In this method, it converts partial derivatives conservation equations into algebraic equations, which can subsequently be solved numerically.

The decisive advantage of this method over other methods is that it is distinguished by the reliability of its results and solution speed, its ability to deal with complex geometries, its guarantee for the conservation of mass and momentum, its adaptation to the physical problem.

The technique of the control volumes consists of integration of partial derivatives equations on each control volume to obtain discretized equations. The different steps of the finite volume method are:

- The discretization of the domain considered in control volume
- Writing algebraic equations at the nodes of the mesh;

- Solving the algebraic system obtained

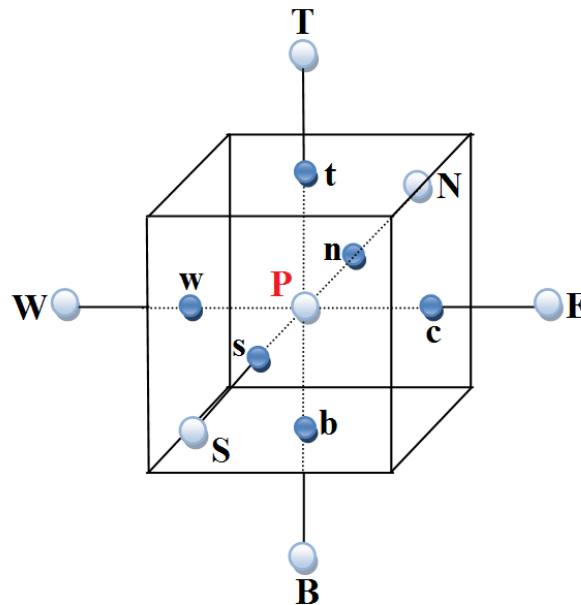


Figure (III.10): A cell or control volume in three dimensions

An example of control volume is shown in the figure below (Figure III.10). A point is positioned at the center of each and is called the control volume center, it will be denoted P (principal node), the nodes of neighboring volumes will be noted according to their positions NSWET and B (relating to the North, South, West, Top and Bottom directions respectively) .

III.8. Mesh

The discretization of the domain is obtained by a mesh made up of nodes. Thus a volume element (control volume) is defined around each node.

The scalar quantities (pressure, temperature) are stored in the node (P) of the mesh, while the vector quantities (u, v and w) are stored in the middle of the segments connecting the nodes. The general transport equation is integrated on the control volume associated with the scalar variables and the momentum equations are integrated on the control volume associated with the velocity components.

The control volume of the longitudinal component (u) is shifted in direction (X) relative to the main control volume, while the transverse component (v) is shifted in direction (Y) and the transverse component (w) is shifted in direction (Z). This type of mesh is known as: "staggered grid" allows a good approximation of the convective flows and a numerical stabilization of the solution as well as a better evaluation of the pressure gradients.

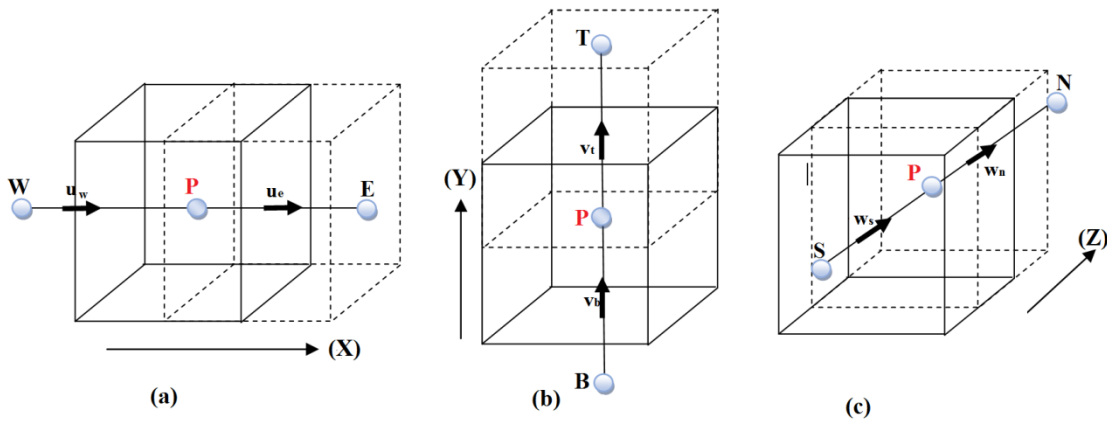


Figure (III.11): (a) staggered mesh for u (b), staggered mesh for v and (c) staggered mesh for w

III.9. Choice of mesh

Before performing the numerical simulations, we create the geometric model using the ANSYS Geometry Workbench (ANSYS R15.0). The choice of mesh is a crucial step in digital simulation. It is therefore important to choose a mesh that best adapts to the problems considered. In this thesis, we used the meshing the geometry in the ANSYS meshing application and the ANSYS FLUENT software as a solver.

ANSYS meshing application that allows you to mesh geometry domains of a CFD problem, it generates files (*.mesh) for ANSYS Fluent.

Fluent is a software which solves by the finite volumes method of the problems of fluid mechanics and heat transfers.

ANSYS Workbench gathers several functions including: definition of the geometry of the problem, the mesh and its checking, the definition of the borders (types of boundary conditions) and definitions of the domains of calculation (fluid or solid).

In this thesis we have chosen a hexahedron and tetrahedron mesh in the three directions.

In the figures shown below, the mesh form is represented in three selected cases of the research: the Figure (III.12) for case 4 of application N° 3 and Figure (III.13) for case 13 of application N°5 Figure (III.14) for case 15 of application N°6. The mesh produced is a structured grid of cells evenly distributed in the computational domain.

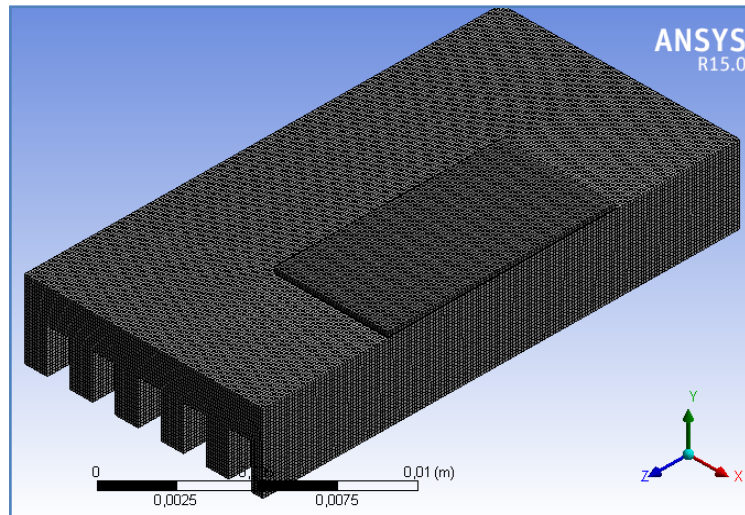


Figure (III.12): Diagram of the mesh used

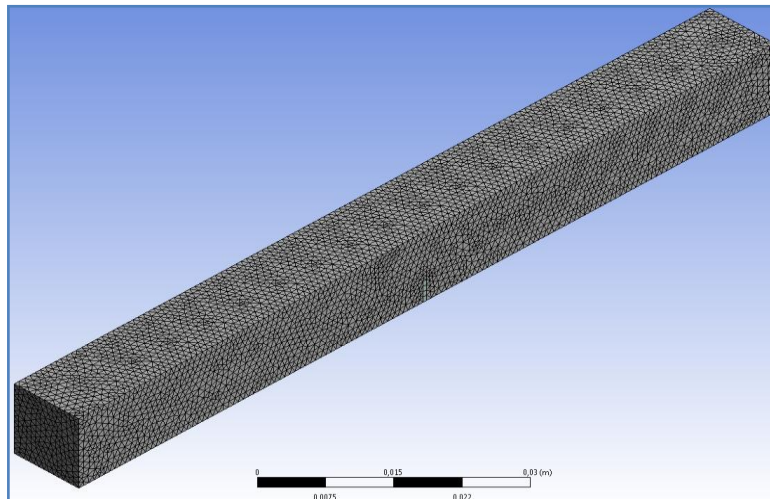


Figure (III.13): Diagram of the mesh used (case 13 of application N°5)

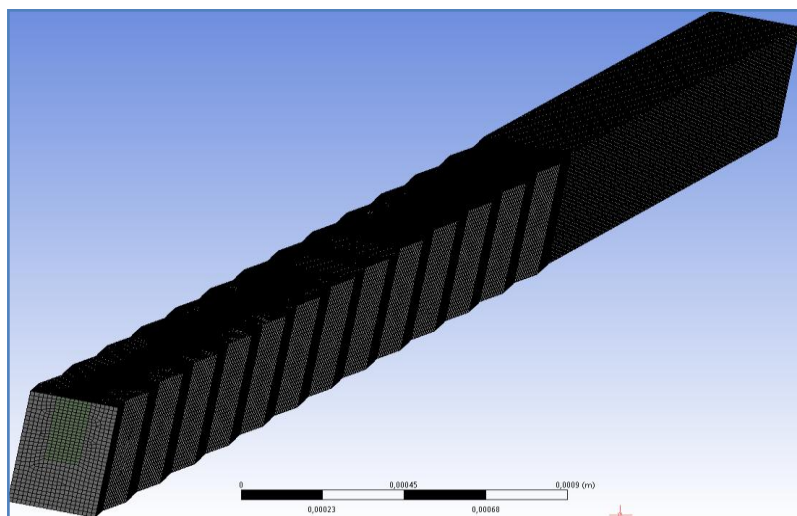


Figure (III.14): Diagram of the mesh used (case 15 of application N° 6)

In this thesis, the problems are solved by the FLUENT software, which is based on the finite volume method, as well as the SIMPLE algorithm for velocity-pressure coupling. The calculation steps described below proper to the steady flow regime Generally, we distinguish:

- Integration of transport equations.
- The discretization.
- The pressure- velocity coupling.
- The convergence.

III.10. Discretization of equations

Discretization consists of transforming differential equations to approximate algebraic equations. The conservation equations can be written in a common form. This formulation makes it possible not to repeat the discretization for each equation. So these equations can be reduced to a single general equation in Cartesian coordinates for a flow of an incompressible fluid and three-dimensional in the following form [135]:

$$\underbrace{\frac{\partial}{\partial t}(\rho\phi)}_T + \underbrace{\sum_{j=1} \frac{\partial}{\partial x_j}(\rho u_j \phi)}_C = \underbrace{\sum_{j=1} \frac{\partial}{\partial x_j} \left(\Gamma_\phi \frac{\partial \phi}{\partial x_j} \right)}_D + \underbrace{S_\phi}_S \quad (\text{III. 75})$$

Avec :

T: Transitional term;

C: Convection term;

D: Diffusion term;

S: Source term.

For each variable ϕ , the transport equation is written in the stationary, three-dimensional case in the following way:

$$\begin{aligned} \frac{\partial}{\partial x}(\rho u \phi) + \frac{\partial}{\partial y}(\rho v \phi) + \frac{\partial}{\partial z}(\rho w \phi) \\ = \frac{\partial}{\partial x} \left(\Gamma \frac{\partial \phi}{\partial x} \right) + \frac{\partial}{\partial y} \left(\Gamma \frac{\partial \phi}{\partial y} \right) + \frac{\partial}{\partial z} \left(\Gamma \frac{\partial \phi}{\partial z} \right) + S_\phi \end{aligned} \quad (\text{III. 76})$$

Where :

ϕ is general dependent variable; Γ Indicates the diffusion coefficient .

This equation (III.76) is discretized according to the finite volume technique and the system of equations retained is solved for each successive value of ϕ , see reference [136].

The tables below present the different values of the variable ϕ and its coefficients for each transport equation and each application studied.

Equations	Variable ϕ	Diffusion coefficient Γ	Source term S_ϕ
continuity	1	0	0
Quantity of movement following x	U	$\frac{\mu_{nf}}{\rho_{nf} \alpha_f}$	$-\frac{\partial P}{\partial X}$
Quantity of movement following y	V	$\frac{\mu_{nf}}{\rho_{nf} \alpha_f}$	$-\frac{\partial P}{\partial Y}$
Quantity of movement following z	W	$\frac{\mu_{nf}}{\rho_{nf} \alpha_f}$	$-\frac{\partial P}{\partial Z}$
Energy	θ	$\frac{\alpha_{nf}}{\alpha_f}$	0
Energy (solid)	θ	1	0

Table (III.8): Different terms of the transport equation. (Application N°1 and N°2)

Equations	Variable ϕ	Diffusion coefficient Γ	Source term S_ϕ
continuity	1	0	0
Quantity of movement following x	U	$\frac{\mu_{nf}}{\rho_{nf} \alpha_f}$	$-\frac{\partial P}{\partial X}$
Quantity of movement following y	V	$\frac{\mu_{nf}}{\rho_{nf} \alpha_f}$	$-\frac{\partial P}{\partial Y} + \frac{(\rho\beta)_{nf}}{\rho_{nf} \beta_f} Ra.Pr\theta$
Quantity of movement following z	W	$\frac{\mu_{nf}}{\rho_{nf} \alpha_f}$	$-\frac{\partial P}{\partial Z}$
Energy	θ	$\frac{\alpha_{nf}}{\alpha_f}$	0
Energy (solid)	θ	1	0

Table (III.9): Different terms of the transport equation. (Application N°3 and N°4)

Equations	Variable ϕ	Diffusion coefficient Γ	Source term S_ϕ
continuity	1	0	0
Quantity of movement following x	U	$\frac{\mu_{nf}}{\rho_{nf} \alpha_f}$	$-\frac{\partial P}{\partial X}$
Quantity of movement following y	V	$\frac{\mu_{nf}}{\rho_{nf} \alpha_f}$	$-\frac{\partial P}{\partial Y} + \frac{(\rho\beta)_{nf}}{\rho_{nf} \beta_f} Ra.Pr \theta$
Quantity of movement following z	W	$\frac{\mu_{nf}}{\rho_{nf} \alpha_f}$	$-\frac{\partial P}{\partial Z}$
Energy	θ	$\frac{\alpha_{nf}}{\alpha_f}$	$\frac{q_v L^2}{(\rho C_p)_{nf} \alpha_f \Delta T}$

Table (III.10): Different terms of the transport equation. (Application N° 5)

Equations	Variable ϕ	Diffusion coefficient Γ	Source term S_ϕ
continuity	1	0	0
Quantity of movement following x	U	$\frac{\mu_{nf}}{\rho_{nf} \alpha_f}$	$-\frac{\partial P}{\partial x}$
Quantity of movement following y	V	$\frac{\mu_{nf}}{\rho_{nf} \alpha_f}$	$-\frac{\partial P}{\partial y}$
Quantity of movement following z	W	$\frac{\mu_{nf}}{\rho_{nf} \alpha_f}$	$-\frac{\partial P}{\partial z}$
Energy	θ	$\frac{\alpha_{nf}}{\alpha_f}$	0
Energy (solid)	θ	1	0

Table (III.11): Different terms of the transport equation. (Application N°6)

In permanent regime, the linear form of discrete equations is as follows:

$$a_p \phi_p = \sum_{nb} a_{nb} \phi_{nb} + b \quad (\text{III.77})$$

Where:

a_p and a_{nb} are linear coefficients for ϕ and ϕ_{nb} .

nb represents the indices of neighboring cells. The number of neighboring cells depends on the topology of the mesh

For each cell we will have similar equations, these linear equations which differ by the coefficients a_p and a_{nb} are solved as a linear system by the iterative implicit method of (Gauss Seidel).

Fluent proposes two discretization schemes:

First order upwind scheme: this scheme allows a certain stability in the calculations but is responsible for numerical diffusion.

Second-order upwind scheme: the use of this method makes it possible to minimize the numerical diffusion but can make the calculation diverge.

III.11. Under-relaxation factors

The relaxation factors help to solve nonlinear equations in the fluent software, which reduces the change of ϕ produced during each iteration. The new value therefore depends on the previous value and the difference between the two values

$$\phi = \phi_{old} + \delta \Delta \phi \quad (\text{III. 78})$$

Where δ is the under-relaxation factor. In the Fluent software, the relaxation factors are between 0 and 1.

In our case, the under-relaxation values are given in the Table (III.12):

	pressure	Quantity of movement	Energy	Density
Laminar model	0.3	0.7	1	1

Table (III.12): default values of under-relaxation factors

III.12 Convergence criterion

The convergence criterion or the criterion for stopping the calculation is the criterion that must be verified to stop the calculation. At each iteration, Fluent makes it possible to judge the state of convergence by means of the calculation of the residuals R_ϕ for each variable (pressure, velocity components, energy, ...). This residue is defined by

$$R_\phi = \frac{\sum |\sum_{nb} a_{nb} \phi_{nb} + b - a_p \phi_p|}{F_{in,\phi}} \quad (\text{III. 79})$$

where :

R_ϕ : the absolute sum of the residuals, corresponding to the variable

$F_{in,\phi}$: the total flow at the input of the variable ϕ .

These residuals tell us about the degree of imbalance of the equation associated with each variable on all the cell of the domain. Convergence is determined from these residuals. It is advisable to examine, on the one hand, the residues as well as their evolution and on the other hand, the values of the calculated quantities. The adequate choice of the initial conditions makes it possible to reach an accelerated convergence and a stable solution.

III.13. Choice of the Pressure – velocity coupling method

The Velocity-Pressure coupling is treated by solving the momentum equations and an equation for pressure derived from a combination of the continuity equation and those of the momentum equation. "Fluent" has three coupling algorithms (SIMPLEC, SIMPLE, PISO).

The SIMPLE (Semi - Implicit Method for a Pressure Linked Equations) is essentially an estimation and correction procedure for calculating the pressure on the staggered grid of the velocity components.

The general idea of this algorithm is to gradually correct the pressure as well as the speed components so that its variables which verify the momentum equations also verify the continuity equation. The sequence of steps in the SIMPLE algorithm is shown in figure (III.15).

The "SIMPLE-C" method (SIMPLE Consistent). This last method differs from the first by the fact that it can be assigned a pressure relaxation factor close to 1, which accelerates convergence in most cases, but can lead to instabilities of the solution.

“PISO” (Pressure-Implicit with Splitting of Operators) algorithm: This method is part of the “SIMPLE” family algorithms. It is recommended for unsteady flows or for meshes containing very oblique cells.

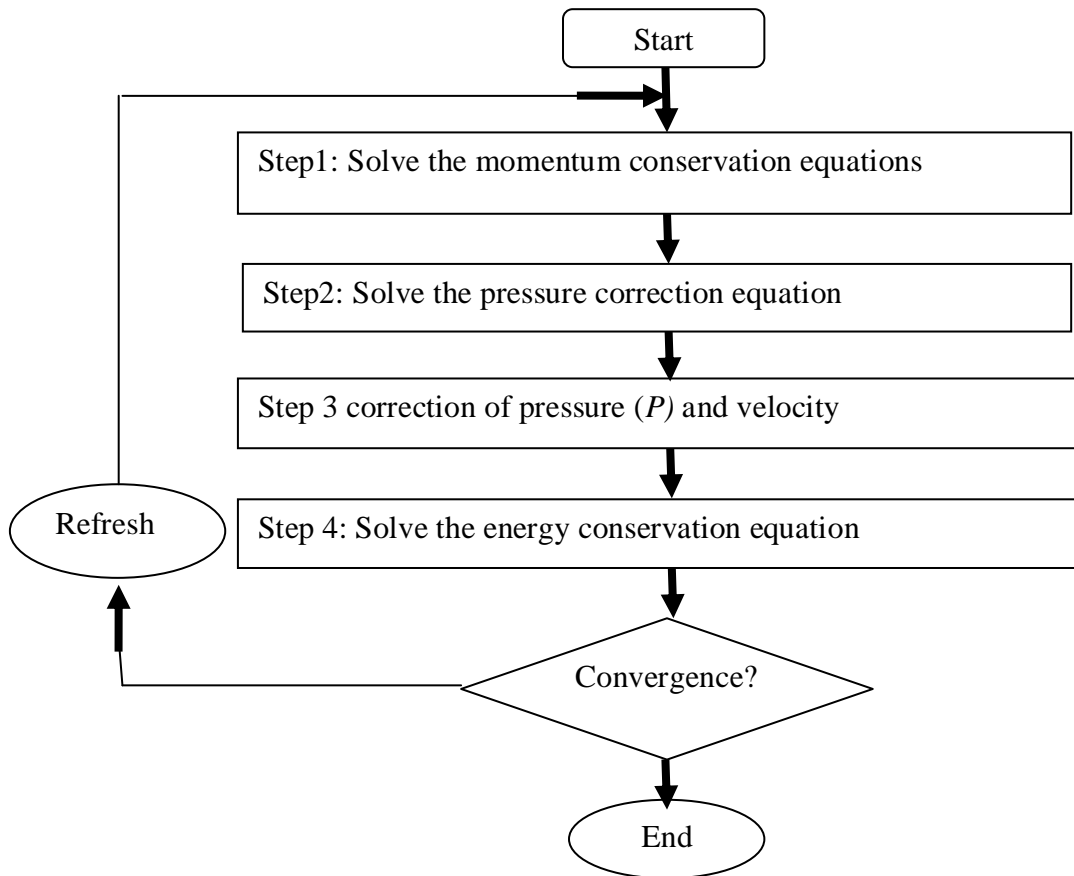


Figure (III.15): The SIMPLE algorithm.

III.14. Different steps to follow for numerical modeling:

The main steps to follow when working on digital simulation software (Fluent) require knowledge of some basic theoretical notions. These notions relate in particular to the definitions of the principal equations governing the flow.

The organogram presented in Figure (III.16) summarizes the methodology and the simulation method which begin with the design of geometric models, the realization of a mesh generator, the resolution of the equations and ending with the analysis and visualization.

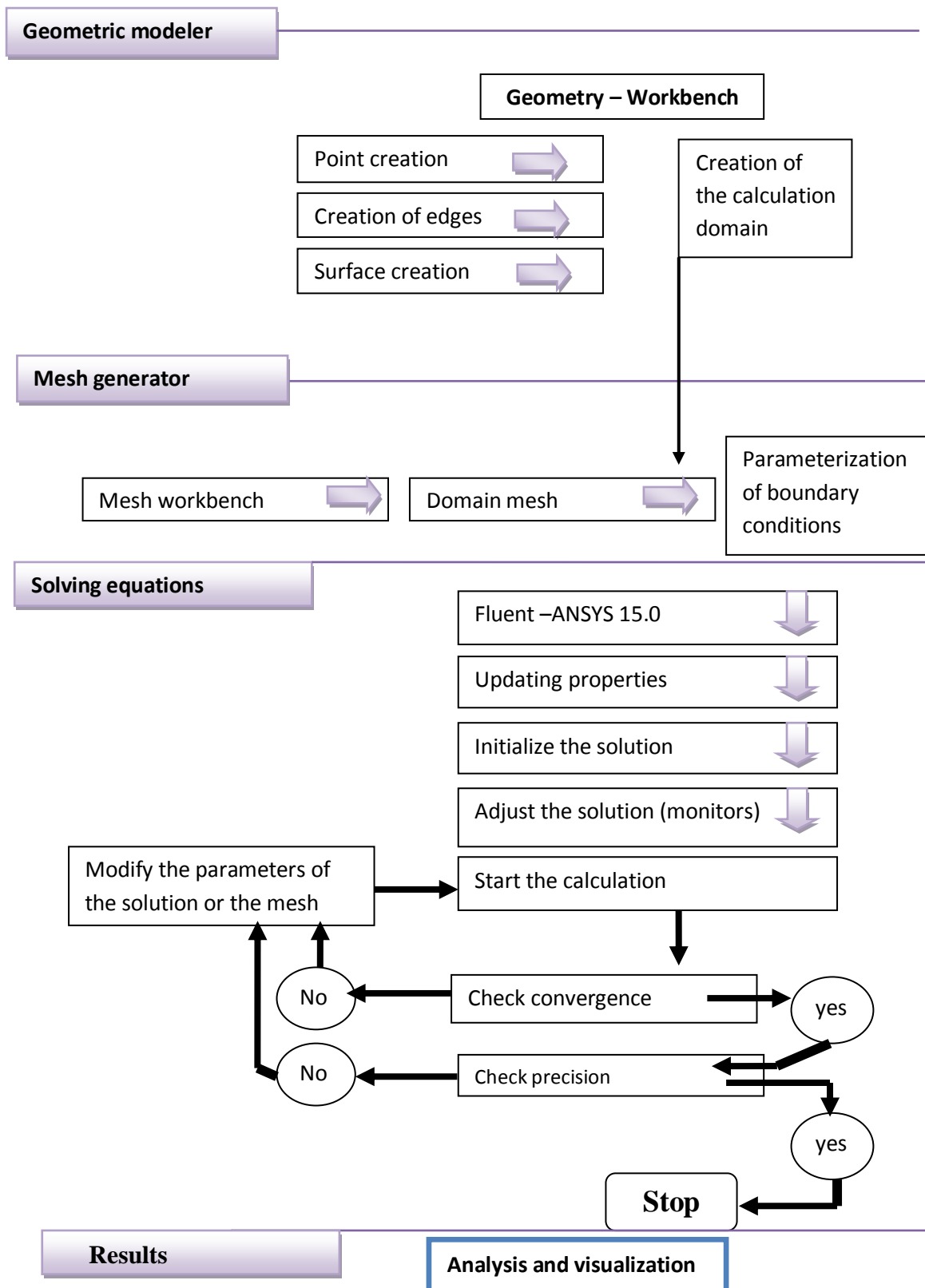


Figure (III.16): Calculation organogram

In the following title, we represent in detail the simulation steps using the ANSYS FLUENT simulation software

III.15. Steps of a CFD simulation using Fluent [137, 138]

III.15.1 Mesh

The generation of the mesh (2D or 3D) is a very important phase in a CFD analysis, given its influence on the calculated solution. A very good quality mesh is essential for obtaining a precise, robust and meaningful calculation result. Good mesh quality is based on the minimization of elements with skewness, and on good "resolution" in regions with a strong gradient. In fact, the quality of the mesh has a serious effect on the convergence, the precision of the solution and especially on the computation time

III.15.1.1 Choice of mesh type

We define structured and unstructured meshes (see **Figure (III.17)**).

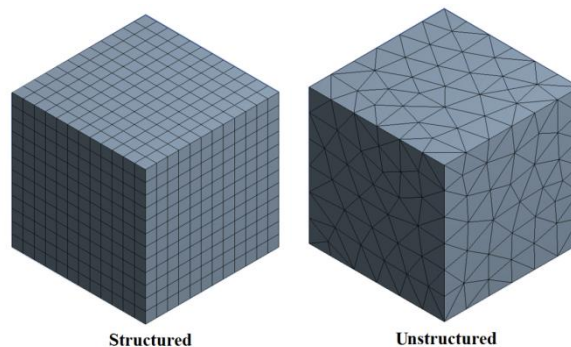


Figure (III.17): Structured and unstructured meshes (3D).

Structured mesh

It has the following advantages:

- Fast to Solve
- When the average flow is aligned with the mesh, a structured mesh reduces the risk of numerical errors.
- Economical in number of elements, has a lower number of meshes compared to an equivalent unstructured mesh.

Its disadvantages:

- Difficult to obtain a good quality of mesh for certain complex geometries.
- Difficult to generate in the case of complex geometry.

Unstructured mesh

The elements of this type of mesh are generated arbitrarily without any constraint as for their arrangement. His advantages:

- Complex geometries easier to mesh
- The algorithms for generating this type of mesh are much automated.

Its disadvantages:

- Slower to solve
- Generate numerical errors which can be more significant if we compare it with the structured mesh.

Hybrid mesh

Mesh generated by a mixture of elements of different types, triangular or quadrilateral in 2D, tetrahedral, prismatic, or pyramidal in 3D. It combines the advantages of structured and unstructured meshes.

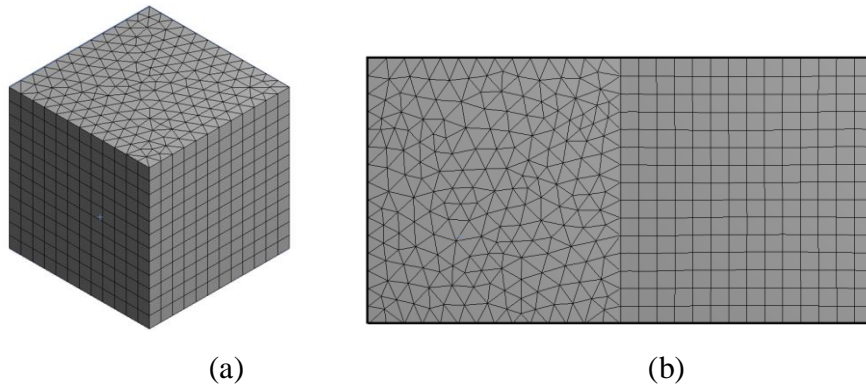


Figure (III.18): Hybrid mesh (a) in 3D (b) in 2D

III.15.1.2 General mesh

In practice, there is no precise rule for the creation of a valid mesh. However, there are different approaches which make it possible to obtain an acceptable grid.

We can summarize these rules as follows:

- Maintain good quality of the elements,
- Ensure good resolution in regions with a strong gradient,
- Ensure a good Smoothing in the transition zones between the parts with fine mesh parts and coarse mesh parts,
- Minimize the Total number of elements (reasonable calculation time).

- **Distortion:**

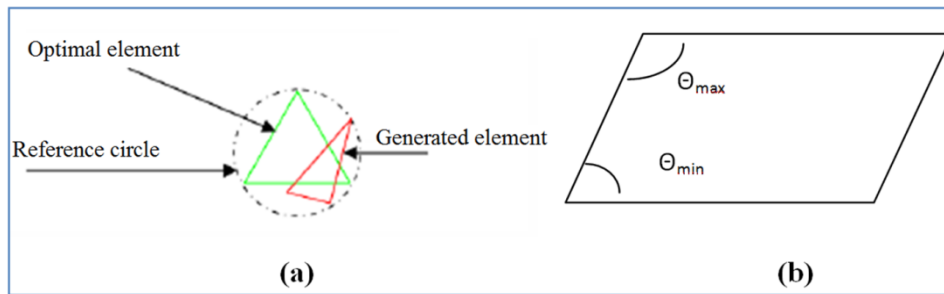


Figure (III.19): Definition of skewness based on (a) equilateral volume (b) angular deviation

The skewness factor F_d can be defined in two different ways. For tetrahedral or triangular elements, the calculation is based on the equilateral volume (see Figure (III.19)):

$$F_d = (\text{size}_{\text{optimal element}} - \text{size}_{\text{generated element}}) / \text{size}_{\text{optimal element}}$$

$$F_d = \max \left\{ \frac{\theta_{\max} - 90}{90}, \frac{90 - \theta_{\min}}{90} \right\} \quad (\text{III.80})$$

The large values of the distortion factor induce calculation errors and considerably slow down the convergence process. Some distortions can be tolerated if they are located in regions with a Weak gradient.

Note: The distortion factor is zero for perfect elements (squares, equilateral triangles)

The table below illustrates the variation in the quality of the mesh elements according to the value of the distortion coefficient F_d :

F_d	0-0.25	0.25-0.50	0.50-0.80	0.80-0.95	0.95-0.99	0.99-1.00
Quality	Excellent	Good	Acceptable	Bad	Very bad	unacceptable

- **Resolution:**

The resolution is particularly related to regions that present strong gradient, and good resolution contributes to good results and makes it possible to better describe physical phenomena which exist in these zones , such as shock waves or those related to layer boundaries. Often used for turbulent flows.

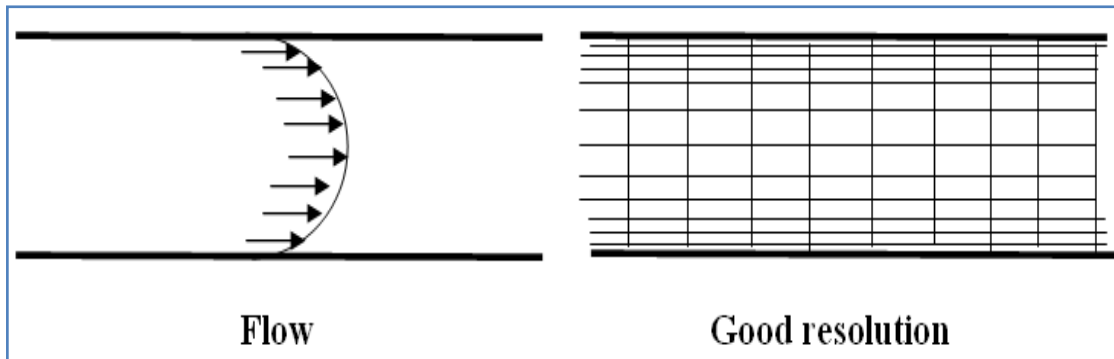


Figure (III.20) : Refinement of the mesh in regions of strong gradient

- **Smoothing :**

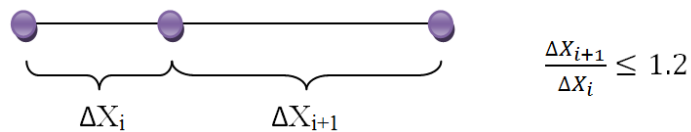


Figure (III.21) : Evolution of the size of the elements.

The change in the size of the elements of the mesh from one meshed zone to another must be progressive, the variation in the size of the elements of two adjacent zones must not exceed 20%

- **Total number of elements:**

The precision of the calculations depends on the quality of the network and the number of its elements. When the latter increases, the precision of the calculations and results improves, but in another way, it penalizes resources in terms of memory, burdens the computer and increases the simulation time. Hence, a compromise is needed between precision and calculation time. Techniques exist to save a certain number of elements:

- Use of hexahedral mesh elements in the appropriate zones.
- Use of the mesh adaptation function to refine only on very specific zones.
- Use of non-uniform meshes, concentrating the good quality of the mesh only in the zones where it is necessary,

- **Convergence en maillage**

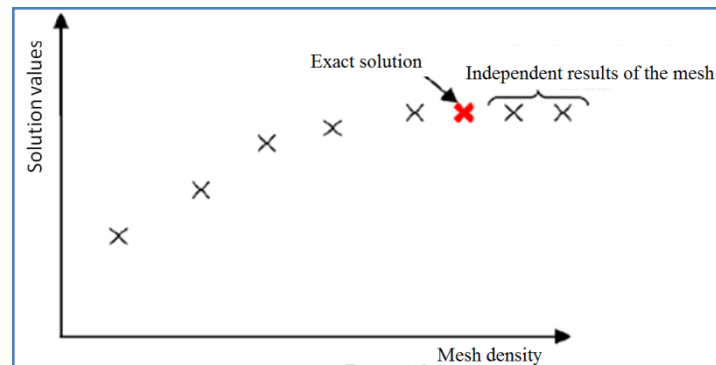


Figure (III.22): Mesh convergence test.

After convergence, the solution must be independent of the density of the mesh to be sure of the realism of the solution (figure (III.22)). One must carry out a convergence test in mesh, by reporting the evolution of a variable, for example the temperature values (variable) according to the size of the mesh which one refines successively.

III.15.2. Simulation

The main steps necessary to successfully simulate a problem in fluid mechanics using the Fluent software.

1. Choice of solver
2. Choice of laminar model
3. Definition of the characteristics of the fluid
4. Operating conditions
5. Boundary conditions
6. Choice of convergence criteria
7. Initialization of calculations
8. Backups
9. Starting of the simulation

III.15.2.1. Choice of solver

We can study the problem by going through these points:

- Stationary or unsteady nature;
- The dimension of the problem, Two-dimensional and three-dimensional or axisymmetric;
- The incompressible or compressible nature of the flow;
- The need or not to take into account the energy balance.
- The taking into account of external forces (gravity, inertial force related to rotation, . . .).

- The possible modeling of turbulence;
- The presence of several phases.

III.15.2.2. Definition of fluid characteristics

The Fluent software has a library of the most common fluids.

III.15.2.3. Operating conditions

The incorrect selection of the reference pressure value makes the simulation results unrealistic and erroneous. To avoid numerical errors during the calculation. The reference pressure value should be determined according to the pressure gauge shown in this relationship:

$$P_{abs} = P_{op} + P_{gauge}. \quad (III.81)$$

By default this is the value of atmospheric pressure as operating pressure.

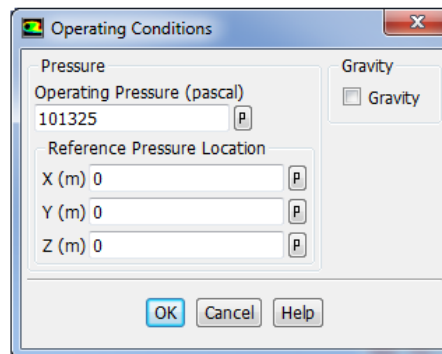


Figure (III.23): Choice of reference pressure

III.15.2.4 Boundary conditions

There are a number of conditions, including:

-Velocity Inlet : Used for incompressible or moderately compressible flows, when the input velocity is known.

-Pressure Inlet : Used for incompressible flow. We then fixes the total inlet pressure.

The total pressure in incompressible flow is given by the following relationship:

$$P_t = p + \frac{1}{2} \rho V^2 \quad (III.82)$$

Pressure Outlet : Specifies the static outlet pressure.

The use of Pressure Outlet used to define the static pressure at the outlet. Use of the condition « Pressure Outlet » instead of Outflow often results in better convergence. Note: Return flow problems (Back Flow). The phenomenon appears when the static pressure in a mesh close to the mesh which is on the border is lower than the pressure imposed in boundary conditions

-**Outflow** : is used to model the outlets of fluid of which one does not know a priori the details of the speed and the pressure at the outlet. It is not suitable for the following cases:

- If you are modeling unsteady flows with variation of the density.
- If a problem includes pressure inlet boundaries.
- If you are modeling compressible flow.

III.15.2.5. Choice of convergence criteria

An iterative solver seeks to balance the conservation equations of mass, momentum and energy. Leaving from an initial solution, the solver makes it evolve into a final solution (the calculations of the simulation are stop).

The residuals are calculated from the corrections in the variables; temperature, pressure, velocity, of the problem between this iteration and the previous iteration. In most cases, the default convergence criterion in FLUENT (residual) is sufficient.

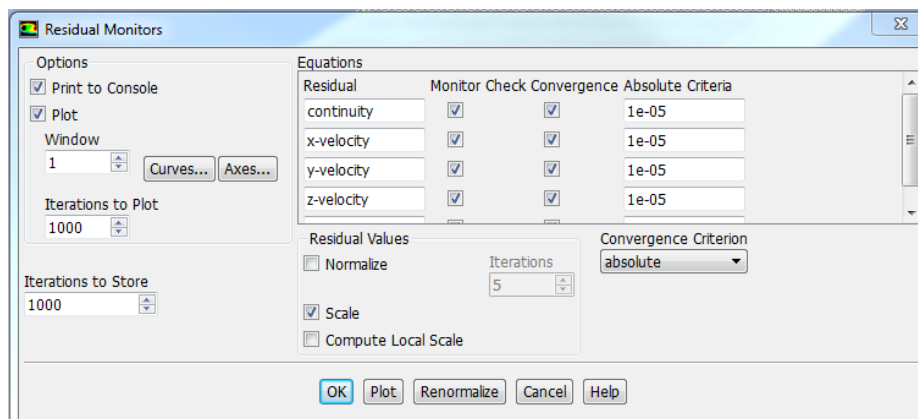


Figure (III.24): Choice of convergence criteria (residuals)

Chapter IV

Applications

IV.1 Application N°1: Numerical study of the thermal transfer in different geometries of the mini-channels

IV.1.1. Introduction

This application contains the results of numerical study of the thermal exchanges between different geometries of a cooler mini-channels of dimensions ($21 \times 21 \times 3.5 \text{ mm}^3$) which has been carried out. Three different shapes have been considered to cool an electronic component of dimensions ($10 \times 10 \times 0.25 \text{ mm}^3$) using a nano-fluid (Cu-water) as a coolant. The mathematical model and the geometry of this study were given in chapter III. In section IV.1.2 we present the results of mesh independence tests. The validation of the calculation code using data drawn from the Tawk *et al.* [126] is presented in section IV.1.3. This section also represents the results in a graphic form with description. The application N°1 is closed with a conclusion bringing together the various observations.

IV.1.2. Effect of the mesh on numerical solutions

The mesh is realized using the fluent software 'Meshing'. After convergence of the calculations of the simulation, the results are represented as follows: Figure (IV.1) shows the variation of the temperature of the upper surface of the mini-channel cooler of the second case along the plane of symmetry for the different applied meshes. Therefore; we conclude that the solution is independent of the mesh.

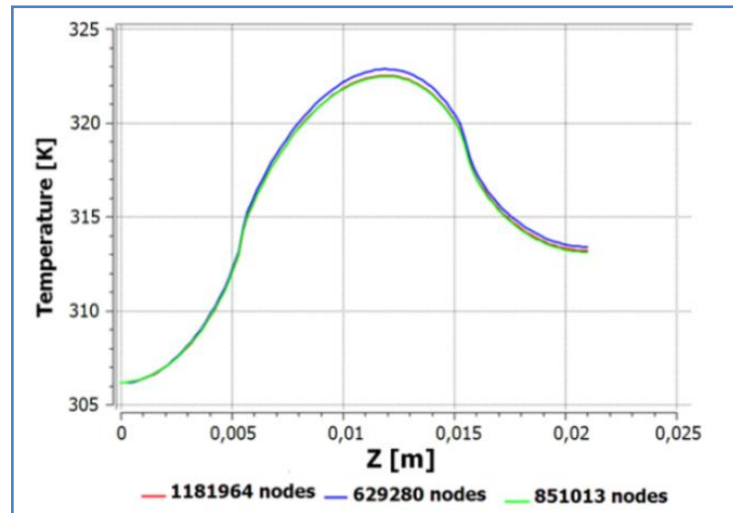


Figure (IV.1): Influence of the mesh on the temperature of the upper surface of the mini-channel cooler of the 2nd case

IV.1.3. Results and interpretations:

Figure (IV.2) shows a comparison of the temperature of this simulation with earlier experimental study [126]. A good agreement was obtained to the cooler case of copper and water (such as liquid cooling). We notice that the temperature increases with the increase of the power dissipated in the chip.

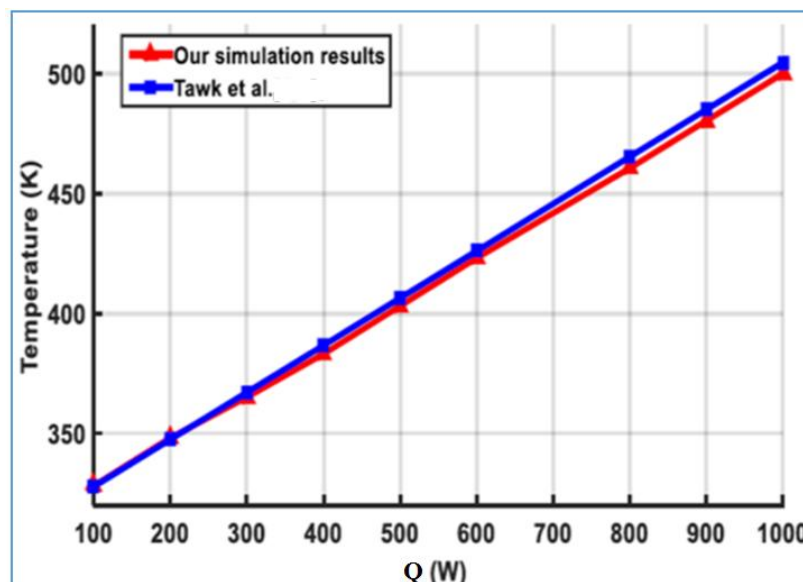


Figure (IV.2): The temperature according to the power dissipated in the chip

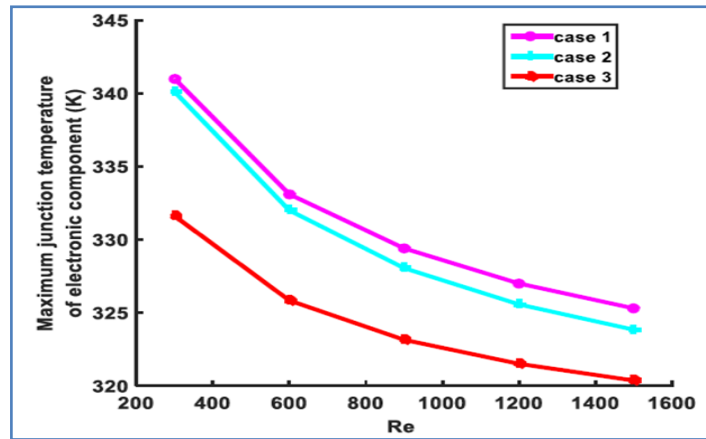


Figure (IV.3): The value of the maximum temperature of the junction of the electronic component obtained by simulations for a volume concentration of Cu- water nano-fluid of 0.05

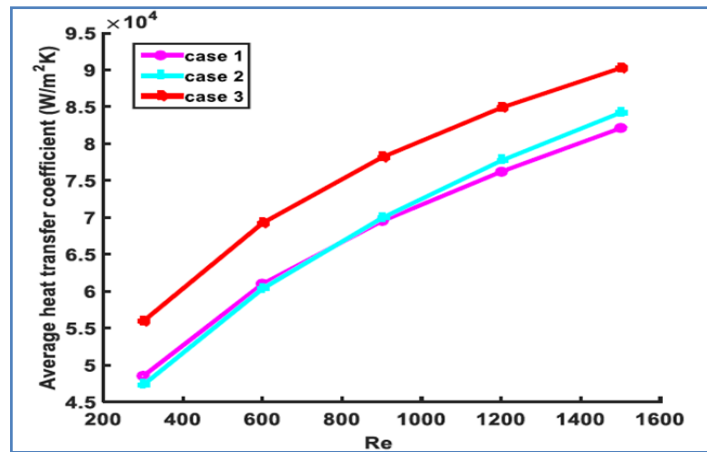


Figure (IV.4). The average heat transfer coefficients as a function of the Reynolds number (Re) for a volume fraction of 0.05

Figure (IV.3) shows the evolution of the maximum junction temperature of electronic component as a function of the Reynolds number. It is observed that the profile of the junction temperature decreases substantially for the three cases of the mini-channels when the Reynolds number increases. The temperature of the electronic component has the highest values for low values of Re. Figure (IV.4) shows the average heat transfer coefficient calculated as a function of Reynolds number for a volume fraction of 0.05, the average heat transfer coefficient is proportional to Reynolds number, varying from 300 to 1500. The comparison of the obtained results of the three studied cases of mini-channels shows that the average heat transfer coefficient of the mini-channel of the third case is greater than those of the mini-channels of the first and second cases.

IV.1.4. Conclusion (Application N°1):

In this application, the thermal exchanges of the different geometries of the mini-channels of a cooler has been studied numerically, using the Fluent 15.0 software, according to the obtained results, it can be concluded that for the three cases of the mini-channels and with a Reynolds number between 300 and 1500, the mini-channels of the third case improve the heat transfer compared to the other cases as well as the value of the maximum temperature of the junction of the electronic component.

IV.2 Application N°2: Numerical study of the influence of nano-fluids on thermal exchange in mini-channels

IV.2.1. Introduction

This application contains the results of the study of the effect of the nature of the nanofluid on thermal exchange in a silicon mini-channels cooler for cooling electronic

Components. The mathematical model, and the studied geometry were given in chapter III. In section IV.2.2 we present the results of mesh independent tests and type of mesh. In section IV.2.3 contains the results in graphical form and their discussion. This application is closed with a conclusion bringing together the various observations. The objective of this study is to study the effect of three types of the nanofluids (Cu-water, Ag-water and Diamond-water) on the temperature of the electronic component and heat transfer in a silicon mini-channels cooler.

IV.2.2. Effect of the mesh on Numerical solutions

In the simulation, we obtained a convergence of the studied model. The nodes used for meshing of the physical domain are affecting the results. The figure (IV.5) shows the number of nodes used for analysis of mini-channel heat sink with a result of the temperature of the electronic component. According to these figures, the results from 1500,000 nodes can be considered to be grid independence.

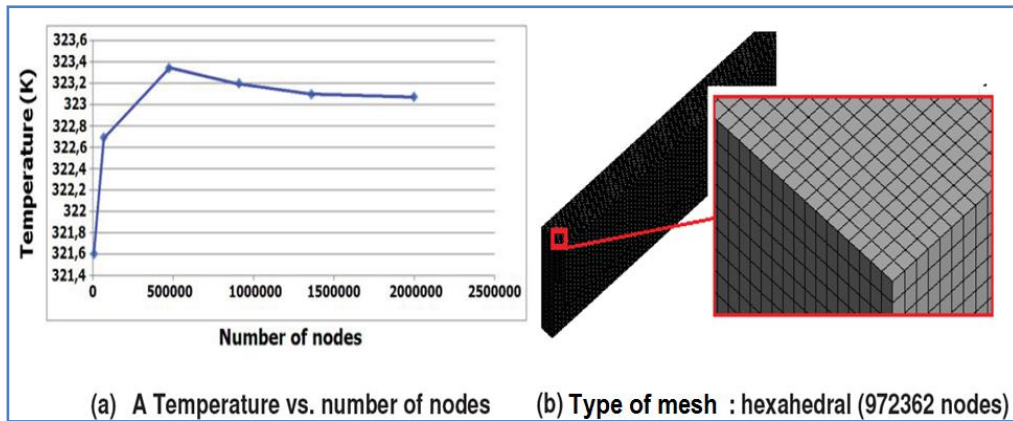


Figure. (IV.5): Grid independence examination

IV.2.3. Results and interpretations

Figure (IV.6) shows the evolution of the temperature value of the electronic component with respect to the Reynolds number. The temperature decreases substantially for the three types of nano-fluids (Cu-water, Ag-water and Diamond-water), when the Reynolds number increases. The electronic components have a high temperature for lowest values of Reynolds number and a minimum temperature for highest one. The more effective nano-fluid to reduce the temperature of the electronic component among the three coolants is diamond-water

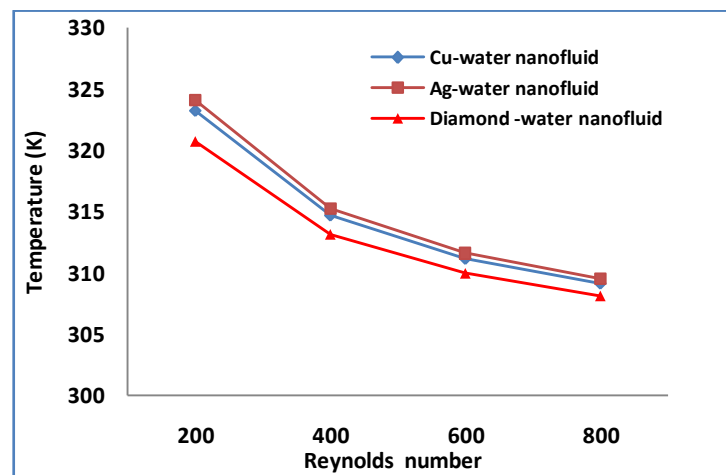


Figure (IV.6): The variation of the temperature of the electronic component according to the number of Reynolds

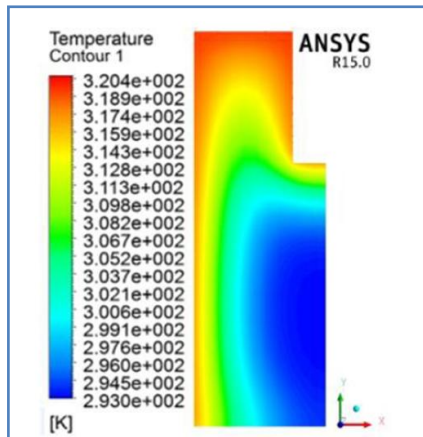


Figure (IV.7): The distribution of the temperature in outlet of mini-channel for diamond -water

Figure (IV.7) shows that distribution of the temperature in outlet of mini-channel for a Reynolds number equal to 200, and the volume concentration of nano-particles equal to 0,05, the isotherms become more curved and tighter on the walls of the mini-channel. The comparison between the three nano-fluids used shows that diamond has a greater heat transfer than copper Cu and silver Ag, as shown in Figure (IV.8)

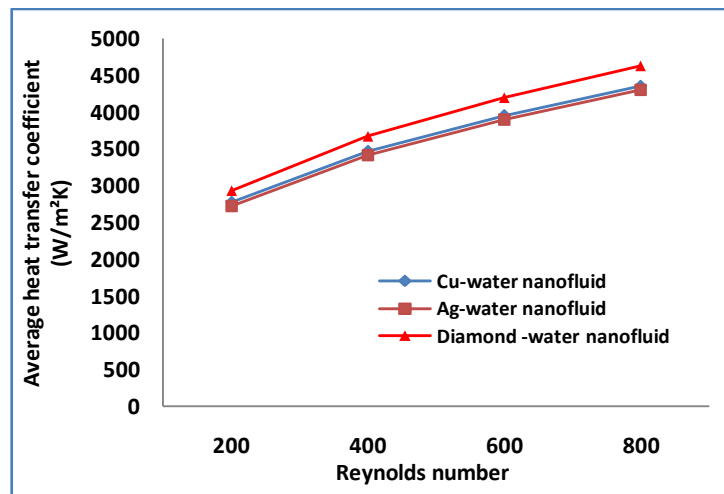


Figure (IV.8) :The average heat transfer coefficient calculated as a function of the Reynolds number at volume fraction =0.05

IV.2.4.Conclusion (Application N°2):

In this application, a numerical study, about the effect of the nano-fluid nature on the electronic component temperature and thermal exchange, has been carried out. The obtained results, confirm that the electronic component temperature decreases with the increase of

Reynolds number. This decrease of the electronic component temperature is most notable for the nano-fluid diamond-Water.

- The use of diamond-water nano-fluid gives significantly higher heat transfer coefficients than water-Ag and water-Cu.

IV.3. Application N°3: A study of thermal exchanges in different geometry sections of mini-channels of a cooler for cooling a chip using nano-fluids

IV.3.1. Introduction

This application represents the results of the study about the thermal exchanges of different geometry sections of mini-channels of a cooler. Particularly, we have chosen a copper mini-channels cooler for cooling an electronic chip IGBT. In our simulation of three-dimensional (3D), we have compared the numerical results to the different forms of the proposed mini-channels and the three different types of nano-fluids by using the Cu-water, the Ag-water, and the Diamond-water with a volume fraction of 0.02. The numerical results are found out by choosing a Reynolds number (Re) between 100 and 900, considering that the flow regime is stationary. The mathematical model, the geometry and the boundary conditions of this research were given in chapter III (section III.4.5). In section IV.3.2 we present the results of mesh independent tests. The validation of the calculation code using data drawn from the Tawk *et al.* [126] is presented in section IV.3.3. In section IV.3.4 contains the results in graphical form and their discussion. The application N°3 is closed with a conclusion bringing together the various observations. The objective of this study (application N°3) is to study and compare the thermal exchange between the different forms of the proposed mini-channels of the cooler size (21 mm x 21 mm x 3.5 mm) using three types of nano-fluids to obtain a better cooling of the electronic chip IGBT 1200 V 75 A and also for the improvement of the heat transfer between the walls of the min-channels and the cooling fluid.

IV.3.2. Effect of the mesh on numerical solutions

Figure (IV.9) shows the variation of the temperature of the upper surface of the mini-channels cooler corresponding to the Fourth case, along the symmetry plane for the different applied meshes. according to these results, we confirm that the solution of the mesh is independent .

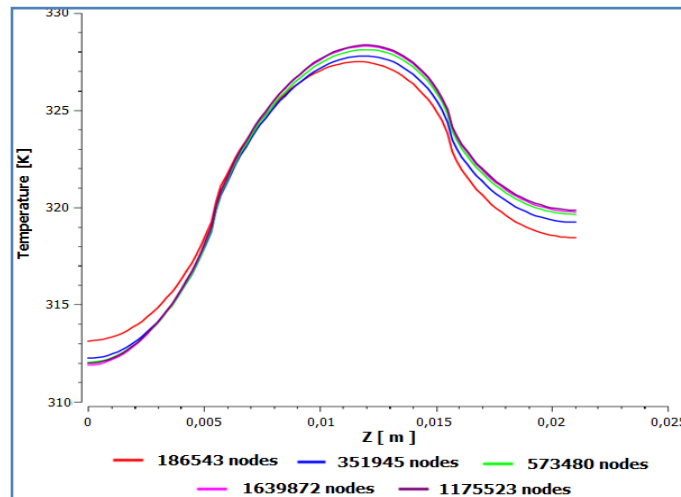


Figure. (IV.9): Influence of the mesh on the temperature of the upper surface of the cooler

IV.3.3. Validation of the results

To validate our numerical results, we choose to compare the results obtained by our numerical simulations with those found by Tawk *et al.*. Figure (IV.10) presents the validation of our simulation for the variation of the surface temperature according to the different values of power (20W, 200W and 400W) compared with experimental and numerical results of Tawk *et al.*

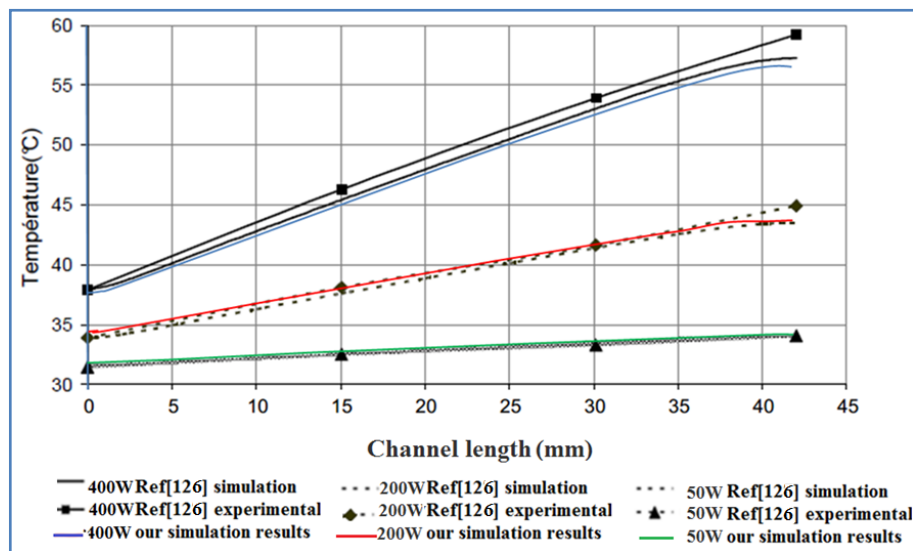


Figure (IV. 10.): Variation of the temperature for different values of power

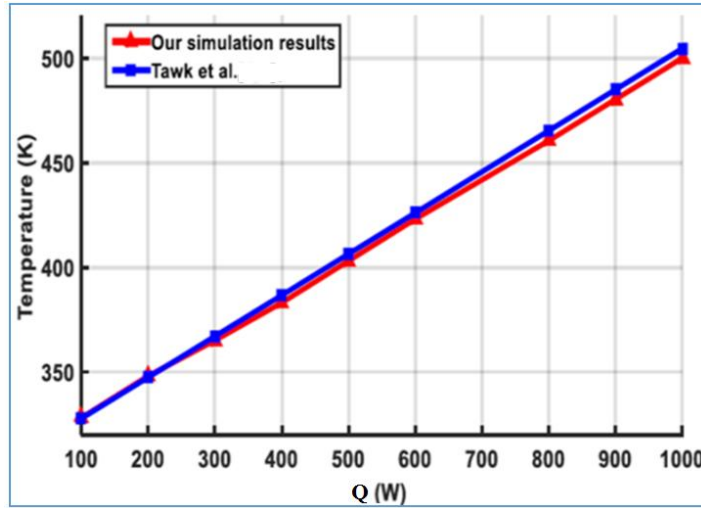


Figure (IV.11): Evolution of the temperature according to the power dissipated in the chip (Q is the power dissipated in the chip)

Figure (IV.11) presents a comparison between the numerical results and the Tawk *et al.* results in terms of the evolution of the maximum temperature of the chip as a function of the power dissipated. In this case, we have considered the copper cooler and the water as a coolant.

From these results, it is clear that the temperature increases as a linear curve with the length. In these conditions, the maximum value of the temperature is equal to

$T = 53^{\circ}\text{C}$. These results show a good agreement with the results of Tawk *et al* [126].

In these conditions, the gap between numerical and experimental results is about 5%. These results confirm the validity of the numerical method.

IV.3.4. Results and discussions

IV.3.4.1. Evolution of the temperature of the upper surface of the mini-channel cooler for all cases

Figure (IV.12) shows the evolution of the temperature of the upper surface of the mini-channel cooler, along the symmetry plane for the different cases of the considered mini-channels cooler. From these results, it has been noted that the values of the temperature of the upper surface of the mini-channel cooler in the Ninth case are inferior in comparison with other cases.

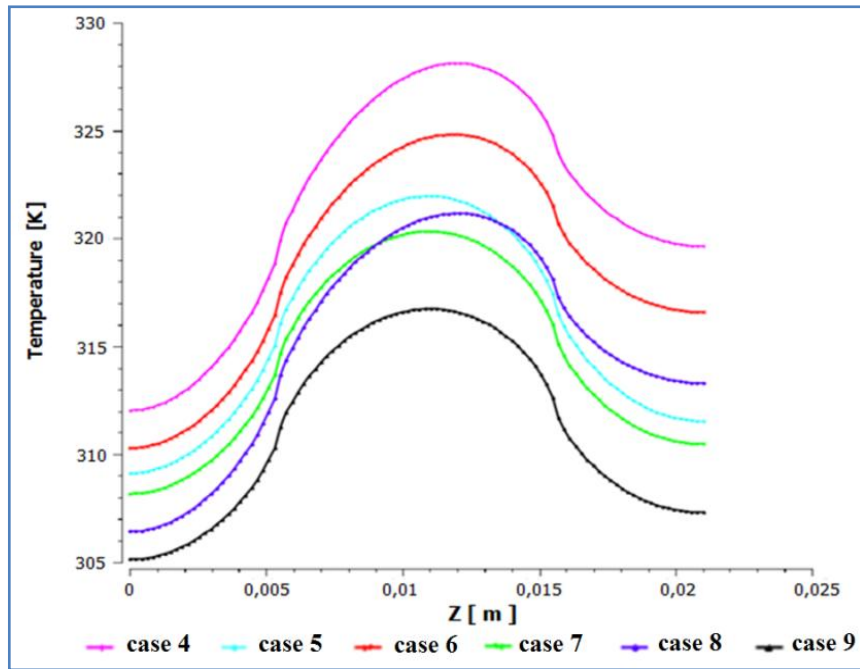


Figure (IV.12): The temperature of the upper surface cooler in 6 cases for $Re=500$, the power is 130W. The inlet temperature is equal to 298.15 K and for Cu- water nano-fluid

IV.3.4.2. Evolution of the junction temperature value of the chip in function of the Reynolds number

Figure (IV.13) shows the evolution of the junction temperature value of the chip IGBT 1200 V 75A in function of the Reynolds number. According to these results, the junction temperature decreases substantially in all cases of the mini-channels of the cooler when the Reynolds number (Re) increases. The chip IGBT presents a high temperature for lowest values of Reynolds number Re and a minimum temperature for highest values of Re . Indeed, it is clear that the maximum junction temperature of the chip in the mini-channel cooler of the Ninth case is lower than that in the other cases and in the used three nano-particles types. According to these results, it has been noted that the nano-fluid is more effective to reduce the temperature of the chip than the three coolants with diamond- H_2O .

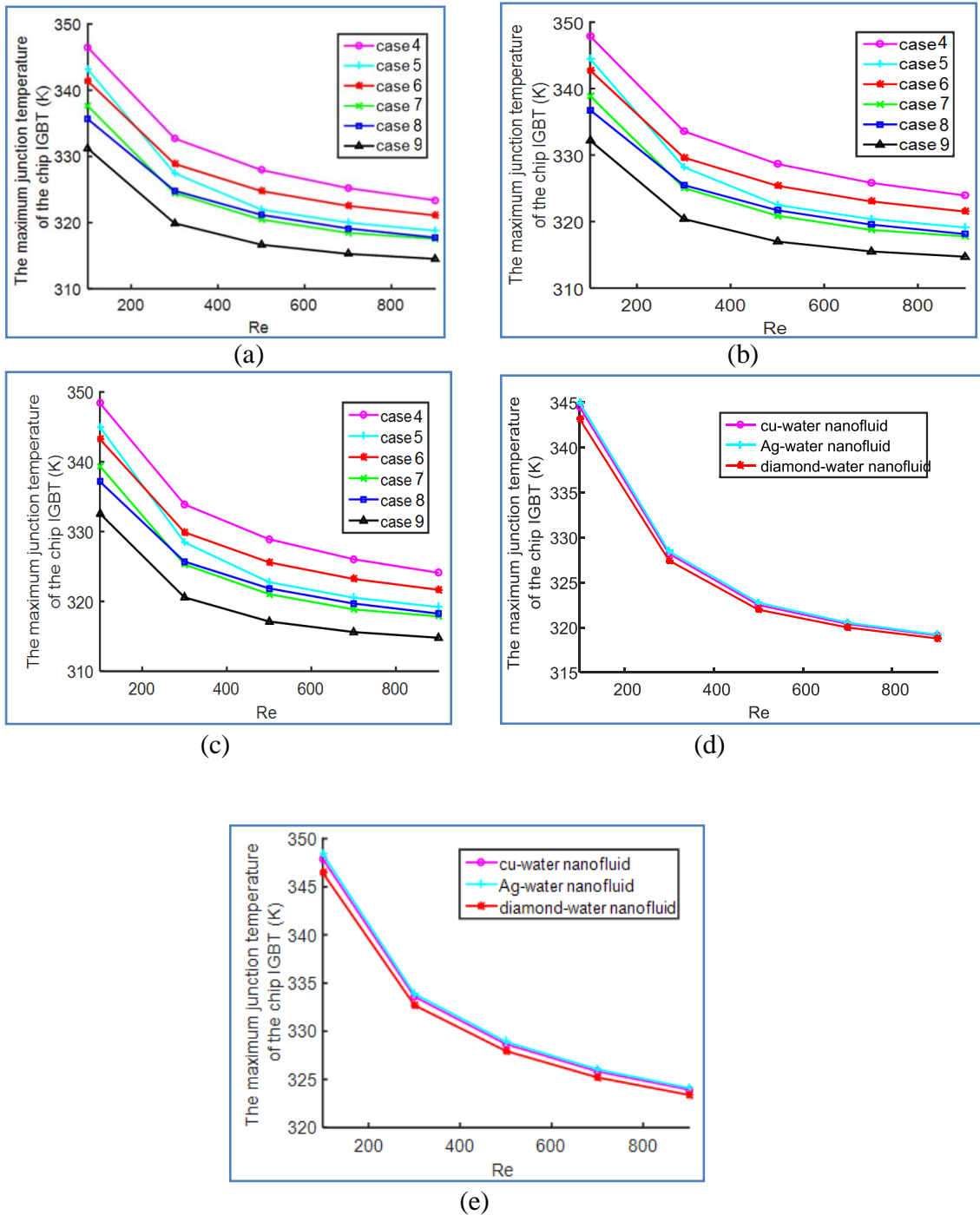


Figure (IV.13): Variation of the maximum temperature obtained from the IGBT chip for a volume concentration equal to 0.02 for various types of nano-fluids: (a) Diamond-water, (b) Cu-water, (c) Ag-water, and different cases: (d) case 5, (e) case 4,

IV.3.4.3. Distribution of the temperature in the surface of the chip for all cases

Figure (IV.14) shows the distribution of the temperature in the surface of the chip IGBT, the plane of symmetry and in the upper surface of the cooler for a Reynolds number equal to $Re = 500$ and for Cu-H₂O nano-fluid with a volume fraction equal to $\phi = 0.02$. From these results, the value of the maximum junction temperature of the chip and the maximum temperature of the

upper surface of the cooler in the Fourth case are the highest ($T_{\max \text{ chip}} = 328 \text{ K}$) compared to other cases. However, the maximum temperature of the upper surface of the cooler and the maximum junction temperature of the chip IGBT in the Ninth case are lower than the others cases. This difference in temperature confirms that when the surface area of exchange between the walls of the mini-channels of the cooler and nano-fluids increases, the maximum junction temperature of the chip decreases. This decrease improves the absorption of the heat through the fins of the cooler.

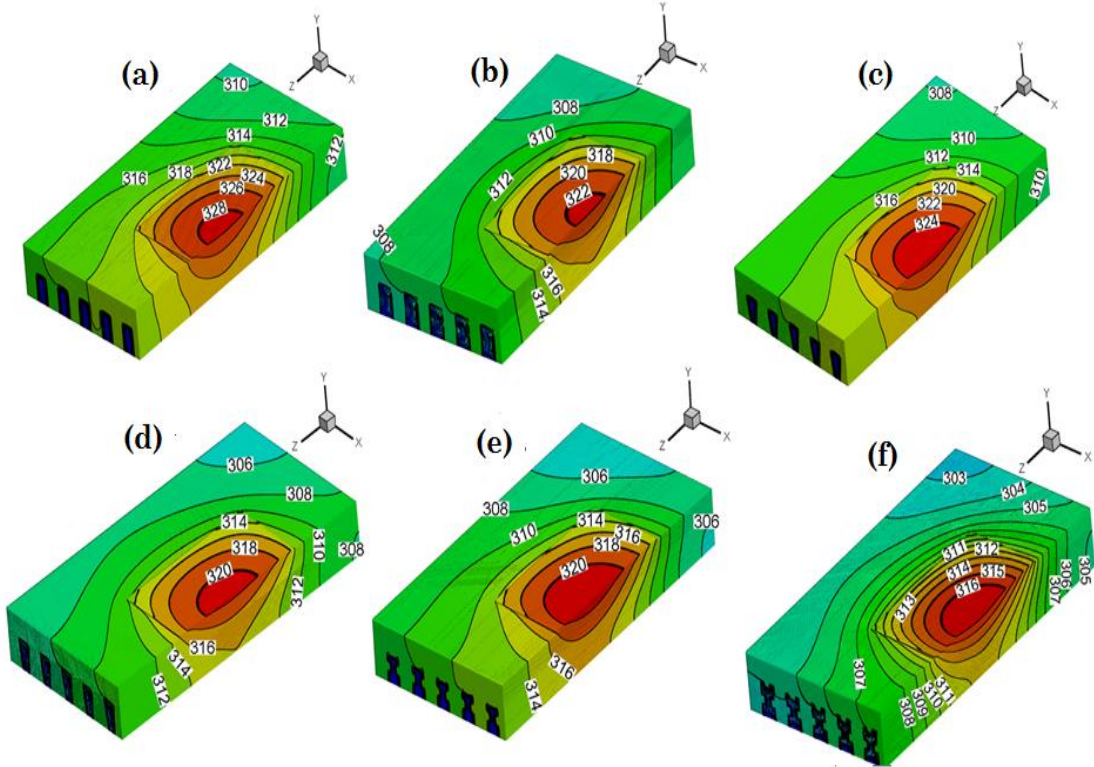
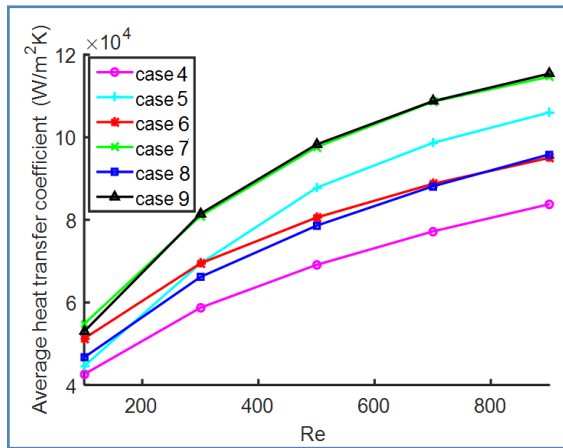


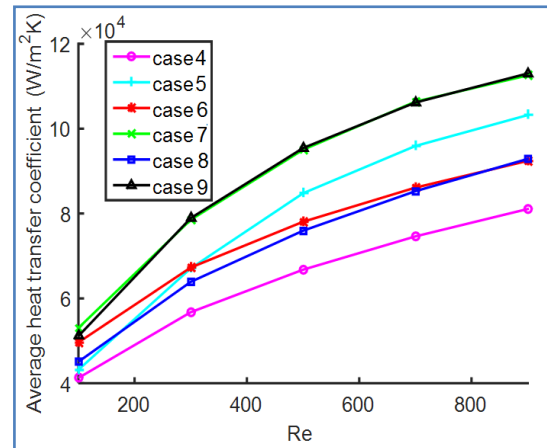
Figure (IV.14): Distribution of the temperature in the surface of the chip IGBT and in the surfaces of the mini-channels of the cooler for $Re=500$ and for cu-water nano-fluid (volume fraction $\phi=0.02$): (a) case 4, (b) case 5, (c) case 6, (d) case 7, (e) case 8, (f) case 9

IV.3.4.4. Evolution of the average heat transfer for all cases

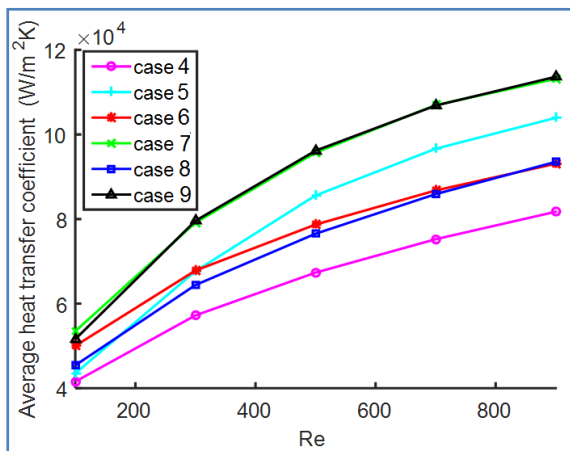
Figure (IV.15) shows the average heat transfer coefficient calculated as a function of the Reynolds number for a volume fraction of 0.02. According to these results, the average heat transfer coefficient is proportional to the Reynolds number varying from 100 to 900. The main heat transfer coefficient values of the mini-channel in the ninth case presents the highest value comparing it to the mini-channel near the symmetry.



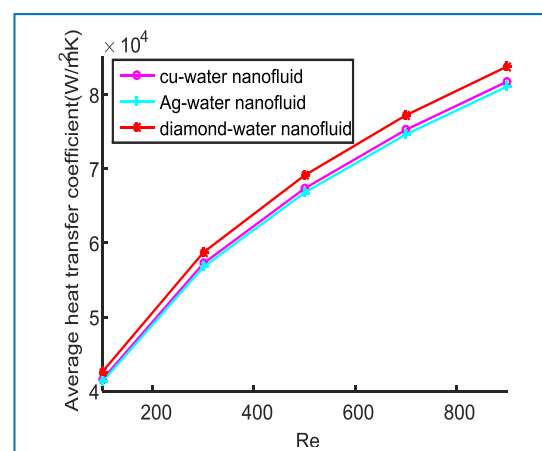
(a) Diamond-water nano-fluid



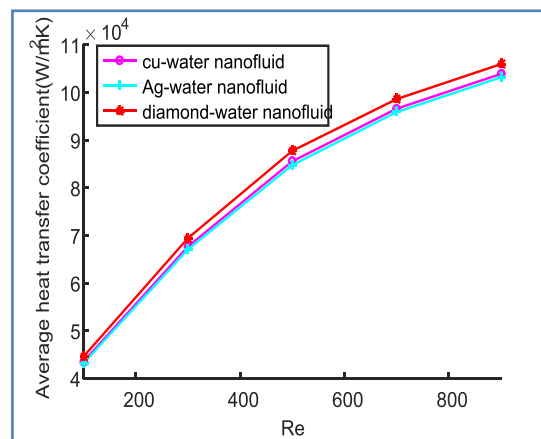
(b) Cu-water nano-fluid



(c) Ag-water nano-fluid



(d) Case 4



(e) case 5

Figure (IV.15): Average heat transfer coefficient for a volume concentration equal 0.02 for various types of nano-fluids: (a),(b),(c) and different cases:(d),(e).

Figure (IV.16.a) illustrates the variation of the average heat transfer coefficient as a function of the range of volume concentration varying from 0.01 to 0.04 of copper nano-particle. From these results, the average convective heat transfer coefficient increases with the increase of the volumetric fraction of the solid for the value of the constant velocity equal to 0.34 m/s. And from

Figure (IV.16.b), it is found that the nanoparticle diameter has a considerable effect on the convective heat transfer coefficient. This effect appears when the size of the nanoparticle decreases. In these conditions, the transfer coefficient increases.

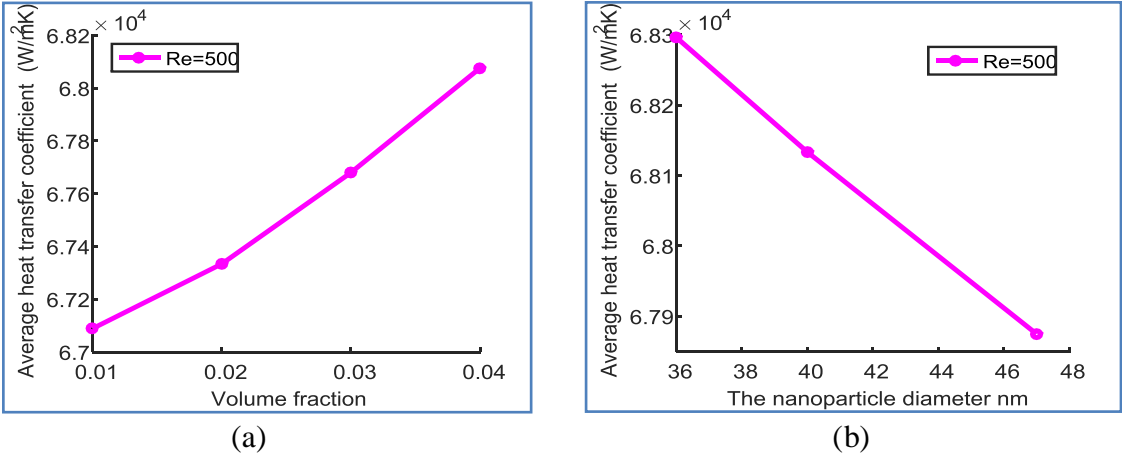


Figure (IV.16): (a) Illustrates the variation of the average heat transfer coefficient as a function of the range of volume concentration varying from 0.01 to 0.04
 (b) Average heat transfer coefficient Vs the nanoparticle diameter

IV.3.4.5. Conclusion (Application N°3)

In this application, we have studied numerically the thermal exchange of different geometry sections of mini-channels using the commercial software ANSYS-Fluent 15.0. From the obtained results, for the different mini-channels, it has been found that in the Reynolds number ranging from 100 to 900, the mini-channel cooler in the Ninth case gave a heat transfer improvement over other cases. Furthermore, an improvement in the maximum temperature value of junction of the electronic chip is also observed. In these conditions, the types of nano-particles have considerable effects on the improvement of the heat transfer, especially with the decrease in the nano-particle diameter and increase in the volumetric fraction. In this study, we found that the best heat transfer fluid among the nano-fluids studied is the nano-fluid containing the diamond nano-particles.

IV.4 Application N°4: Influence of the types of nano-particles, nano-particles volume concentration, and the types of cooler metals on the heat transfer in a mini-channels cooler

IV.4.1. Introduction

This application contains the results of the study of the effect of three different types of nano-particles, nano-particles volume concentration and types of cooler metals on heat transfer in a mini-channel cooler numerically. In these simulations, we have considered the Cu-H₂O, the Ag-H₂O and the Diamond-H₂O with different volume fractions in the range of 0,02-0,1 with two types of cooler materials (copper cooler and aluminum cooler) for cooling an electronic component. In these conditions, the inlet velocity is constant for the three different types of nano-fluids. The power of the electronic component is equal to 130 W. The mathematical model and the studied geometry were given in chapter III. We present the validation of the calculation code using data drawn from the Tawk *et al.* [126] in figure (IV.17). Section IV.4.2 contains the results in graphical form and their discussion. Application N°4 is closed with a conclusion bringing together the various observations. The objective of this application is to study the influence of nano-particles types, the volume concentration of nano-particles and cooler materials types on the heat transfer in a proposed mini-channel cooler. Particularly, we have chosen two types of cooler materials: the aluminum cooler and the copper cooler.

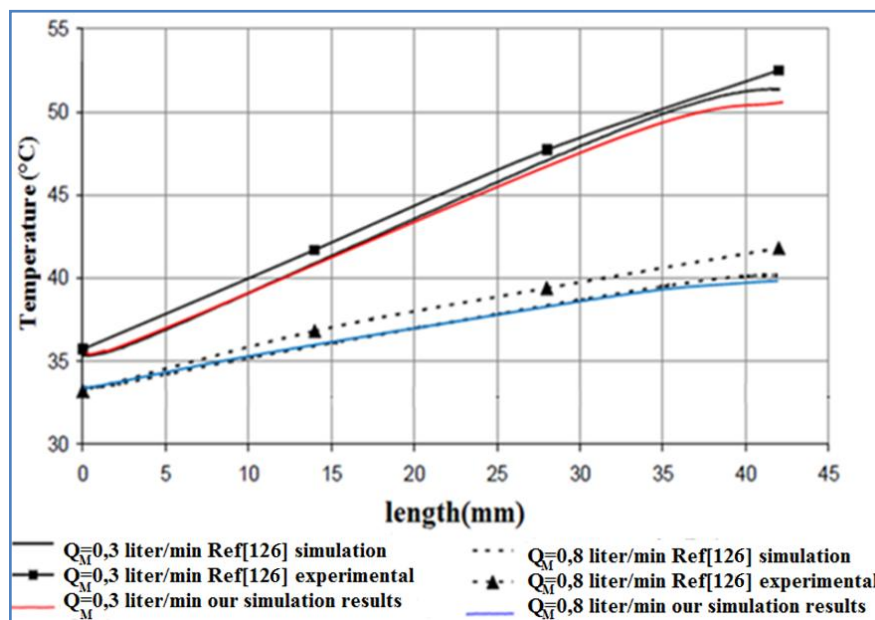


Figure (IV.17): Variation in the surface temperature for different values of mass flow. (Q_M is the mass flow, liter/min)

Figure (IV.17) represents a comparison between our numerical results and the results of Tawk *et al.* [126] in terms of the evolution of the surface temperature of the cooler; at a dissipated power equal to 200 W and volume flow equal to 0.3 - 0.8 l/min. Either in Figure (IV.18), the surface temperature comparison is presented in three cases. Case 1A corresponds to the molybdenum cooler and the coolant is the gallium. This case was studied also by Tawk *et al.* Case 2A corresponds to the molybdenum cooler and the coolant is the Cu-water nano-fluid with a volume concentration equal to 0.7%.

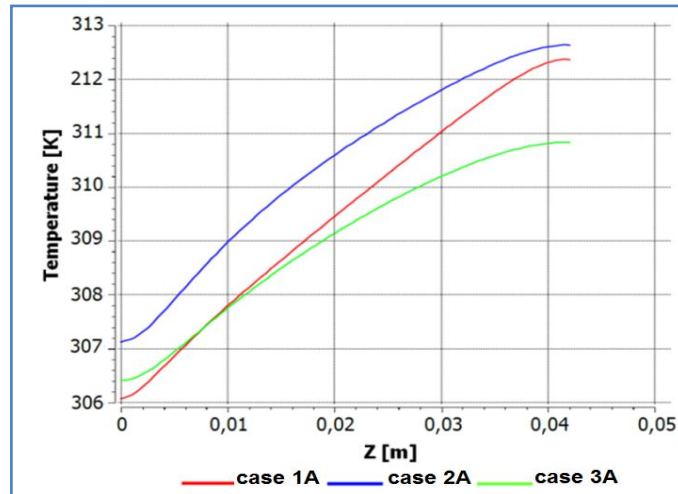


Figure (IV.18): Comparison of the surface temperature within three cases.

In case 3A, we consider that the copper cooler and the coolant are the Cu-H₂O nano-fluid with a volume fraction equal to 0.7%. From these results, we find that the temperatures of the upper surface of the cooler in case 3A are less than that in case 1A and case 2A. This difference is due to the physical properties and particularly to the value of the thermal conductivity of the metal in the cooler. Furthermore, it can be explained by the type and concentration of the coolant.

IV.4.2. Results and discussions

IV.4.2.1. Variation in the temperature of the mini-channels cooler with the three nano-fluids used and two metals of the cooler

Figure (IV.19) shows the variation in the temperature of the upper surface of the mini-channels cooler along the plane of symmetry with the three nano-fluids used and two metals of the cooler (copper cooler and aluminum cooler). From these results, it has been observed that the temperature value increases in the three types of the nano-fluids. According to these results, the values of temperature of the upper surface of the copper cooler are lower than those of the aluminum cooler, especially with the coolant H₂O–diamond nano-fluid.

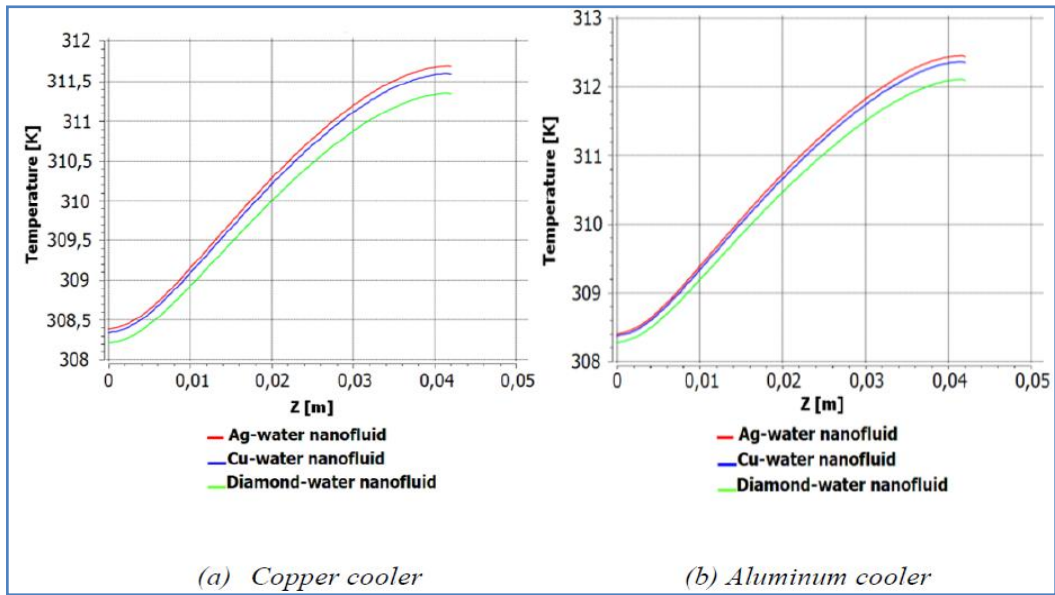


Figure (IV.19): Profiles of the temperatures of the three nano-fluids and the two cooler metals at $Re = 1414$ and $\phi = 0,02$.

IV.4.2.2. Effects of three different types of nano-particles on the temperature of the electronic component and the average heat transfer coefficient

Figures (IV.20) and (IV.21) illustrate the effect of different types of nano-particles and volume fraction of nano-particles (Cu, Ag, Diamond) on the maximum temperature of the electronic component and the average heat transfer coefficient for the value of the Reynolds number equal to $Re = 1414$. From these results, it is clear that adding a low volume concentration of nano-particles for the base fluid (water) leads to a significant decrease in the maximal temperature of the electronic component, along an increase in the heat transfer coefficient. In figure 6, the results show that among the three used liquids, the liquid containing the diamond nano-particle and water is the best in terms of the heat transfer coefficient. In these conditions, the electronic component temperature is also reduced. This fact is attributed to the convection facilitated by the higher thermal conductivities of the diamond-water nano-fluid compared to that of the Cu-water and Ag-water nano-fluid.

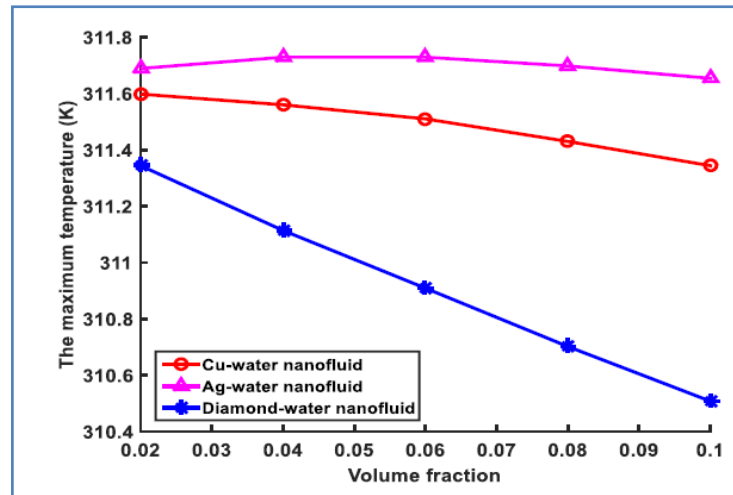


Figure (IV.20): Variation in the maximum temperature vs. the volume fraction

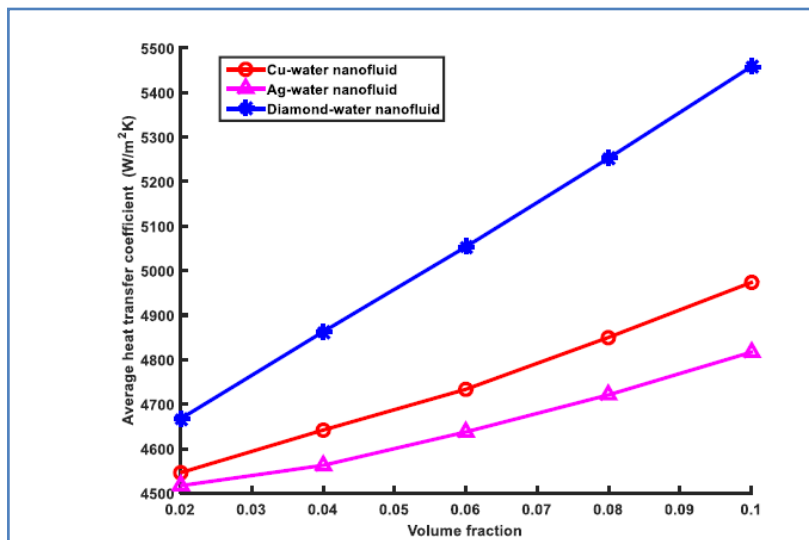


Figure (IV.21): Variation of the average heat transfer coefficient vs. the volume fraction.

IV.4.2.3. Evolution of the temperature of the electronic component for the two metals

Figure (IV.22) shows the evolution of the maximum temperature value of the electronic component in the function of the volume fraction of Cu-H₂O nano-fluid of both metals. From these results, it is clear that the maximum value of the temperature decreases substantially in both metals when the Reynolds number is constant. Indeed, the temperature value of the electronic component in the copper cooler is higher than that of the aluminum cooler. The copper cooler allows us to better cool the component with the increase in the volume concentration of Cu-water nano-fluid.

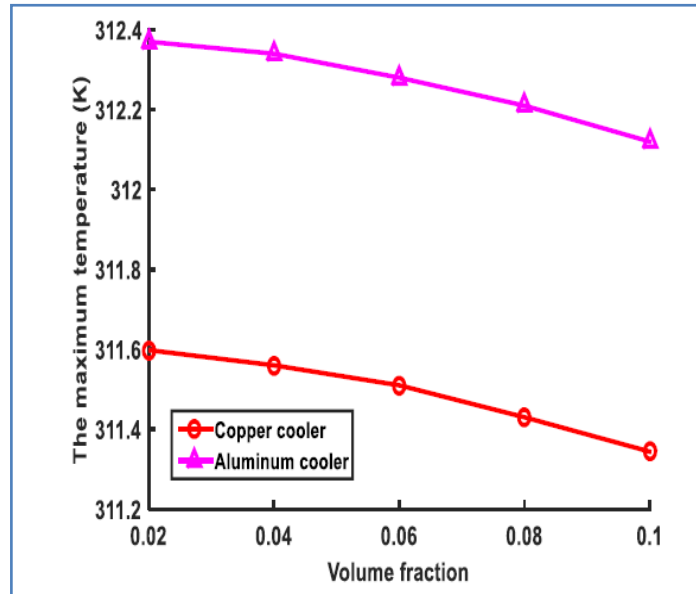


Figure (IV.22): Variation of the maximum temperature vs. the volume fraction.

IV.4.2.4. Distribution of the temperature of the mini-channel with three nano-fluid and two metals of the cooler

Figure (IV.23) shows that; for a Reynolds number equal to $Re = 1414$, and an imposed power of the component equal to 130 W, the distribution of the temperature in 3D configuration within the mini-channel, the maximum temperature of the surface of the mini-channel is close to $T = 311.7$ K for the copper cooler and 312.4 K for the aluminum cooler. Comparing the three nano-fluids, we find that the temperature of the electronic component in the diamond-water nano-fluid is lower than that of the other liquids and therefore more appropriated for cooling.

Moving from the mini-channels of the cooler inlet to its outlet, we find that the temperatures in the mini-channels increase. This increase indicates the amount of heat transfer between the walls of cooler mini-channels and the coolant (nano-fluid).

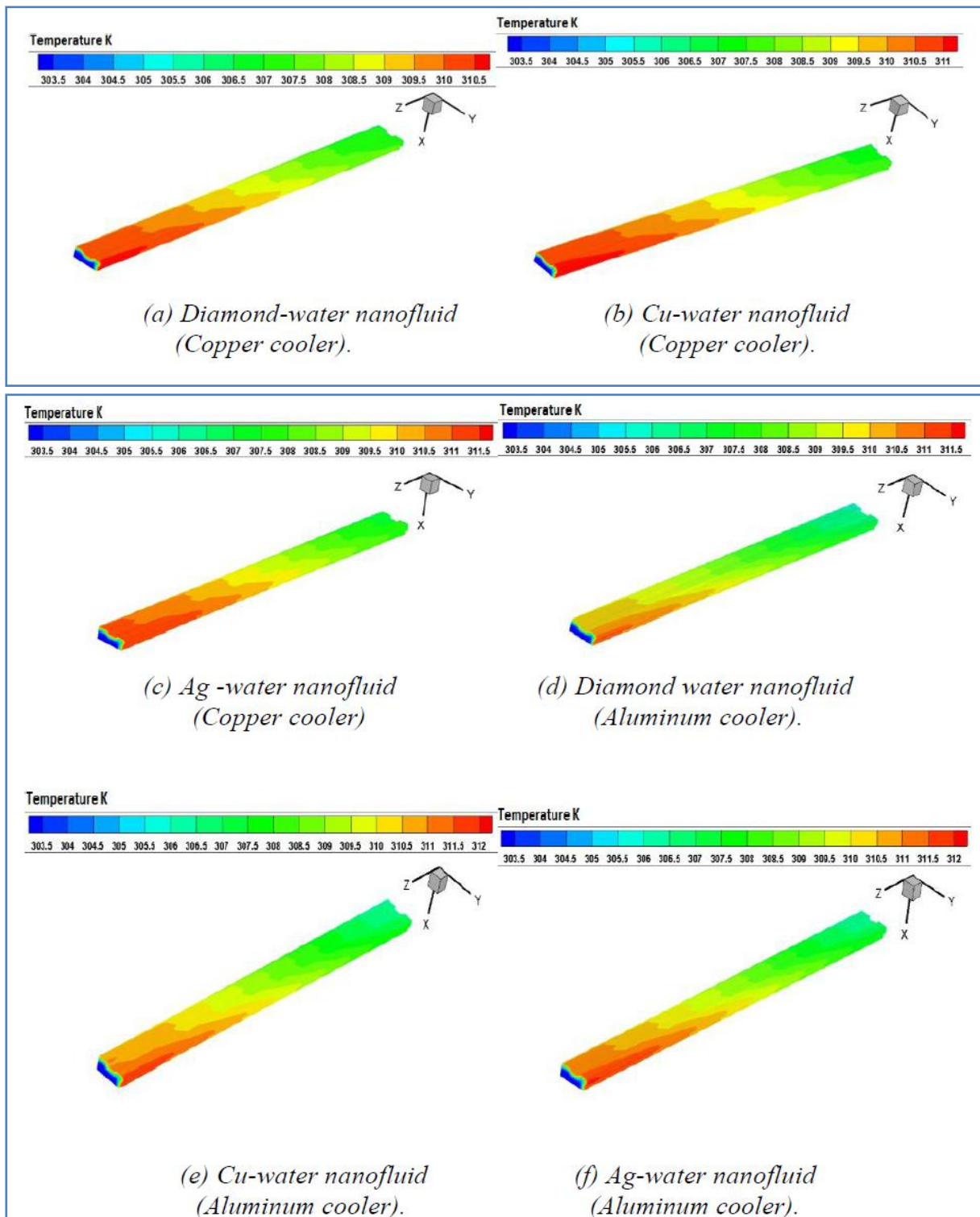


Figure (IV.23): Distribution of the temperature in the surfaces of the mini-channel for $Re = 1414$ and three different nano-fluids (volume fraction = 0.06).

IV.4.2.5. Conclusion (Application N°4)

In application N°4, we have studied the effect of different types of nano-particles numerically, by considering different volume fractions and types of cooler metals on heat transfer in a mini-channel cooler by using the commercial software, ANSYS-Fluent 15.0. The obtained results conclude that:

- For the Reynolds number equal to 1414 and the power of electronic component equal to 130W, the temperature of the electronic component is the lowest for the diamond-H₂O and it is the highest for the Ag-H₂O and Cu-H₂O nano-fluids.
- For the two cooler metal types, the copper cooler is better in the reduction of the temperature followed by aluminum.
- The use of diamond-H₂O nano-fluid significantly gives higher heat transfer coefficients than that of the Ag-H₂O and Cu-H₂O nano-fluids.
- The increase in the percentage of nano-particle in basic fluid (water) allows ameliorating the heat transfer coefficient in a mini-channels cooler.

These results will be used in the design and improvements of the mini-channels cooler.

IV.5 Application 5: Numerical study in three dimensions of the influence of the fluids' nature and obstacle position on cooling of electronic component

IV.5.1. Introduction

This application presents the results of a numerical study of the influence of the nature of nano-fluids and the obstacle position within the mini-channel of dimensions (10 x 10 x 108 mm³) on the electronic component cooling. The mathematical model and the studied geometry were given in chapter III (see section III.4.7). The power of the electronic component is constant. In these simulations, we consider the Al₂O₃-water, SiO₂-water and TiO₂-water as coolants with volume fraction of nano-particles $\varphi=0,05$. The numerical results are obtained by choosing a Reynolds number (Re) between 300 and 500; considering the flow regime to be stationary.

IV.5.2. Independence of the mesh

Figure (IV.24) shows the variation in the maximum temperature of the component in the tenth case along the different number of cells applied. According to the figure, we can conclude that the solution is independent of the mesh.

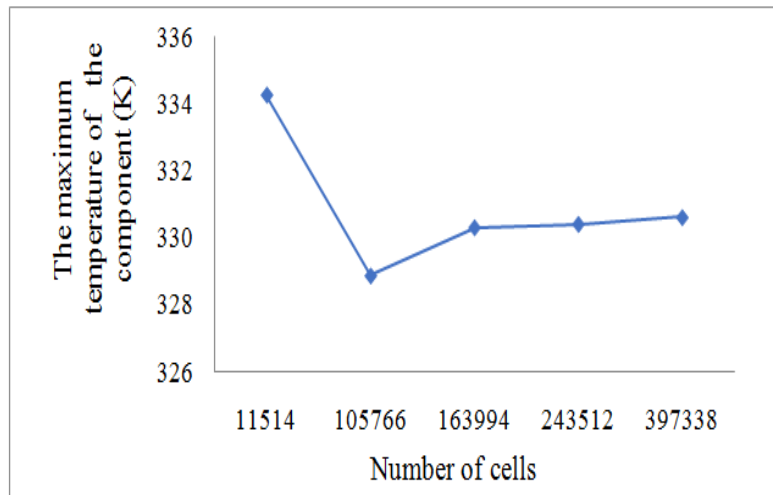


Figure (IV.24): Influence of the number of cells on the temperature of the component for the first case (Re = 500 and volume fraction = 0.05).

IV.5.3. Results and Interpretations

The results of the simulation are represented in application N°5 to determine the effect of the obstacle position inside a horizontal mini-channel on the cooling of the electronic component, as well as choosing the appropriate coolant from the set nano-fluids used in this study. We found out the following results:

Figure (IV.25) shows the evolution in the temperature value of the electronic component according to the Reynolds number. The temperature decreases substantially within the three types of nano-fluids, when the Reynolds number increases. The electronic components have a high temperature for lowest values of the Reynolds number and a minimum temperature for higher values of Re. Additionally, we find that when cooling with SiO₂-H₂O nano-fluid, the maximum temperature of the electronic component changes from 340.36 K to 331.86 K at various Reynolds numbers ranging from 300 to 500. Whereas, we find that the maximum temperature of the electronic component ranges between 338,77 K and 330,4 K for Al₂O₃-H₂O nano-fluid. Comparing these results, we find that Al₂O₃-water nano-liquid is more effective at reducing the temperature of the electronic component.

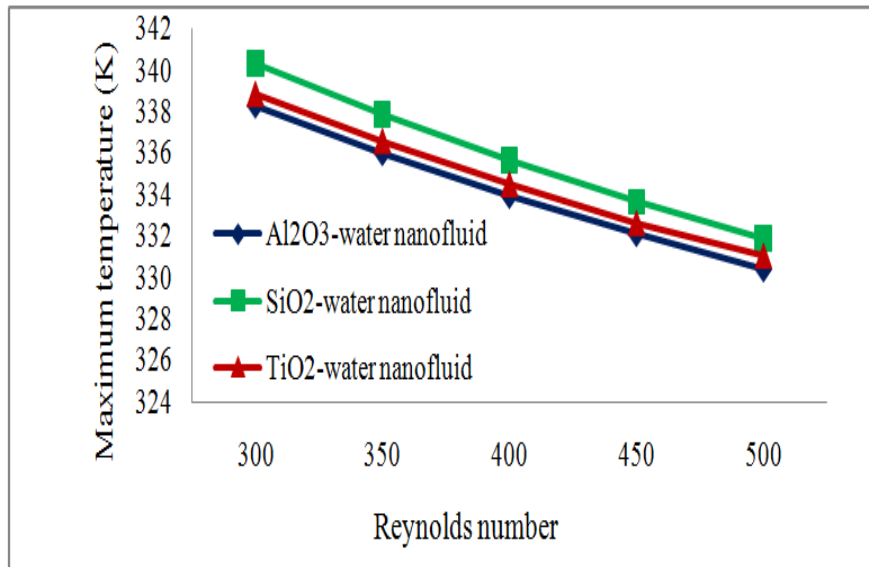


Figure (IV.25): The variation in the temperature of the electronic component according to the number of Reynolds.

Figure (IV.26) shows that for a Reynolds number equal to 500, and a volume fraction of nano-particles Al_2O_3 equal to 0.05, the distribution of temperature in the walls of the electronic component depends on the obstacle position. In fact, we find out that the temperature of the electronic component walls located near the entrance to the canal is low compared to the walls near the channel outlet for three cases. We also find that the position of the obstacle in the eleventh case helps in an acceptable way to improve and reduce the temperature of the walls of the electronic component compared to the thirteenth case, which is the best comparison with the tenth case. Exceptionally, the twelfth case gave a low temperature on the walls of the electronic compared to other cases (case 10, case 11 and case 13) as shown in Figure. 6.

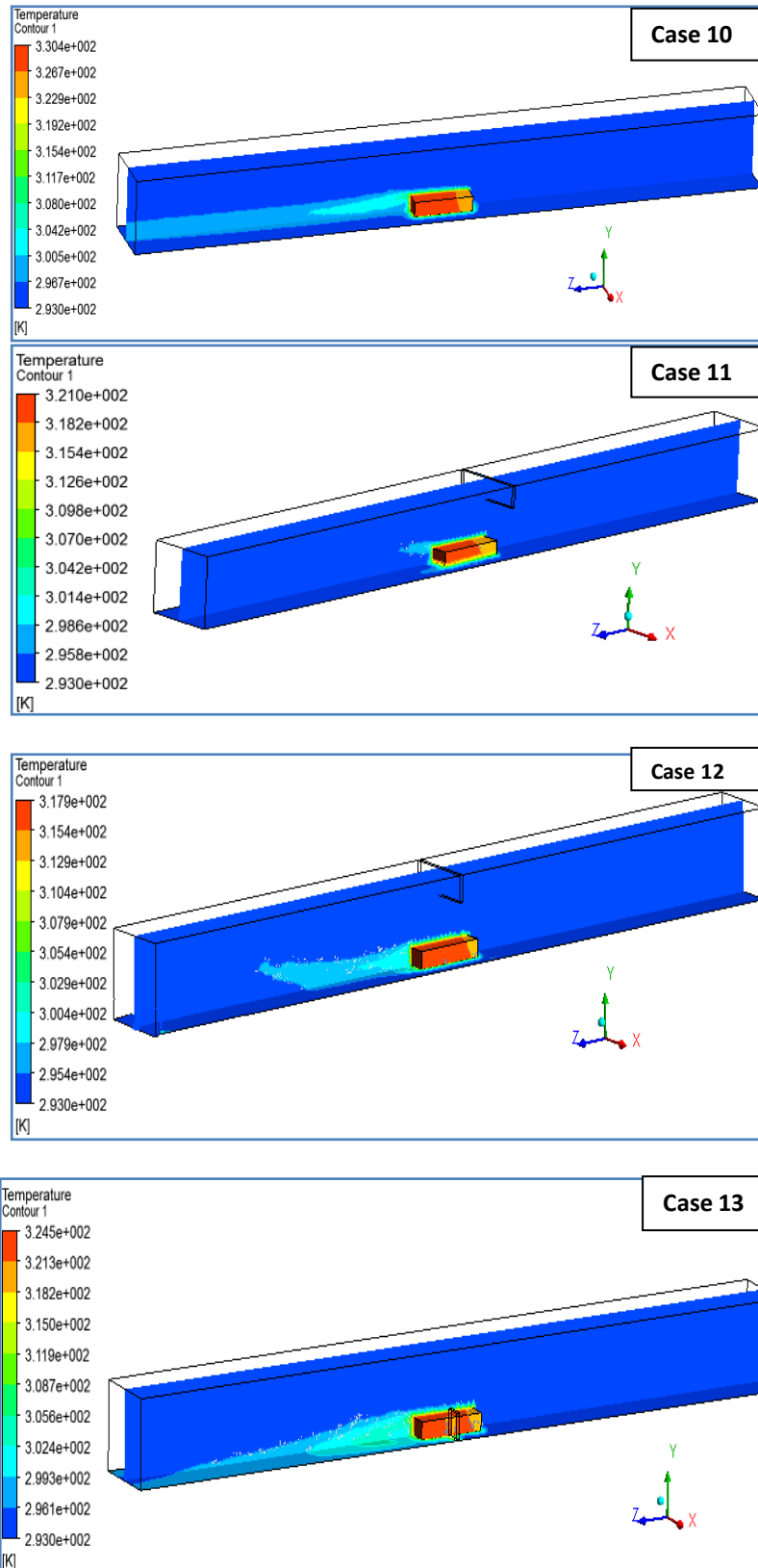


Figure (IV.26): Isotherms at the electronic component and in the middle of the mini-channel corresponding to $Re = 500$, volume fraction $\phi = 0,05$ in four cases.

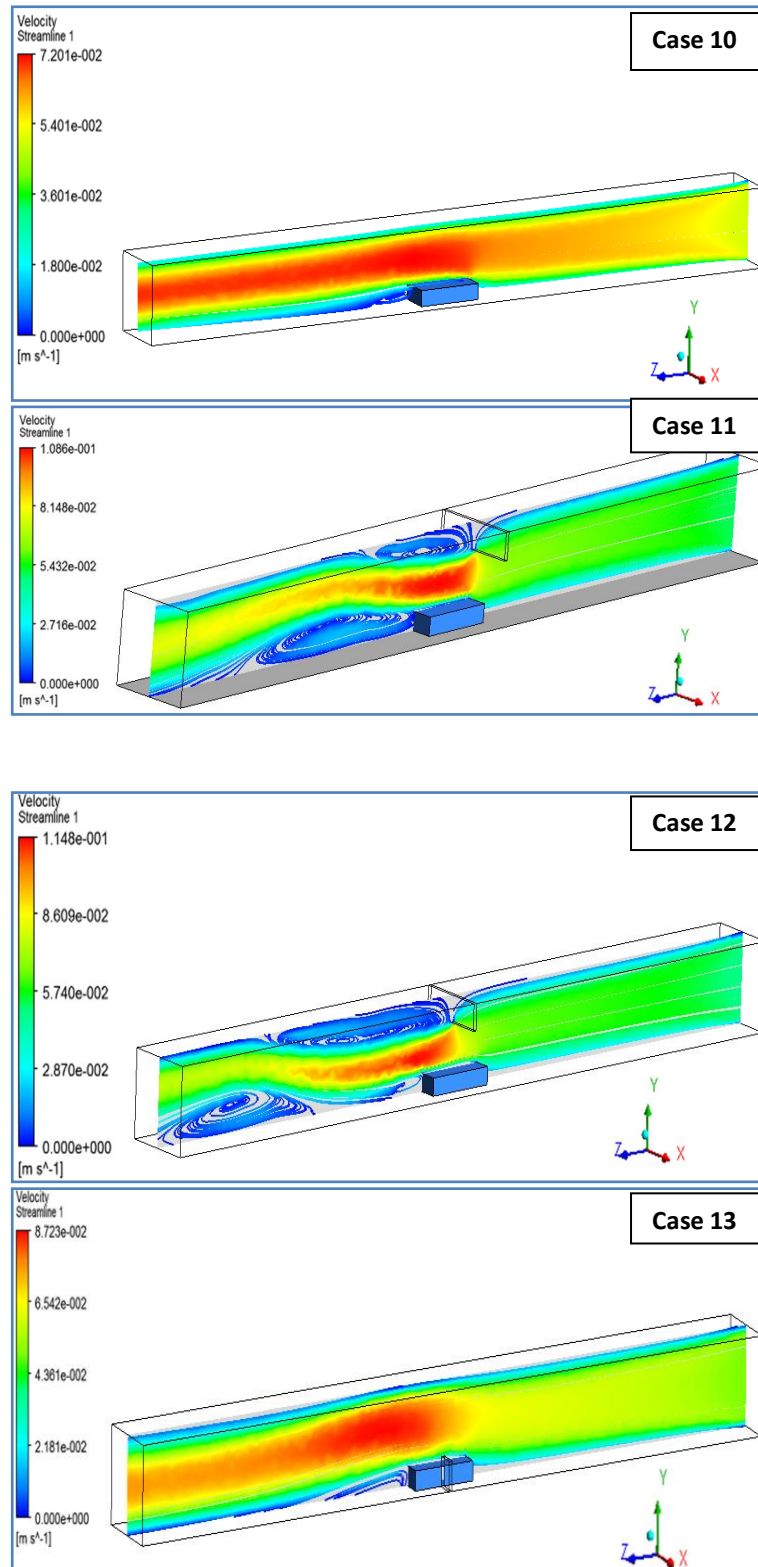


Figure (IV.27): Velocity contour of Al_2O_3 -water nano-fluid flow in mini-channel corresponding to $\text{Re} = 500$, volume fraction $\phi = 0,05$ in four cases.

Figure (IV.27) shows the velocity distribution of Al_2O_3 -water nano-fluid at the plane $x = 5 \text{ mm}$ for a Reynolds number equal to 500, and for a volume concentration of nano-particles equal to 0,05.

The comparison between the four cases shows that when obstacles are placed near the electronic component, the flow velocity increases at these obstacles and the flow inside the channel is unstable, contrary to what we notice in the thirteenth case, the position of the obstacle does not give an increase in the flow velocity at the walls of the electronic component compared to the eleventh and the twelfth case. Moreover, we find the maximal of the flow velocity in case 13 (0,1148 m/s), while we find it in the tenth, eleventh and thirteenth case equal to $V_{\text{case1}}= 0.072$ m/s, $V_{\text{case2}}= 0.10$ m/s and $V_{\text{case4}}= 0.087$ m/s respectively.

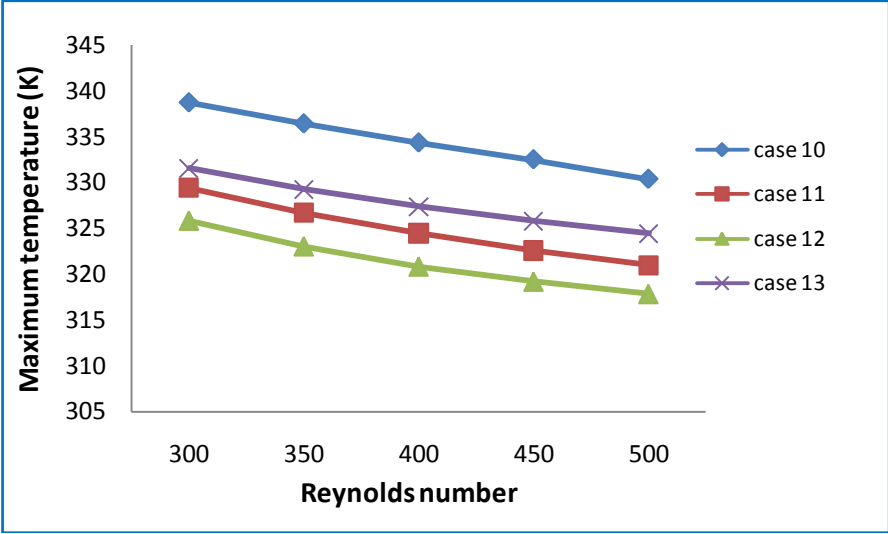


Figure (IV.28): The values of the component temperature according to Re for four cases.

The comparison of the four cases studied (Figure (IV.28)) shows that when the obstacle is placed near the electronic component, the temperature of the electronic component decreases and vice versa. The reason is that when the obstacle is placed near the electronic component and at the top of the mini-channel, the velocity values between the obstacle and the electronic component are high compared to the flow velocity in the mini-channel. Thus, the heat exchange between the liquid and the electronic component improves, and we find that the maximum temperature of the electronic component is 338.7 K to 330.4 K at various Reynolds numbers ranging from 300 to 500 for case 10. However, we find that the maximum temperature ranges between 325.84 K and 317.89 K for case 12. We also find that when the Reynolds number changes between 300 and 500, the maximum temperature of the electronic component in the eleventh case has been the lowest value of the component temperature in the thirteenth case.

IV.5.4 Conclusion (Application N°5)

In this study, we examined the influence of the nature of nano-fluids and obstacle position on cooling of electronic component. The obtained results confirm that:

With the increase of Reynolds number for all cases, we found that the maximum temperature of the electronic component decreases, we also find the temperature values of the electronic component of the twelfth case are low compared to the other studied cases.

The liquid containing nano-particles Al_2O_3 is better for cooling electronic component.

In this study, the mini-channel with the position of the obstacle in the twelfth case provides much better thermal performance than the other cases. It is suggested that the appropriate obstacle form and design positions within the mini-channel can be used to improve the overall thermal performance.

IV.6 Application N°6: A numerical study on the effect of the addition of the pie shape ribs and parallelogram ribs in micro- channels on thermal performance using Diamond - water nanofluid

IV.6.1. Introduction

This application presents the results of a numerical study in three dimensions, the Influence of the addition of the parallelogram ribs and pie shape ribs in microchannel on thermal exchange. In this study, we designed four cases of micro channel heat sinks, the Fourteenth and fifteenth cases do not contain the ribs in micro channel, unlike the Sixteenth case in which we added the ribs in a pie shape, while the seventeenth case contains the parallelogram ribs. The geometry, the mathematical model and the boundary conditions for these studies were given in chapter III (see section III.4.8). Particularly, we have chosen silicon micro channel heat sinks in four cases. A constant heat flux is applied to the bottom wall of microchannels heat sinks and we used a nano fluid diamond-water with $\phi=0,05$ volume concentration of diamond nano-particle as a coolant, and also using the commercial software ANSYS Fluent Reynolds number (Re) has been taken between 200 and 600 and the flow regime has been assumed to be stationary.

In this study, the results of mesh independence tests are presented in section IV.6.2. The validation of the calculation code using data drawn from the Chai *et al.* [139] is presented in section IV.6.3. Section IV.6.4 contains the results in graphical form and their discussion. This application is closed with a conclusion bringing together the various observations.

IV.6.2. Independence of the mesh

After the simulation calculations converged, we tested mesh independence. Figure (IV.29) shows meshing view in three dimensions. Meshing details are like number of nodes 972972, maximum skewness 0,00816. Maximum and minimum orthogonal quality is 1 and 0.999, respectively for case 14.

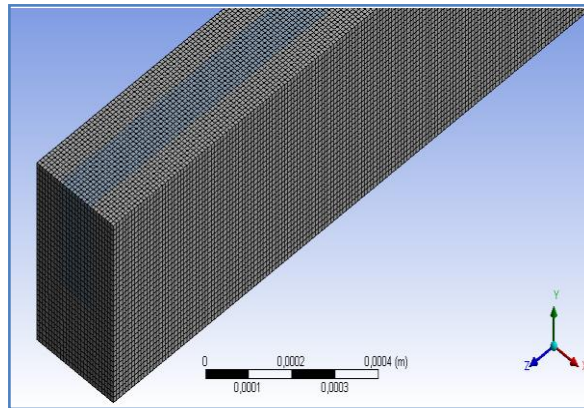


Figure (IV.29) :Meshing of microchannel of case 14

The nodes used for meshing the physical domain are affecting the results.

Figure (IV.30) shows the number of nodes used in the analysis of micro channel heat sink in case 14 with the result of Nusselt number. According to this figure, we can conclude that the solution is independent of the mesh.

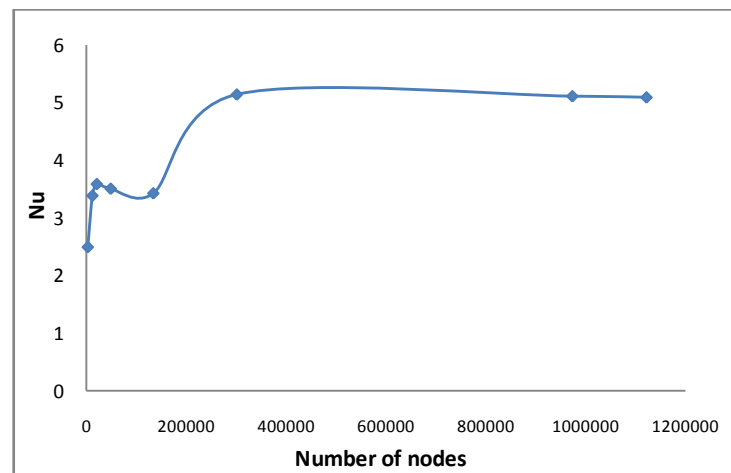


Figure (IV.30): Grid independence examination at $Re = 200$ and the heat flux is 100 W/cm^2 .

IV.6.3. Validation of the results

To validate our numerical results, we choose to compare the results obtained by our numerical simulations with those found by Chai *et al.* [139].

Figure (IV.31) represents the validation of our simulation for the variation of the Nusselt number according to the different values of inlet Reynolds number with experimental data results of Chai *et al.* for the smooth micro channel.

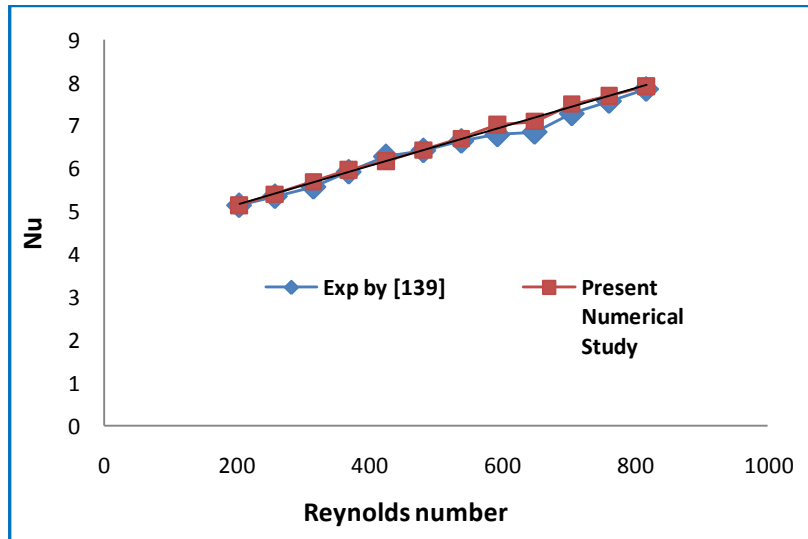


Figure (IV.31): Comparison of numerical results of Nusselt number vs Re with resultants of ref [139] for the smooth micro channel

From these results, it is clear that the Nusselt number increases to the inlet Reynolds number between 200 and 800.

These results show a good agreement with the results of Chai *et al.*

The results of the simulation are represented in this study to determine the effect of the addition of the pie shape ribs and parallelogram ribs in micro-channels on thermal performance. The results we found are as follows:

IV.6.4. Results and Discussions

Figure (IV.32) shows the variation in the temperature of the heated bottom wall in the different cases studied. From these results, we noted that low temperature is on the inlet side, it goes on increasing towards the outlet of micro channel as in the Fourteenth and the fifteenth cases, adding a wave to the micro channel reduces a value temperature compared to the first case, while in the Sixteenth and seventeenth cases we find that the temperature decrease from

$z = 2.5 \text{ mm}$ to $z = 4 \text{ mm}$ and then rises slowly, due to the ribs positioned at the end of the micro channel,

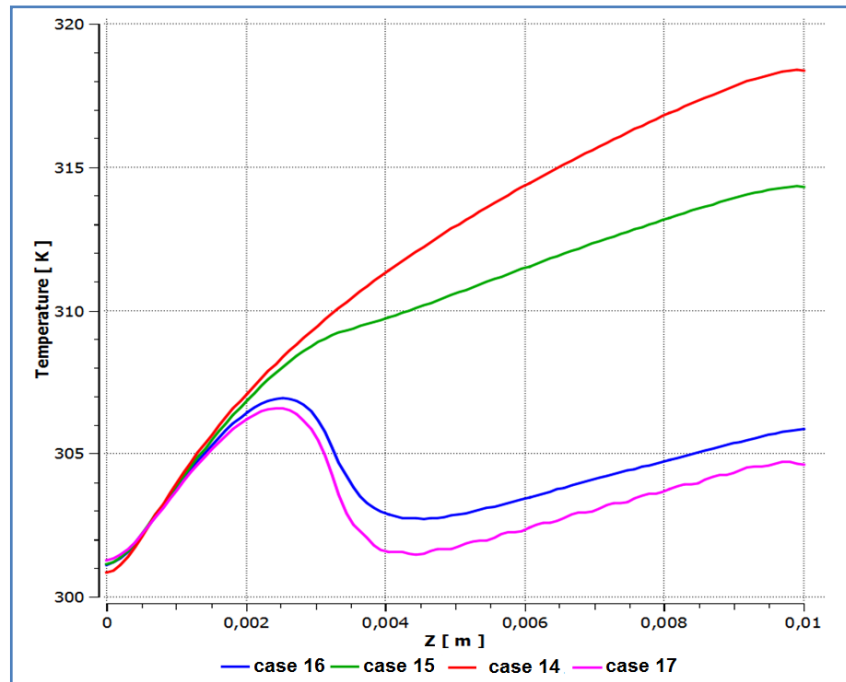


Figure (IV.32): Comparisons of temperature profiles on the heated bottom wall for all cases at $Re= 600$ and the heat flux is $100W/cm^2$

Furthermore, we observe that the temperature values of the bottom surface of the substrate in the seventeenth case is inferior in comparison to other cases. Also, figure (IV.33) represents the distribution in two dimensional temperatures on the bottom wall for all cases.

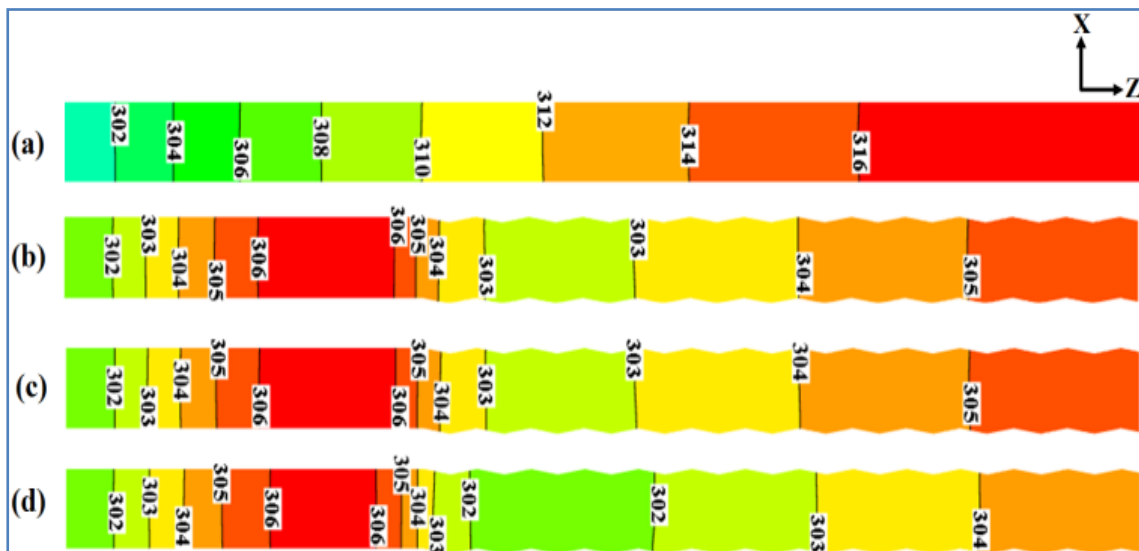


Figure (IV.33): The two-dimensional temperature distribution on the bottom wall in four cases (a: case 14, b: case 15, c: case 16 and d: case 17), at $Re=600$ and $\phi=0.05$, the unit of temperature is Kelvin

The results of Figure (IV.34) show the evolution of the maximum temperature on the bottom wall of the substrate with Reynolds number (Re) in four cases. The maximum temperature on the bottom wall of the substrate decreases substantially in all cases when the Reynolds number increases. The bottom wall of the substrate has a high temperature for low values of the Reynolds number and a minimum temperature for higher values of Re. Besides, we find in rectangular micro-channel heat sinks (case 14), the temperature at bottom face is 333.24 K to 318.46 K at various Reynolds numbers ranging from 200 to 600. Whereas, we find that the temperature at the lower wall ranges between 317.91 K and 306.58 K in the seventeenth case (micro-channel with parallelogram ribs).

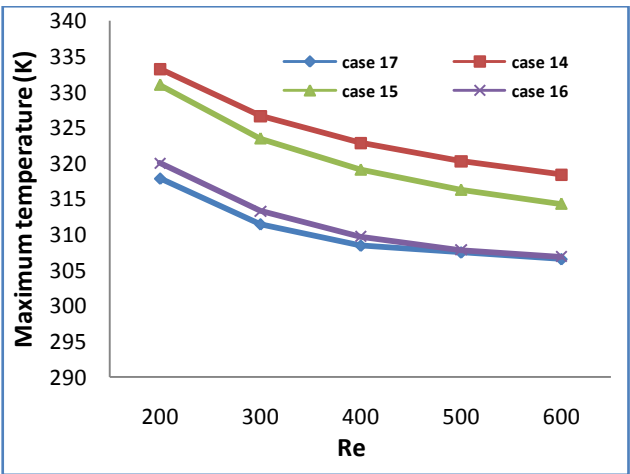
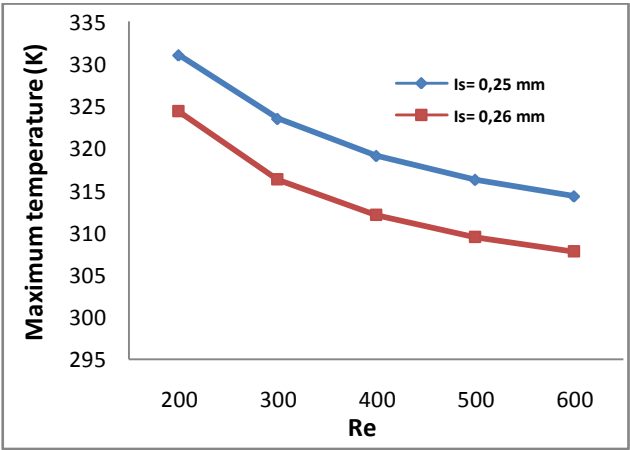
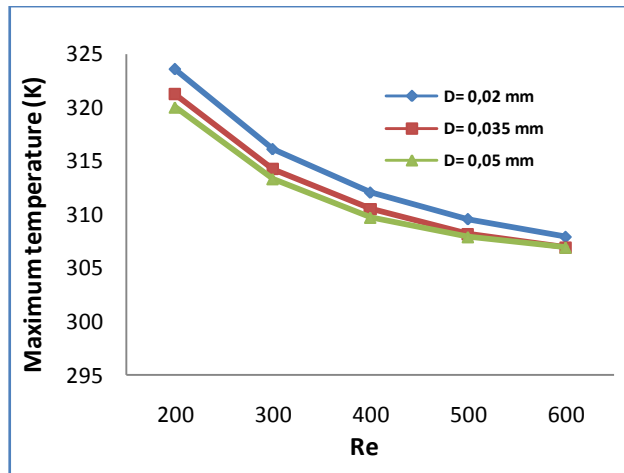


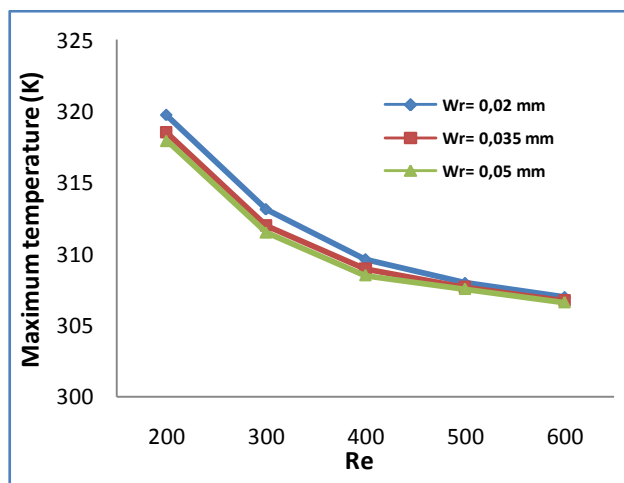
Figure (IV.34): The maximum temperature on the heated bottom wall with the inlet Reynolds number ranging from 200 to 600 for all cases.



(a)



(b)



(c)

Figure (IV.35): Evolution of the maximum temperature on the bottom wall in function with Re and with the geometric parameter in three cases

Figure (IV.35) shows the evolution of the maximum temperature on the bottom wall in function with the Reynolds number and with the geometric parameter (I_s , W_r and D) in three cases (case 15, case 16 and case 17). In the fifteenth case (show figure 8. a) when the length I_s increases, the temperature value decreases. Likewise, the same observation can be deduced in case 16 (figure 8. b) and case 17 (figure 8. c), when W_r and D increases, the maximum temperature of the bottom surface decreases.

Figure (IV.36) shows the evolution of the Nusselt number in function with a number of the Reynolds and with the geometric parameter in three cases (case 15, case 16 and case 17). We note that when increasing the I_s , D and W_r , the Nusselt number increases with different proportions.

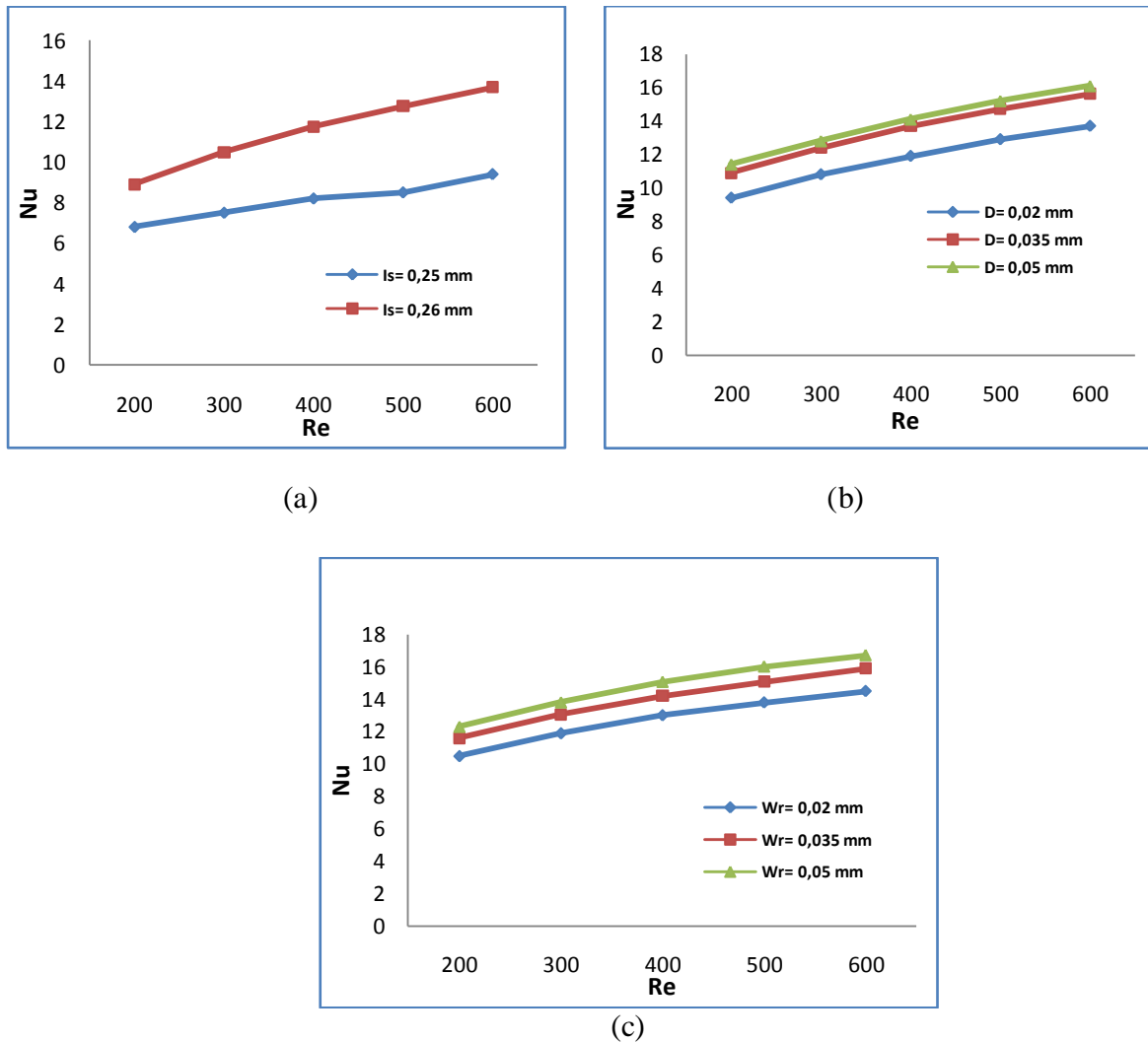


Figure (IV.36): Evolution of the Nusselt number in function with the number of Reynolds and with the geometric parameter.

The temperature, contour of inlet, middle and outlet is shown in Figure (IV.37) at Reynolds number is equal to 600 and the volume fraction is equal to 0,05. In all cases, they found that the high temperature region takes place at the limit of the heat sinks since there is no heat loss by nano-fluid convection. In addition, in the case 14 the temperature gradient for nano-fluid raises along the longitudinal z orientation from the channel inlet to the outlet due to convection heat exchange. We find when adding the sides and increasing the contact surfaces between the coolant and the channel walls in the Sixteenth and seventeenth, we notice a difference in the coolant temperature values along the channel compared to the fourteenth case (rectangular microchannel).

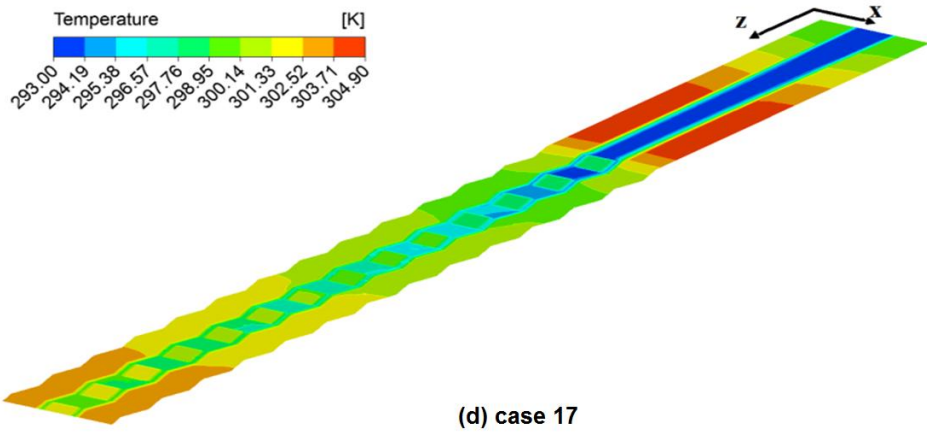
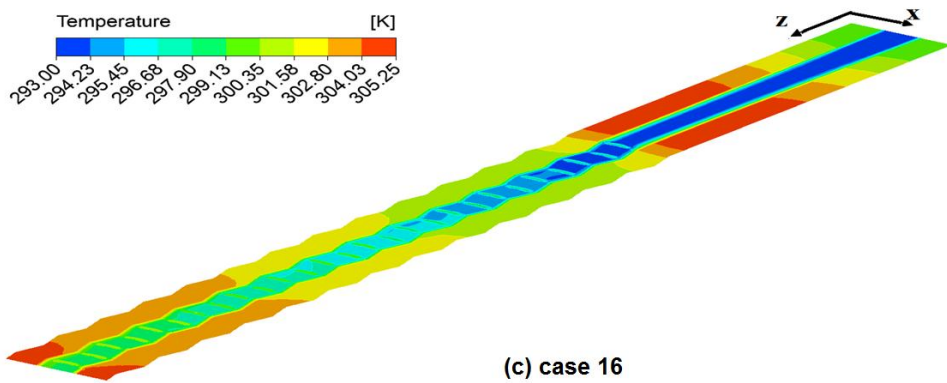
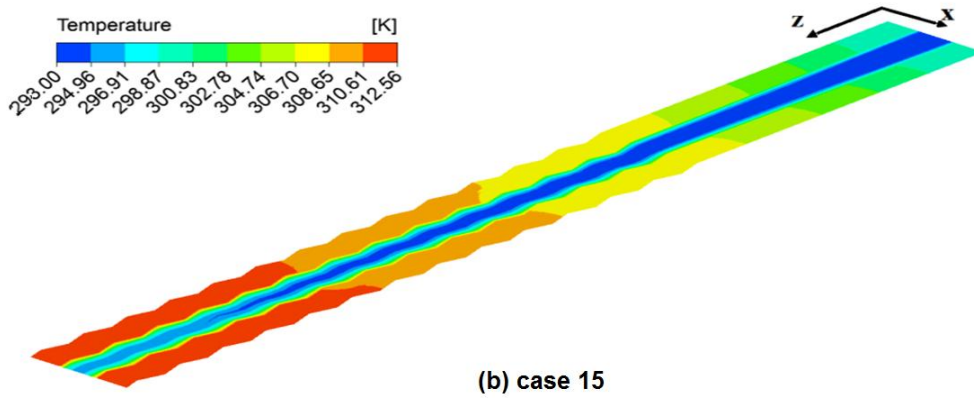
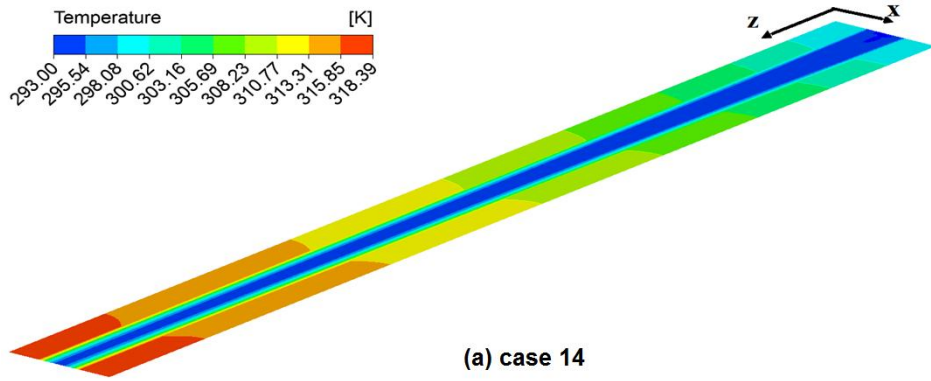


Figure (IV.37): Static temperature contours for plane $y = 0.25$ mm along the length of the microchannel for different cases at Reynolds number of 600 and volume fraction equal 0.05

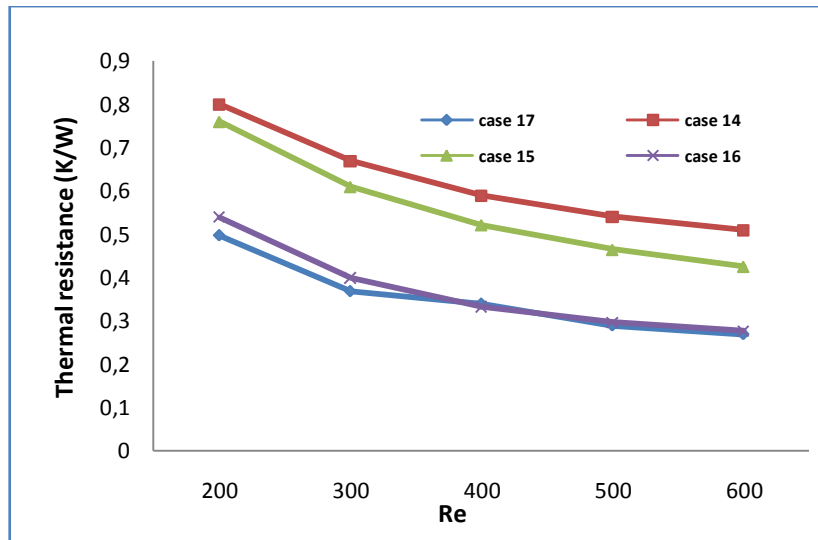


Figure (IV.38): Thermal resistance of micro channel heat sinks with the inlet Reynolds number in four cases.

Figure (IV.38) shows, the variation of the thermal resistance with Reynolds number in four different micro channel heat sinks, we found that the micro channel of the fourteenth case has the highest value of the thermal resistance and the lowest resistance we find in the micro channel of the sixteenth and seventeenth cases.

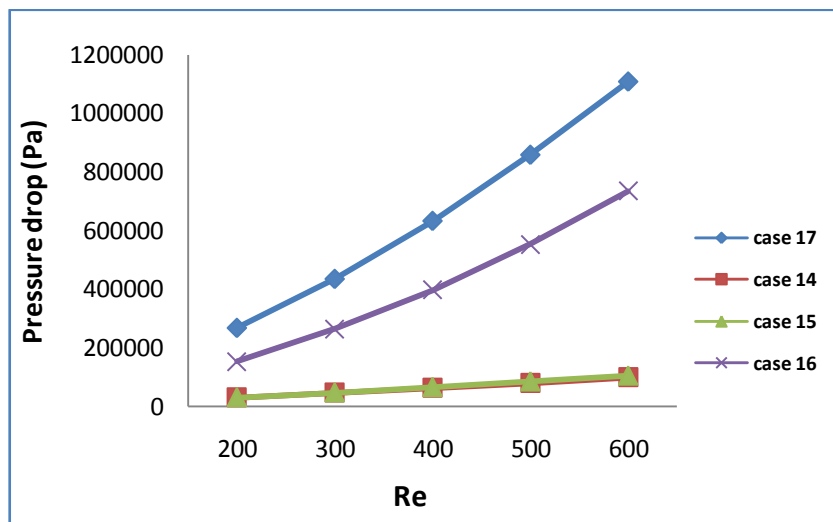


Figure (IV.39): The variation between pressure drop and inlet Reynolds number in all cases

Figure (IV.39) shows the variation between pressure drop and Reynolds number in four cases. The pressure drop is estimated for various Re numbers ranging from 200 to 600. We found that the pressure drop increases linearly with the Reynolds number. We observe that the pressure drop of case 17 is upper than that of all the other cases, however, the lowest pressure drop is obtained for the rectangular microchannel without ribs in case 15.

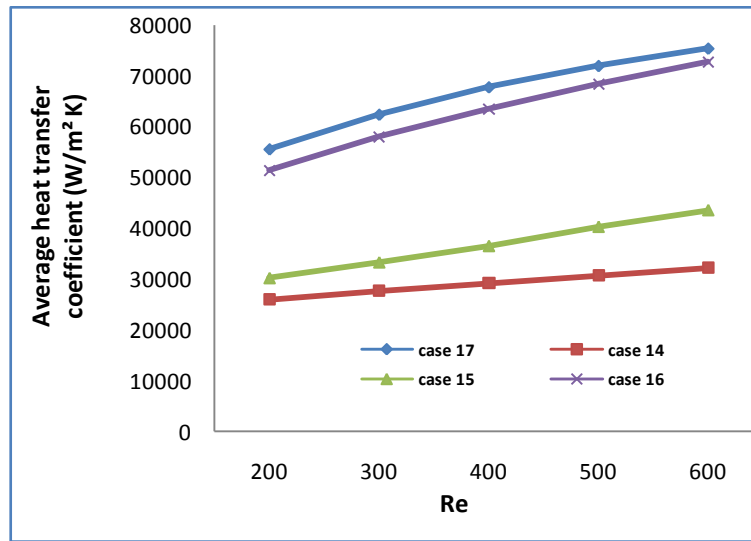


Figure (IV.40): Average heat transfer coefficient of micro channel heat sinks with the Reynolds number in four cases

Figure (IV.40) shows the average heat transfer coefficient calculated as a function of the Reynolds number in a volume fraction of 0.05 in four cases. The average heat transfer coefficient is proportional to the Reynolds number varying from 200 to 600. Comparing the four micro channel heat sinks, case 17 has the highest values among the four cases, as the micro channel heat sinks in the seventeenth case gives a better average heat transfer coefficient than case 16, and case 16 is better than case 15 and case 14. It is found that, in all cases, the average heat transfer coefficient increases linearly with the inlet Reynolds number. The same thing is observed in Figure (IV.41), the Nusselt number with a Reynolds number in different cases, the rise in Nusselt number with the inlet Reynolds number. The reason is that when the velocity is increased, the flow rate of the fluid is increased as well, so its ability of removing heat is larger. Also, as it increases the contact surfaces by adding the ribs in the micro channel, it contributes to increasing the heat exchange between coolant and walls of micro channel heat sinks. Furthermore, in our study, we found that the parallelogram ribs in the seventeenth case are the best in the process of improving the heat exchange and thus reduce the temperature of the surface heat in the bottom of microchannels.

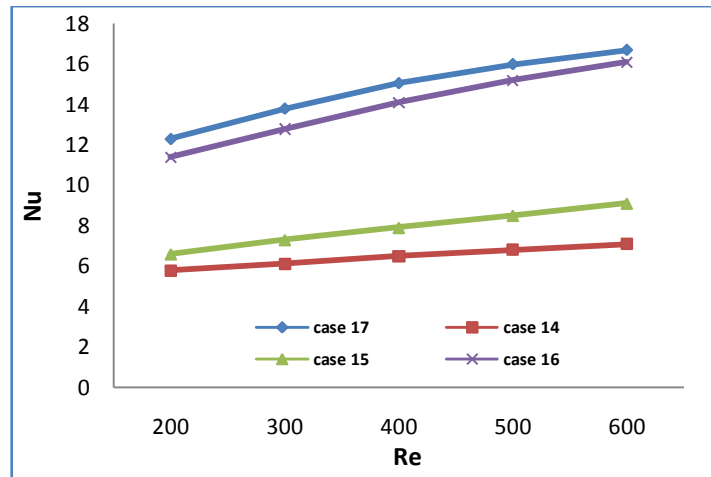


Figure (IV.41): Variation of Nusselt number with Reynolds number in all cases

As shown in figure (IV.42), the evolution of the friction factor with Reynolds number for four cases studied. The results show that the friction factor is lowering with the raise of Reynolds number in the different cases of micro channels. We also note that the friction factor decreases by a small percentage in the Fourteenth and fifteenth cases compared to the sixteenth and seventeenth cases in which we find the friction coefficient decreasing by a large percentage. It can be inferred that the addition of parallelograms and pie shape, ribs to the micro channel to give an increase in the friction factor compared to rectangular micro channel (case 14) and micro channel is in the fifteenth case for all values of the Reynolds number.

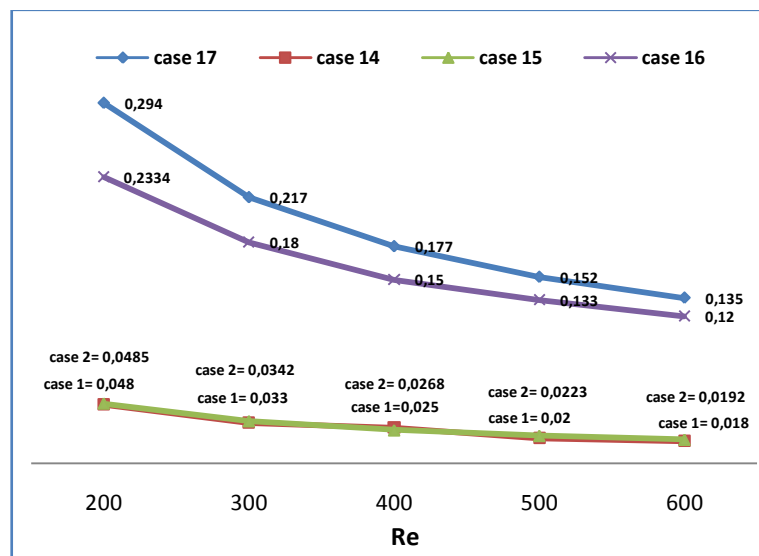


Figure (IV.42): Average friction factor of all cases with Reynolds number for $q=100 \text{ W/cm}^2$

However, we found that the friction factor of case 17 channels is still higher than that of the case 16, case 15 and case 14.

IV.6.5. Conclusion (Application N°6)

In this application we studied the effect of the addition of the pie shape ribs and parallelogram ribs in micro- channels on thermal performance using Diamond - water fluid, and finally obtained the following results:

- With the increase of Reynolds number in all cases, we found that the temperature on the heated bottom wall decreases, also we find the temperature values on the heated bottom in the case 17 (micro channels containing the parallelogram ribs) are low compared to the other studied cases.
- For the Reynolds number ranging from 200 to 600, the microchannels with ribs can significantly increase the heat transfer performance. According to our studies, we find that the micro channels with parallelogram ribs are effective compared to micro channel with pie shape ribs.
- Increasing the flow velocity reduces the thermal resistance and increases the friction coefficient simultaneously in all cases. It shows the friction factor of the micro channels with parallelogram ribs (case 17) is still higher than that of the micro channels with parallelogram ribs (case 16), case 15 and rectangular micro channels (case 14). And also, the micro channels of the Fourteenth and fifteenth cases have the highest value of the thermal resistance, while, we find the least resistance found in the micro channels with pie shape and parallelogram ribs.

Annex international publications

Annex:1

Publication from application N°1

This work has been the subject of an international conference on **nano-fluids**
1st International Conference on Nano-fluids (ICNf2019)
2nd European Symposium on Nano-fluids (ESNf2019)
26-28 June 2019, Castelló, Spain

(K. Chadi, B. Guerira, N. BELGHAR, M. Falek, C.E. Bensaci and A. Messaoudi)

The title of the article is:

Numerical study of the influence of nano-fluids on thermal exchange in mini-channels

Annex:2

Publication from application N°2

This work was the subject of an international conference on **nano-fluids**
1st International Conference on Nano-fluids (ICNf2019)
2nd European Symposium on Nano-fluids (ESNf2019)
26-28 June 2019, Castelló, Spain

(K. Chadi, N. BELGHAR, B. Guerira, M. Falek, C.E. Bensaci and A. Messaoudi)

The title of the article is:

Numerical study of the thermal transfer in different geometries of the mini-channels

Annex:3

Publication from application N°3

This work has been the subject of an international publication in *Metallurgical and Materials Engineering (2020) Vol 26 (1) 2020 p. 103-119*

(Kamel Chadi, Nourredine Belghar, Belhi Guerira, Aissam Messaoudi)

The title of the article is:

Three-dimensional numerical study of thermal exchanges in different geometry sections of mini-channels using three different nano-particles

Annex:4

Publication from application N°4

This work has been the subject of an international publication in *Metallurgical and Materials Engineering (2020) Vol 26 (1) 2020 p. 121-135*

(Kamel Chadi, Nourredine Belghar, Belhi Guerira, Zied Driss)

The title of the article is:

Influence of types of nano-particles, nano-particles volume concentration and types of cooler metals on the heat transfer in a mini-channel cooler

Annex:3

*Metallurgical and Materials Engineering
Association of Metallurgical Engineers of Serbia AMES*

*Research paper
<https://doi.org/10.30544/455>*

THREE-DIMENSIONAL NUMERICAL STUDY OF THERMAL EXCHANGES IN DIFFERENT GEOMETRY SECTIONS OF MINI-CHANNELS USING THREE DIFFERENT NANOPARTICLES

Kamel Chadi^{1}, Nouredine Belghar¹, Belhi Guerira¹, Aissam Messaoudi²*

¹Laboratory of Materials and Energy Engineering, University of Mohamed Khider Biskra, Algeria

²Abbes Laghrour University of Khenchela, Algeria

Received 04.12.2019

Accepted 08.04.2020

Abstract

In the present work, we have studied the thermal exchanges of different geometry sections of mini-channels of a cooler numerically. Particularly, we have chosen a mini channels cooler copper for cooling an electronic chip IGBT. In our simulation of three-dimensional (3D), we have compared the numerical results for the different forms of the proposed mini-channels and the three different types of nano-fluids by using the Cu-water, the Ag-water, and the Diamond-water with a volume fraction of 0.02%. The numerical results are obtained by choosing a Reynolds number (Re) between 100 and 900 and considering that the flow regime is stationary.

The simulation was performed using commercial software, ANSYS-Fluent 15.0. The results obtained show that the increase of the exchange surface between the walls of the mini channels and the cooling fluid makes increases the heat exchange coefficient and the improvement of the maximum junction temperature of the electronic chip IGBT with the increase of the Reynolds number.

The choice of nanoparticles has considerable effects on improving the heat transfer and the maximum junction temperature of the chip IGBT.

Keywords: heat exchange; mini-channels; numerical simulation; nanofluid; fluent.

Introduction

Temperature is an important factor in the performance of the electronic component. This temperature can be high enough to reduce in a significant manner the life of the component. To ameliorate this temperature, it is necessary to ameliorate the

*Corresponding author: Kamel Chadi, chadikamel_dz@yahoo.fr

Annex:4

*Metallurgical and Materials Engineering
Association of Metallurgical Engineers of Serbia AMES*

*Research paper
<https://doi.org/10.30544/457>*

INFLUENCE OF TYPES OF NANOPARTICLES, NANOPARTICLES VOLUME CONCENTRATION AND TYPES OF COOLER METALS ON THE HEAT TRANSFER IN A MINI-CHANNEL COOLER

Kamel Chadi^{1}, Nourredine Belghar¹, Belhi Guerira¹, Zied Driss²*

¹Laboratory of Materials and Energy Engineering, University of Mohamed Khider Biskra, Algeria

²Laboratory of Electromechanical Systems (LASEM), National School of Engineers of Sfax (ENIS), University of Sfax (US), B.P. 1173, Road Soukra km 3.5, 3038, Sfax, Tunisia.

Received 05.12.2019

Accepted 05.04.2020

Abstract

In the present work, we have studied the effect of three different types of nanoparticles, nanoparticles volume concentration and types of cooler metals on heat transfer in a mini channel cooler numerically. In these simulations, we have considered the Cu-H₂O, the Ag-H₂O and the Diamond-H₂O with different volume fractions in the range of 0.02%-0.1% and for two types of cooler materials for cooling an electronic component. In these conditions, the inlet velocity is constant for the three different types of nano-fluids. The power of the electronic component is equal to 130 W. The numerical results are developed for a Reynolds number equal to 1414 and a steady-state.

The simulation was performed using commercial software, ANSYS-Fluent 15.0. The obtained results show that the average heat transfer coefficient increases with the increase of the volume fraction of the nanoparticles (Cu, Ag, Diamond) and with the decrease of the temperature of the electronic component. In these conditions, the average heat transfer coefficient is the highest for the H₂O–diamond nanofluid compared with the other nanofluids the Cu-H₂O and the Ag-H₂O. Furthermore, the types of cooler metals have considerable effects on the amelioration of the temperature of the electronic components.

Keywords: heat transfer; nanofluid; mini channels; cooler; fluent.

Introduction

Heat transfer is a process of great importance in the field of industry and technology, particularly in the field of cooling the electronic components by micro-

*Corresponding author: Kamel Chadi, chadikamel_dz@yahoo.fr

Conclusions and recommendations

This thesis presents the results in 3D of the six studies: The first relates to a numerical study of the thermal transfer in three different geometries of the mini-channels with the dimensions (21x21x3.5mm³). While the second study is related to the influence of nano-fluids on thermal exchange in mini-channels.

In this study, the power of electronic component is constant, the solid volume fraction equals 0.05. The parameters studied are the nature of three nano-fluids, the Reynolds number is in the range $200 \leq Re \leq 800$.

The results in both studies allowed us to draw the following results: The mini-channels of the third case improve the heat transfer compared to the other cases as well as the value of the maximum temperature of the junction of the electronic component. And the use of diamond-water nano-fluid gives significantly higher heat transfer coefficients than water-Ag and water-Cu nano-fluid.

The third study relates to the numerical modeling of the thermal transfer in different geometry sections of the mini-channels using nano-fluids. The geometry of the Fourth case was used in an experimental and numerical study of a cooling system of electronic components by a liquid metal. This cooler is formed of 10 channels and 11 fins. The power of the chip IGBT 1200 V 75 A is equal to 130 W with thermal insulation on all the outside faces of the cooler. The inlet temperature of the nano-fluid in the cooler in all cases is equal to $T = 298.15\text{K}$. In these simulations, we consider the Cu-water, the Ag-water, and the Diamond-water as coolants with a volume fraction of 0.02.

This study allowed us to obtain the following results:- the mini-channel cooler in the ninth case gave a transfer improvement over other cases also, improvement of the maximum temperature value of junction of the electronic chip is observed. In these conditions, the types of nano-particles also have considerable effects on the improvement of the heat transfer, especially with the decrease of the nanoparticle diameter and with the increase of volumetric fraction.

As for the fourth study, in which we studied the influence of types of nano-particles, nano-particles volume concentration and types of cooler metals on the heat transfer in a mini-channel cooler. The obtained results conclude that:

The increase of the percentage of nano-particle in basic fluid (water) allows ameliorating the heat transfer coefficient in a mini-channels cooler.

- For the two cooler metal types, the copper cooler is better in the reduction of the temperature.

The fifth study concerns the influence of the fluids' nature and obstacle position on cooling of electronic component. In this study, we mounted in a mini-channel with the addition of obstacles in three cases, while one case does not contain the obstacles in mini channel (case 10), within the mini-channel of dimensions (10 x 10 x 108 mm³) on cooling of electronic component. The power of the electronic component is constant. In this study, we consider the Al₂O₃-water, SiO₂-water and TiO₂-water as coolants and The Reynolds number (Re) between 300 and 500. The results obtained allowed us to draw the following conclusions:

- The liquid containing nano-particles Al₂O₃ is better for cooling of the electronic component.

- The mini-channel with the position of the obstacle in the twelfth case provides much better thermal performance than the other cases. It is suggested that the appropriate obstacle form and design positions within the mini-channel can be used to improve the overall thermal performance.

The sixth study concerns the effect of the addition of the pie shape ribs and parallelogram ribs in micro-channels on thermal performance using Diamond - water nanofluid. In this study, the heat supplied to the silicon MCHS substrates through a bottom surface where the electronic chips are attached. The heat flux is generated by the chips equal $q=100 \text{ W/cm}^2$ and thermal insulation on all the outside faces of the heat sinks. We used a nano-fluid diamond-water with $\phi=0,05$ volume concentration of diamond nano-particle as a coolant. The results obtained allowed us to draw the following conclusions:

- With the increase of Reynolds number for all cases, we found that the temperature on the heated bottom wall decreases, moreover, we find the temperature values on the heated bottom in case 17 (micro channels containing the parallelogram ribs) are low compared to the other studied cases.

- For the Reynolds number ranging from 200 to 600, the microchannels with ribs can significantly increase the heat transfer performance. According to our studies (sixth study), we find that the micro channels with parallelogram ribs are effective compared to micro channel with pie shape ribs.

As recommendations to complete this study, we can suggest:

- a) The use of low Reynolds number models to better capture the turbulence near the walls.

- b) It is possible to use nano-fluids with excellent physical properties.
- c) New shapes of barriers can be created inside the channel to increase cooling.
- d) The shapes of the ribs inside the channel can be changed and tested.

Bibliographic references

- [1] E. C. Okonkwo, I.Wole-Osho, I. W. Almanassra, Y. M. Abdullatif, T. Al-Ansari, “An updated review of nanofluids in various heat transfer devices”, *Journal of Thermal Analysis and Calorimetry*, 2020.
- [2] I. Mjallal , H. Farhat, M. Hammoud , S. Ali and I. Assi, “Improving the cooling efficiency of heat sinks through the use of different types of phase change materials”, *Technologies*. Vol. 6 (1) 5, 2018.
- [3] S.M.Sohel Murshed, C.A.Nieto de Castro, “A critical review of traditional and emerging techniques and fluids for electronics cooling”, *Renewable and Sustainable Energy Reviews* Vol. 78, pp. 821-833, 2017.
- [4] K. Chavda, “Effect of nanofluid on heat transfer characteristics of double pipe heat exchanger: part-ii: effect of copper oxide nanofluid”, *International J. Research in Engineering and Technology*, Vol. 04, Issue: 04, 2015.
- [5] M. H. Esfe, A. A. A. Arani, A. H. Niroumand, W.-M. Yan, and A. Karimipour, “Mixed convection heat transfer from surface-mounted block heat sources in a horizontal channel with nanofluids”, *International Journal of Heat and Mass Transfer*, vol. 89, pp. 783–791, 2015.
- [6] W. Gui-Lian, Y. Da-Wei, W. Yan, N. Di, Z. Xiao-Lin, D. Gui-Fu, “Heat transfer and friction characteristics of the microfluidic heat sink with variously-shaped ribs for chip cooling”, *Sensors*, Vol.15, pp. 9547-9562, 2015.
- [7] C. Nonino, S. Savino , S. Del Giudice, “FEM for the 3-D analysis of conjugate conduction-convection heat transfer in cross-flow micro heat exchangers”, *International J. Numerical Methods for Heat & Fluid Flow*, 2015.
- [8] D. Ciloglu, A. Bolukbasi, and H. Cifci, “The Effect of type of nanoparticles on the quenching process”, *International J. Materials and Metallurgical Engineering*, Vol. 9, No:6, 2015.
- [9] A.S. Navaei, H.A. Mohammed, K.M. Munisamy, H.Yarmand, S. Ghareh khani, “Heat transfer enhancement of turbulent nanofluid flow over various types of internally corrugated channels”, *Powder Technology*, Vol. 286, pp. 332 – 341, 2015.
- [10] W. Hongtao, C. Zhihua and G. Jianguo, “ Influence of geometric parameters on flow and heat transfer performance of micro-channel heat sinks”, *Applied Thermal Engineering*, Vol. 107, pp. 870-879, 2016.
- [11] A. A. Ammar, H. K. Wissam, “A numerical study of the heat transfer and fluid flow in different shapes of microchannels”, *Al-Nahrain University, College of Engineering Journal (NUCEJ)*, Vol.19, pp. 66 -75, 2016.
- [12] C. Lei, D. Guo, S. Hua, “Numerical study of laminar flow and heat transfer in microchannel heat sink with offset ribs on sidewalls”, *Applied Thermal Engineering*, Vol. 92, pp. 32-41, 2016.
- [13] R. Sharma, A. Singh Gill, V. Dhawan , “Experimental analysis of heat transfer and fluid flow in micro-channel heat sink”, *International Journal of Recent advances in Mechanical Engineering (IJMECH)*, Vol.5(3), 2016.

- [14] H. Togun, “Laminar CuO-water nano-fluid flow and heat transfer in a backward-facing step with and without obstacle”, *Applied Nanoscience*. Vol.6, pp.371-378, 2016.
- [15] N.S. Chemloul, and M.A. Belmiloud, “Effet des nanoparticules sur l’amélioration du transfert thermique dans une cavité carrée”, *Revue des Energies Renouvelables*, Vol. 19 N°3, pp. 397-408, 2016.
- [16] A. Andreozzi, O. Manca, S. Nardini, D. Ricci, “Forced convection enhancement in channels with transversal ribs and nanofluids”, *Applied Thermal Engineering*, 2016.
- [17] P.Kumar , D. Dey , S. Samantaray , “A recent review on thermo-physical properties of nanofluid”, *International Conference on Electrical, Electronics, and Optimization Techniques (ICEEOT)*, 2016.
- [18] M. Zunaid, A. Jindal, D. Gakhar, A. Sinha, “Numerical study of pressure drop and heat transfer in a straight rectangular and semi cylindrical projections microchannel heat sink”, *Journal of Thermal Engineering*, Vol. 3(5), pp. 1453-1465, 2017.
- [19] A. Behnampour, O. A. Akbari, M. R. Safaei, M. Ghavami, A. Marzban, G. A.S. Shabani, M. zarringalam, R. Mashayekhi, “Analysis of heat transfer and nanofluid fluid flow in microchannels with trapezoidal, rectangular and triangular shaped ribs”, *Physica E: Low-dimensional Systems and Nanostructures*, Vol. 91, pp. 15 – 31, 2017.
- [20] A. Elazem and A. Ebaid, “Effects of partial slip boundary condition and radiation on the heat and mass transfer of MHD-nanofluid flow”, *Indian J. Physics*, 2017.
- [21] C Qi, Y L Wan, G Q Wang and D T Han, “Study on stabilities, thermophysical properties and natural convective heat transfer characteristics of TiO₂-water nanofluids”, *Indian J. Physics*, 2017.
- [22] R. Mohebbi, M. Izadi, and A. J. Chamkha, “Heat source location and natural convection in a C-shaped enclosure saturated by a nanofluid”, *J. Physics of Fluids* , 2017.
- [23] S.E. Ghasemi, A.A. Ranjbar, M.J. Hosseini, “Thermal and hydrodynamic characteristics of water-based suspensions of Al₂O₃ nanoparticles in a novel minichannel heat sink”, *J. Mol. Liq* , 2017.
- [24] G. Colangelo, E. Favale, M. Milanese, A.de Risi, D.Laforgia, “Cooling of electronic devices: Nanofluids contribution”, *Applied Thermal Engineering* Vol. 127, pp. 421-435, 2017.
- [25] P. Mangalkar , Dr. V.M.Kriplani, “A Review on Heat Transfer Enhancement using Nanofluid for Cooling of Electronic Components”, *International Journal of Engineering Science and Computing*, February, Vol. 7 issue No 2, 2017.
- [26] G. Munish, V. Singh, R. Kumar, Z. Said, “A review on thermophysical properties of nanofluids and heat transfer applications”, *Renewable and Sustainable Energy Reviews* Vol.74, , pp. 638-670, 2017.
- [27] D. P. Sharad , C. W. Sagar, “Numerical investigation on effect of geometrical variations in microchannel heat sink”, *International Research Journal of Engineering and Technology (IRJET)* Vol. 05(02), pp. 1519-1525, 2018.
- [28] S. V. Jadhav, P. M. Pawar, B. P. Ronge, “Effect of pin-fin geometry on microchannel performance”, *Journal of Chemical Product and Process Modeling*, Vol.14(1), pp. 1934-2659, 2018.

- [29] S. M. Sohel Murshed and C. A. Nieto de Castro, "Nanoparticles-loaded fluids for cooling modern electronics", AIP Conference Proceedings, 050015, 2018.
- [30] I. Mjallal, H. Farhat, M. Hammoud, S. Ali, A. AL Shaer and A. Assi, "Cooling Performance of Heat Sinks Used in Electronic Devices", MATEC Web of Conferences Vol.171, 02003, 2018.
- [31] B. Mehdi, H. Saeed, "Electronics cooling with nanofluids: A critical review", Energy Conversion and Management, Vol. 172, pp. 438-456, 2018.
- [32] R. Rezazadeh, N. Pourmahmoud, S. Asaadi, "Numerical investigation and performance analyses of rectangular mini channel with different types of ribs and their arrangements", International journal of thermal sciences, Vol.132, pp.76-85, 2018.
- [33] M. Kmiotek and A. Kucaba-piętal, "Influence of slim obstacle geometry on the flow and heat transfer in microchannels", Bulletin of the Polish Academy of Sciences Technical Sciences, Vol. 66, No. 2, 2018.
- [34] A. Abdollahi, H.A. Mohammed, Sh.M. Vanaki, R. N. Sharma, "Numerical investigation of fluid flow and heat transfer of nanofluids in microchannel with longitudinal fins", Ain Shams Engineering Journal, Vol. 9, Issue 4, pp. 3411-3418, 2018.
- [35] P. Kangude, D. Bhatt and A. Srivastava, "Experiments on the effects of nanoparticle on subcooled nucleate pool boiling", J. Physics of fluids, 2018.
- [36] D. Fernando, S. Gao, S. J. Garrett, "On the heat transfer effects of nanofluids within rotor-stator cavities", J Physics Fluids, Vol.30, 082007, 2018.
- [37] E. Belahmadi, R. Bessaih, "Heat transfer and entropy generation analysis of Cu-water nanofluid in a vertical channel", World J. Engineering, 2018.
- [38] M. Saeed, and M. Kim, "Heat transfer enhancement using nanofluids ($\text{Al}_2\text{O}_3\text{-H}_2\text{O}$) in mini-channel heat sink", International Journal of Heat and Mass Transfer, Vol. 120, pp. 671–682, 2018.
- [39] H. Bakhshi, E. Khodabandeh, O. Akbari, D. Toghraie, M. Joshaghani, A. Rahbari, "Investigation of laminar fluid flow and heat transfer of nanofluid in trapezoidal microchannel with different aspect ratios", International J. Numerical Methods for Heat & Fluid Flow, 2018.
- [40] A. Naser, J. A. Teixeira, and A. Addali, "A Review on Nanofluids: Fabrication, stability, and thermophysical properties", Journal of Nanomaterials, ID 6978130 | 33 pages, 2018.
- [41] SX. Wang, Z. Wan, Y. Tang, "Thermodynamic and experimental study on heat transfer mechanism of miniature loop heat pipe with water-copper nanofluid", J. Physics of Fluids, 2018.
- [42] A. Khanlari, A. Sözen, H. İ. Variyenli, "Simulation and experimental analysis of heat transfer characteristics in the plate type heat exchangers using $\text{TiO}_2\text{/water}$ ", International J. Numerical Methods for Heat & Fluid Flow, 2018.
- [43] I. Khan, K. A. Abro, M. N. Mirbhar, and I. Tlili, "Thermal analysis in Stokes' second problem of nanofluid", Applications in thermal engineering, Case Studies in Thermal Engineering, vol. 12, pp. 271–275, 2018.

- [44] V.Y. Rudyak, A.V. Minakov, “Thermophysical properties of nanofluids”, *European Physical Journal E* 41, 15, 2018.
- [45] S. V. Jadhav, P. M. Pawar, “Performance analysis of microchannel with different pin fin layouts”, *International Journal of Numerical Modelling*, e2697, 2019.
- [46] X. Yang, L. Wei, F. Cao, L. Zhang, Z. Lu, X. Meng, L. Jin, “A parametric study of laminar convective heat transfer in fractal minichannels with hexagonal fins”, *International Journal of Energy Res*, pp. 1-17, 2019.
- [47] S. Gulbanu, M. Kaya, E. Gedik and M. Kayfeci, “Numerical investigation on turbulent convective heat transfer of nanofluid flow in a squar cross-sectioned duct”, *International J. Numerical Methods for Heat & Fluid Flow*, 2019.
- [48] F. Mebarek-Oudina, R. Bessaïh, “Numerical simulation of natural convection heat transfer of copper-Water nanofluid in a vertical cylindrical annulus with heat sources”, *Thermophysics and Aeromechanics*, Vol. 26 (3), pp. 325-334, 2019.
- [49] A. Ahad, E. Saeed, A. Taher, “Numerical analysis of mixed convection of different nanofluids in concentric annulus”, *Int. J. Numerical Methods Heat Fluid Flow*, Vol. 29, pp. 1506-1525, 2019.
- [50] F. Mebarek-Oudina, “Convective heat transfer of Titania nanofluids of different base fluids in cylindrical annulus with discrete heat source”, *Heat Transfer-Asian Research*, Vol. 48 (1), pp.135-147, 2019.
- [51] B. Mahanthesh, G. Lorenzini, F. Mebarek-Oudina and I. L. Animasaun, “Significance of exponential space- and thermal-dependent heat source effects on nanofluid flow due to radially elongated disk with Coriolis and Lorentz forces”, *Journal of Thermal Analysis and Calorimetry*, 2019.
- [52] R. Mohebbi, M. Izadi, H. Sajjadi, A. A. Delouei, M.A. Sheremet, “Examining of nanofluid natural convection heat transfer in a Γ -shaped enclosure including a rectangular hot obstacle using the lattice Boltzmann method”, *Physica A: Statistical Mechanics and its Applications*, Vol. 526, 120831, 2019.
- [53] N. Rehana, M. Hasanuzzaman, N.A. Rahim, “Effect of nanofluids on heat transfer and cooling system of the photovoltaic/thermal performance”, *International J. Numerical Methods for Heat & Fluid Flow*, 2019.
- [54] S. Kumar, K. S. Pawan, “Effects of flow inlet angle on flow maldistribution and thermal performance of water cooled mini-channel heat sink”, *International J. thermal sciences*, Vol.138, pp. 504–511, 2019.
- [55] M. Bezaatpour, M. Goharkhah, “Three dimensional simulation of hydrodynamic and heat transfer behavior of magnetite nanofluid flow in circular and rectangular channel heat sinks filled with porous media”, *Powder Technology*, Vol 344, pp. 68-78, 2019.
- [56] K. P. Yogesh, “Influence of fin height on heat transfer and fluid flow characteristics of rectangular microchannel heat sink”, *International Journal of Heat and Mass Transfer*, Vol. 137, pp. 1041-1052, 2019.

- [57] A. Deriszadeh and F. de Monte, "On heat transfer performance of cooling systems using nanofluid for electric motor applications", XII International Conference on Computational Heat, Mass and Momentum Transfer, ICCHMT 2019.
- [58] V. Murali Krishna, M. Sandeep Kumar, "Numerical analysis of forced convective heat transfer of nanofluids in microchannel for cooling electronic equipment", Materials Today Proceedings, Vol.17, pp. 295-302, 2019.
- [59] M. Bahiraei, M. Jamshidmofid, M. Goodarzi, "Efficacy of a hybrid nanofluid in a new microchannel heat sink equipped with both secondary channels and ribs", Journal of Molecular Liquids, Vol.273, pp. 88-98, 2019.
- [60] G. Wang, T. Chen, M. Tian, G. Ding, "Fluid and heat transfer characteristics of microchannel heat sink with truncated rib on sidewall", International Journal of Heat and Mass Transfer, Vol. 148, 119142, 2020.
- [61] H. Laouira, F. Mebarek Oudina, A. K. Hussein, L. Kolsi, A. Merah, O. Younis, "Heat transfer inside a horizontal channel with an open trapezoidal enclosure subjected to a heat source of different lengths", Heat Transfer-Asian Research, Vol.49, pp 406-423, 2020.
- [62] F. Mebarek-Oudina, S. Marzougui, A. Abderrahmane, M. Magherbi, Z. Shah, K. Ramesh, "Entropy generation on Magneto-Convective flow of Copper-Water nanofluid in a cavity with chamfers", Journal of Thermal Analysis and Calorimetry, 2020.
- [63] G. Huminic, A. Huminic, "Entropy generation of nanofluid and hybrid nanofluid flow in thermal systems, A review", Journal of Molecular Liquids, Vol. 302, 112533, 2020.
- [64] J. Alsarraf, A. Shahsavar, M. Khaki, R. Ranjbarzadeh, A. Karimipour, M. Afrand, "Numerical investigation on the effect of four constant temperature pipes on natural cooling of electronic heat sink by nanofluids: A multifunctional optimization", Advanced Powder Technology, Vol. 31, pp. 416-432, 2020.
- [65] F. Selimefendigil, H. F. Öztop, "Control of natural convection in a CNT-water nanofluid filled 3D cavity by using an inner T-shaped obstacle and thermoelectric cooler", International Journal of Mechanical Sciences, Vol. 169, 105104, 2020.
- [66] M. A. Hssain, R. Mir and Y. El Hammami, "Numerical Simulation of the cooling of heated electronic blocks in horizontal channel by mixed convection of nanofluids", Journal of Nanomaterials, 11 pages, 2020.
- [67] P.C. Mukesh Kumar and C.M. Arun Kumar, "Numerical study on heat transfer performance using Al₂O₃/water nanofluids in six circular channel heat sink for electronic chip", Materials Today: Proceedings, Vol. 21, pp. 194-201, 2020.
- [68] P.S. Arshi Banu, A. Krishnan, S.M. Shafee and A. Gnana Sagaya Raj, "Numerical investigation of micro-pin-fin heat exchanger using nanofluids", Materials Today: Proceedings, Vol. 22, Part 3, pp.1020-1025, 2020.
- [69] W. Abbas and M. M. Magdy, "Heat and mass transfer analysis of nanofluid flow based on and over a moving rotating plate and impact of various nanoparticle shapes", Mathematical Problems in Engineering, 12 pages, 2020.

- [70] W.V. Vicki, M.Z. Abdullah, P. Gunnasegaran, “Thermophysical properties of Al₂O₃-CuO hybrid nanofluid at different nanoparticle mixture ratio: An experimental approach”, *Journal of Molecular Liquids*, Vol. 313, 113458, 2020.
- [71] X. Chong, X. Shanglong, W. Shiteng, C. Pengyan, “Experimental investigation of heat transfer for pulsating flow of GOPs-water nanofluid in a microchannel”, *International Communications in Heat and Mass Transfer*, Vol. 110, 104403, 2020.
- [72] T. Ambreen, M-H. Kim, “Influence of particle size on the effective thermal conductivity of nanofluids: A critical review”, *Applied Energy*, Vol. 264, 114684, 2020.
- [73] K. A. Jehhef, R. H. Khanjar and M. A. Siba, “Convection heat transfer enhancement in square cross-section with obstacle using nanofluids”, *IOP Conf. Series: Materials Science and Engineering*, Vol.518, 2019.
- [74] W. Chamsa-ard, S. Brundavanam, C.C. Fung, D. Fawcett and G. Poinern, “Nanofluid Types, Their Synthesis, Properties and Incorporation in Direct Solar Thermal Collectors: A Review”, *Nanomaterials*, 2017,
- [75] Z. Han, “Nanofluids with enhanced thermal transport properties, Departement of Mechanical Engineering”, University of Maryland at College Park, College Park, Maryland, 2008.
- [76] Y. Wang, Z. Iqbal, S. Mitra. Rapid, “low temperature microwave synthesis of novel carbon nanotube-silicon carbide composite”, *Carbon*, Vol. 44, pp.2804-2808, 2006.
- [77] S. Berber, Y. K. Kwon, D. Tomanek, “Unusually high thermal conductivity of carbon nanotubes, physical review letters, Vol. 84, pp. 4613-4616, 2000.
- [78] S. Jana, A. Salehi-Khojin, and W.-H. Zhong, “Enhancement of fluid thermal conductivity by the addition of single and hybrid nano-additives”, *Thermochimica Acta*, Vol. 462, no. 1-2, pp. 45–55, 2007.
- [79] S. P. Jang, S. U. S. Choi, “Role of Brownian motion in the enhanced thermal conductivity of nanofluids”, *Applied Physics Letters*, Vol. 84, 21, 2004.
- [80] P. Keblinski, S.R. Phillpot, S.U.S Choi, J.A. Eastman, “Mechanisms of heat flow in suspensions of nano-sized particles (nanofluids)”, *International Journal of Heat and Mass Transfer*, Vol. 45, pp. 855-863, 2002.
- [81] W. Yu, H. Xie, “A review on nanofluids: preparation, stability mechanisms, and applications”, *J. Nanomater*, Vol. 87, pp. 228–40, 2012.
- [82] L. Kong, J. Sun, and Y. Bao, “Preparation, characterization and tribological mechanism of nanofluids”, *RSC Advances*, Vol. 7, No. 21, pp. 12599–12609, 2017.
- [83] E. Pop, V. Varshney, A. K. Roy, “Thermal properties of graphene: Fundamentals and applications”, *MRS Bull*, Vol. 37, pp.1273-1281, 2012.
- [84] F. Mashali, E. Mohseni Languri, J. Davidson, D.Kerns, W. Johnson, K. Nawaz, and G. Cunningham, “Thermo-physical properties of diamond nanofluids: A review”, *International Journal of Heat and Mass Transfer*, Vol.129, pp. 1123-1135, 2019.

- [85] B. C. Pak and Y. I. Cho, “Hydrodynamic and heat transfer study of dispersed fluids with submicron metallic oxide particles”, *Experimental Heat Transfer*, Vol. 11, pp. 151–170, 1998.
- [86] Y. Xuan and W. Roetzel, “Conception for heat transfer correlation of nanofluids”, *International Journal of Heat and Mass Transfer*, Vol. 43, pp. 3701-3707, 2000.
- [87] A. Bejan, “Convection Heat Transfer”, 3rd Edition, Wiley, New-York, 2004.
- [88] J. Kim, Y. T. Kang, C.K. Choi, “Analysis of convective instability and heat transfer characteristics of nanofluids”, *Physics of Fluids*, Vol. 16, pp. 2395-2401, 2004.
- [89] J.C. Maxwell, “A Treatise on Electricity and Magnetism”, Clarendon Press, U.K, 1881.
- [90] R.L. Hamilton and O.K. Crosser, “Thermal conductivity of heterogeneous two component systems”, *Industrial and Engineering Chemistry Fundamentals*, Vol. 1, pp. 187- 191, 1962.
- [91] W. Yu and U.S. Choi, “The role of interfacial layers in the enhanced thermal conductivity of nanofluids: a renovated Maxwell model”, *Journal of Nanoparticles Research*, Vol. 5, pp. 167- 71, 2003.
- [92] D.A.G. Bruggeman, “Berechnung verschiedener physikalischer konstanten von heterogenen substanzen, I. Dielektrizitätskonstanten und leitfähigkeiten dermischkörper aus isotropen substanzen”, *Ann. Phys. Leipzig*, Vol. 24, pp. 636– 679, 1935.
- [93] E. M. Hemmat, M. Afrand, A. Karimipour, WM. Yan, N. Sina, “An experimental study on thermal conductivity of MgO nanoparticles suspended in a binary mixture of water and ethylene glycol”, *Int Commun Heat Mass Transf*, Vol. 67, pp.173–5, 2015.
- [94] E. M. Hemmat, S. Saedodin, A. Naderi, A. Alirezaie, A. Karimipour, S. Wongwises, M. Goodarzi, M. bin Dahari, “Modeling of thermal conductivity of ZnO-EG using experimental data and ANN methods”, *Int Commun Heat Mass Transf*, Vol. 63, pp.35–40, 2015.
- [95] E. M. Hemmat, PM. Behbahani, AA. Abbasian Arani, MR. Sarlak, “Thermal conductivity enhancement of SiO₂–MWCNT (85: 15%)–EG hybrid nanofluids”, *J Therm Anal Calorim*, Vol. 128, pp.249–258, 2017.
- [96] RM. Mostafizur, MH. Bhuiyan, R. Saidur, AA. Aziz, “Thermal conductivity variation for methanol based nanofluids”, *Int J Heat Mass Transf*, Vol. 76, pp.350–356, 2014.
- [97] M. Xing, J. Yu, R. Wang, “Experimental study on the thermal conductivity enhancement of water based nanofluids using different types of carbon nanotubes”, *Int J Heat Mass Transf*, Vol. 88, pp.609–616, 2015.
- [98] X. Li, C. Zou, X. Lei, W. Li, “Stability and enhanced thermal conductivity of ethylene glycol-based SiC nanofluids”, *Int J Heat Mass Transf*, Vol. 89, pp.613–619, 2015.
- [99] A. Einstein, “Eine Neue Bestimmung der Molekuldimensionen”, *Ann. Phys. Leipzig*, Vol. 19, pp. 289–306, 1906.
- [100] G. K. Batchelor, “Brownian Diffusion of particles with Hydrodynamic Interaction”, *Journal of Fluid Mechanics*, Vol. 74, pp. 1-29, 1976.

- [101] H.C. Brinkman, “The Viscosity of Concentrated Suspensions and Solutions”, *J. Chemical Physics*, Vol. 20, pp. 571, 1952.
- [102] S. Maiga, S.J. Palm, C.T. Nguyen, G. Roy, N. Galanis, “Heat transfer enhancement by using nanofluids in forced convection flows”, *International Journal of Heat and Fluid Flow*, Vol. 26, pp.530–546, 2005.
- [103] H. E. Patel, T. Sundararajan, S. K. Das, “An experimental investigation into the thermal conductivity enhancement in oxide and metallic nanofluids”, *J. Nanopart. Res*, Vol. 12, pp.1015–1031, 2010.
- [104] C.H. Chon, K.D. Kihm, S.P. Lee, S.U.S. Choi, “Empirical correlation finding the role of temperature and particle size for nanofluid (Al_2O_3) thermal conductivity enhancement”, *Appl. Phys. Lett*, Vol. 87, 153107, 2005.
- [105] G. Paul, T. Pal, I. Manna, “Thermo-Physical property measurement of nano-gold dispersed water based nanofluids prepared by chemical precipitation technique”, *J. Colloid Interface Sci*, Vol. 349, pp.434–437, 2010.
- [106] S. Simpson, A. Schelfhout, C. Golden and S. Vafaei, “Nanofluid Thermal Conductivity and Effective Parameters”, *Applied Sciences*, Vol. 9, 87, 2019.
- [107] F.M. Ali, W.M.M. Yunus, M.M. Moxsin, Z.A. Talib, “The effect of volume fraction concentration on the thermal conductivity and thermal diffusivity of Nanofluids, numerical and experimental”, *Rev. Sci. Instrum*, Vol. 81, 074901, 2010.
- [108] S. Choi, Z. Zhang, W. Yu, F. Lockwood, E. Grulke, “Anomalous thermal conductivity enhancement in nanotube suspensions”, *Appl. Phys. Lett*, Vol. 79, pp. 2252–2245, 2001.
- [109] M. E. Hemmat, A. Naderi, M. Akbari, M. Afrand, A. Karimipou, “Evaluation of thermal conductivity of COOH-functionalized MWCNTs/water via temperature and solid volume fraction by using experimental data and ANN methods”, *Journal of Thermal Analysis and Calorimetry*, Vol. 121, pp. 1273–1278, 2015.
- [110] SH. Kim, SR. Choi, D. Kim, “Thermal conductivity of metal-oxide nanofluids: Particle size dependence and effect of laser irradiation”, *J. Heat Transfer*, Vol. 129, pp. 298–307, 2007.
- [111] H. Xie, J. Wang, T. Xi, Y. Liu, “Thermal conductivity of suspensions containing nanosized SiC particles”, *Int J Thermophys*, Vol. 23, pp. 571–580, 2002.
- [112] H. Xie, J. Wang, T. Xi, Y. Liu, F. Ai, Q. Wu, “Thermal conductivity enhancement of suspensions containing nanosized alumina particles”, *J. Appl Phys*, Vol. 91, pp. 4568–4572, 2002.
- [113] X. Wang, X. Xu, S. Choi, “Thermal Conductivity of Nanoparticle–Fluid Mixture”, *J. Thermophys. Heat Transf*, Vol. 13, pp. 474–480, 1999.
- [114] R. Agarwal, K. Verma, NK. Agrawal, RK. Duchaniya, R. Singh, “Synthesis, characterization, thermal conductivity and sensitivity of CuO nanofluids”, *Appl Therm Eng*, Vol. 102, pp. 1024–1036, 2016.
- [115] M. Chopkar, S. Sudarshan, PK. Das, I. Manna, “Effect of Particle Size on Thermal Conductivity of Nanofluid”, *Metall Mater Trans A*, Vol. 39, pp. 1535–1542, 2008.

- [116] A. H.A. Al-Waeli, M. T. Chaichan, K. Sopian, A.K. Hussein, “Influence of the base fluid on the thermo-physical properties of PV/T nanofluids with surfactant”, *Case Studies in Thermal Engineering*, Vol. 13, 100340, 2019.
- [117] S. K. Vandurangi, S. Hassan, K.V. Sharma, S. Akilu, S. Emani, N. Nabipour, “Effect of base fluids on thermo-physical properties of SiO₂ nanofluids and development of new correlations”, *Mathematical methods in the applied sciences*, 2020.
- [118] P.B. Maheshwary, C.C. Handa, K.R. Nemade, “A comprehensive study of effect of concentration, particle size and particle shape on thermal conductivity of titania/water based nanofluid”, *Appl. Therm. Eng.*, Vol. 119, pp. 79–88, 2017.
- [119] J. Boussinesq, “*Theorie analytique de la chaleur*”, Gauthier-Villars, Paris, Vol.2, 1903.
- [120] A. Oberbeck, “Ueber die warmeleitung der flussigkeiten bei berucksichtigung der stromungen infolge von temperaturdifferenzen”, *Annalen der physic und Chemie*, Vol. 243(6), pp. 271–292, 1879.
- [121] S. Fohanno, G. Polidori, C. Popa, “*Nanofluides et transfert de chaleur par convection naturelle*”, Université de reims champagne-Ardenne, France, 2012.
- [122] I. Zakaria, W.A.N.W Mohamed, A.M.I Bin Mamat, R. Saidur, W.H. Azmi, R. Mamat, K.I Sainana and H. Ismail, “Thermal analysis of heat transfer enhancement and fluid flow for low concentration of Al₂O₃ Water – Ethylene Glycol Mixture Nanofluid in a Single PEMFC Cooling Plate”, *Energy Procedia*, Vol. 79, pp. 259–264, 2015.
- [123] G.A. Sheikhzadeh, A. Arefmanesh, M.H. Kheirkhah, R. Abdollahi, “Natural convection of Cu-water nanofluid in a cavity with partially active side walls”, *European Journal of Mechanics B/Fluids*, Vol. 30, pp. 166–176, 2011.
- [124] M. K. Moraveji, R. M. Ardehali and A. Ijam, “CFD investigation of nanofluid effects (cooling performance and pressure drop) in mini-channel heat sink”, *International Communications in Heat and Mass Transfer*, Vol. 40, pp. 58–66, 2013.
- [125] B. Gladés, “*Contribution à l’étude de la convection naturelle dans les nanofluides en configuration de Rayleigh-Bénard*”, (thèse de doctorat), L’Université Toulouse III- Paul Sabatier, 2010.
- [126] M. Tawk, Y. Avenas, et al, “*Etude d’un système de refroidissement de composants électroniques de puissance par métal liquide*”, 13ème édition de la Conférence, Électronique de Puissance du Futur (EPF), Saint-Nazaire, France, 2010.
- [127] K. A. Jehhef, R. H. Khanjar and M. A. Siba, “Convection heat transfer enhancement in square cross-section with obstacle using nanofluids”, *IOP Conf. Series: Materials Science and Engineering*, Vol.518, 2019.
- [128] G. Ali Sheikhzadeh, A. Aghaei, S. soleimani, “Effect of nanoparticle shape on natural convection heat transfer in a square cavity with partitions using water-SiO₂ nanofluid”, *Trans. Phenom. Nano Micro Scales*, Vol. 6, pp. 27–38, 2018.
- [129] S. Tippa, M. Narahari, and R. Pendyala, “Unsteady natural convection flow of nanofluids past a semi-infinite isothermal vertical plate”, *AIP Conference Proceedings*, Vol. 1787, 020014, 2016.

- [130] P. Gunnasegaran, N.H. Shuaib, H.A. Mohammed, M.F. Abdul Jalal and E. Sandhita, “Heat transfer enhancement in microchannel heat sink using nanofluids”, *Fluid Dynamics, Computational Modeling and Applications*, pp. 287–326, 2012.
- [131] X. Gongnan, L. Shian, S. Bengt, Z. Weihong, and L. Haibin, “A numerical study of the thermal performance of microchannel heat sinks with multiple length bifurcation in laminar liquid flow”, *Numerical Heat Transfer, Part A*, Vol. 65, pp. 107–126, 2014.
- [132] L. Chai, L. Wang, X. Bai, “Thermohydraulic performance of microchannel heat sinks with triangular ribs on sidewalls – Part 2: Average fluid flow and heat transfer Characteristics”, *International Journal of Heat and Mass Transfer*, Vol. 128, pp. 634–648, 2019.
- [133] M. R. Mekideche, “Contribution à la modélisation numérique de torches à plasma d’Induction”, Thèse de doctorat, Université de NANTES, 1993.
- [134] G. D. G. Touzot, “Une présentation de la méthode des éléments finis”, Maloine S.A. Editeur Paris, France, 1984.
- [135] S.V. Patankar and D.B. Spalding, “A calculation procedure for heat, mass and momentum transfer in three dimensional parabolic flows”, *Int. J. Heat Mass Transfer* volume, Vol. 15, pp. 1787–1806, 1972.
- [136] S.V. Patankar, “Numerical Heat Transfer and Fluid Flow”, Hemisphere, NewYork , 1980.
- [137] H. Nouri, F. Ravelet, “Tutoriel introductif à la simulation numérique des écoulements”, Web site.
- [138] F. Bakir, D. Fedala, S. Khelladi, “Simulation numérique des écoulements internes dans les turbomachines”, Web site.
- [139] L. Chai, G. Xia, L. Wang, M. Zhou, Z. Cui, “Heat transfer enhancement in microchannel heat sinks with periodic expansion–constriction cross-sections”, *International Journal of Heat and Mass Transfer*, Vol. 62, pp. 741–751, 2013.